LA-13402-T
Thesis

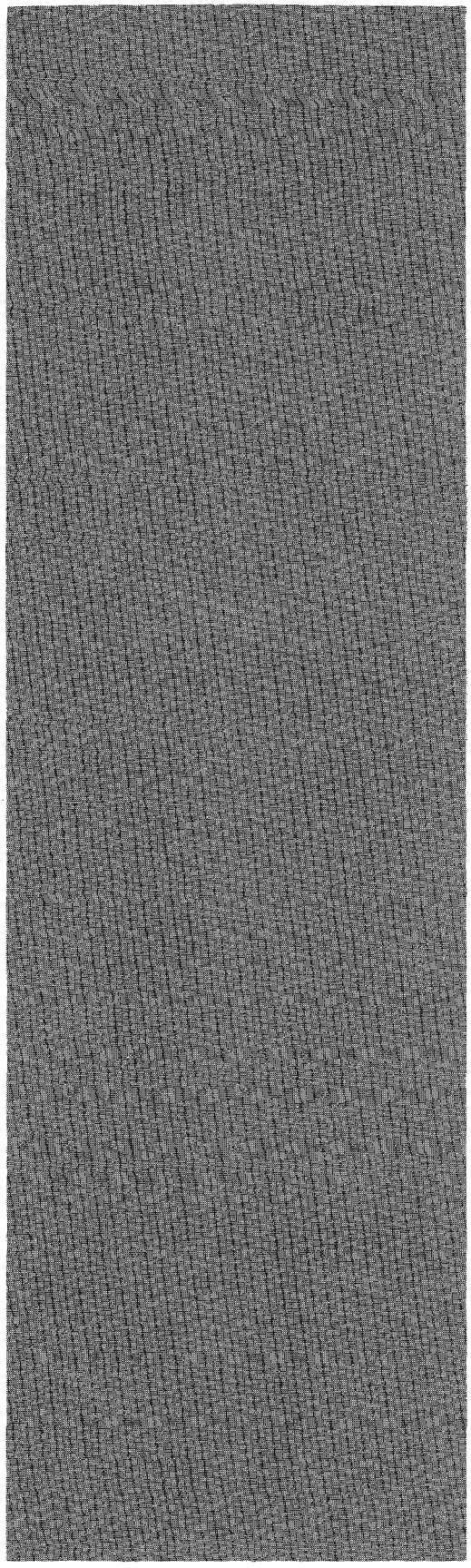

A Simplified Spherical Harmonic Method for Coupled Electron-Photon Transport Calculations

Los Alamos
NATIONAL LABORATORY

Los Alamos National Laboratory is operated by the University of California for the United States Department of Energy under contract W-7405-ENG-36.

This thesis was accepted by the Department of Physics, the Pennsylvania State University, University Park, Pennsylvania, in partial fulfillment of the requirements for the degree of Doctor of Philosophy. The text and illustrations are the independent work of the author and only the front matter has been edited by the CIC-1 Writing and Editing Staff to conform with Department of Energy and Los Alamos National Laboratory publication policies.

An Affirmative Action/Equal Opportunity Employer

LA-13402-T
Thesis

UC-700
Issued: December 1997

A Simplified Spherical Harmonic Method for Coupled Electron-Photon Transport Calculations

John A. Josef

Los Alamos
NATIONAL LABORATORY
Los Alamos, New Mexico 87545

Contents

List of Figures

List of Tables

Acknowledgments

This research was carried out as a visiting Graduate Research Assistant at Los Alamos National Laboratory, group CIC-19. I would like to express sincere thanks to my adviser Jim E. Morel for his continued direction, advice, and knowledge. I would also like to thank him for locating financial support and for carefully reviewing the manuscript.

I would like to thank Joel E. Dendy, Jr. T-7, Victor E. Bandy T-7, and H. Grady Hughes, III X-TM for their technical contributions.

I would like to thank the members of my doctoral committee. Professor Mark Strikman, Professor Jayanth R. Banavar, Professor Douglas H. Sampson, and Professor Richard W. Robinett.

I would like to thank Los Alamos National Laboratory for this unique opportunity to study and learn, and the members of CIC-19 Radiation Transport Team.

Finally, I wish to extend special thanks to Randy M. Roberts for his invaluable instruction, and his many fruitful suggestions. I feel I have benefited greatly from the many enjoyable discussions we have had together.

The assistance of the above named individuals is sincerely appreciated.

A Simplified Spherical Harmonic Method
for Coupled Electron-Photon Transport Calculations

John A. Josef

Abstract

In this thesis we have developed a simplified spherical harmonic method (SP_N method) and associated efficient solution techniques for 2-D multigroup electron-photon transport calculations. The SP_N method has never before been applied to charged-particle transport. We have performed a first time Fourier analysis of the source iteration scheme and the P_1 diffusion synthetic acceleration (DSA) scheme applied to the 2-D SP_N equations. Our theoretical analyses indicate that the source iteration and P_1 DSA schemes are as effective for the 2-D SP_N equations as for the 1-D S_N equations. Previous analyses have indicated that the P_1 DSA scheme is unstable (with sufficiently forward-peaked scattering and sufficiently small absorption) for the 2-D S_N equations, yet is very effective for the 1-D S_N equations. In addition, we have applied an angular multigrid acceleration scheme, and computationally demonstrated that it performs as well for the 2-D SP_N equations as for the 1-D S_N equations. It has previously been shown for 1-D S_N calculations that this scheme is much more effective than the DSA scheme when scattering is highly forward-peaked. We have investigated the applicability of the SP_N approximation to two different physical classes of problems: satellite electronics shielding from geomagnetically trapped electrons, and electron beam problems. In the space shielding study, the SP_N method produced solutions that are accurate within 10% of the benchmark Monte Carlo solutions, and often orders of magnitude faster than Monte Carlo. We have successfully modeled quasi-void problems and have obtained excellent agreement with Monte Carlo. We have observed that the SP_N method appears to be too diffusive an approximation for beam problems. This result, however, is in agreement with theoretical expectations.

Chapter 1

Introduction

Over the past five decades, considerable research effort has been expended upon the development of numerical methods for solving radiation transport problems. There are two primary approaches to modeling transport processes: *deterministic* and *stochastic*. In deterministic methods, one directly solves a discrete approximation to the Boltzmann equation. It is the complexity of this equation which necessitates the use of approximate solution techniques. In stochastic methods, i.e. Monte Carlo, physical processes are directly modeled by statistical methods. Monte Carlo often proves to be more efficient at calculating global quantities, while deterministic methods are often more efficient at calculating local quantities. For large problems in multidimensional (2-D, 3-D) geometries, Monte Carlo often requires enormous computational time. Deterministic methods for neutron transport have been the subject of extensive investigation for decades; however, in the area of multidimensional deterministic charged particle transport, little work has been done to date. In this thesis, we shall focus upon the development of deterministic computational methods for coupled electron-photon transport.

The standard P_N equations have been a classic approximation to the transport equation for over fifty years. The basis of this approximation is to assume that the angular dependence of the angular flux can be represented in a truncated spherical harmonic expansion. Here, the index N is an indicator of the number of terms retained in the expansion, and as N increases without bound, the solution of the P_N

equations converges to the solution of the transport equation. In multidimensional problems, these P_N equations are quite complex and difficult to deal with numerically. Furthermore, the number of unknowns in multidimensional P_N calculations is of order $(N+1)^2$. Since electron scattering is highly anisotropic, high order flux and cross section expansions ($P_7 - P_{15}$) are required, and the P_N method can be prohibitively expensive in terms of both memory and CPU time.

In view of this, Gelbard developed a heuristic simplification of the P_N equations, which he called the simplified P_N method. The method was originally applied to neutron transport problems. The SP_N method abandons the requirement that the exact transport solution is obtained as N approaches infinity. Instead, one obtains approximate transport solutions which are signicantly more accurate than diffusion theory, but significantly less expensive than discrete ordinates (S_N), or full P_N methods. The initial derivation of the SP_N equations was not rigorous. This lack of a theoretical foundation has undoubtedly acted as an obstruction to the widespread use of these equations. However, a recent paper [1] in the literature shows that the SP_N equations represent a formal asymptotic solution to the Boltzmann transport equation. That is, the SP_1 equation, or diffusion equation, is the leading order approximation to the transport equation, and higher order SP_N equations represent higher order corrections to diffusion theory. Furthermore, in multidimensional SP_N the number of unknowns is reduced to order $(N+1)$, thus, offering tremendous computational savings over full P_N when N is large. The condition that N is large will always be met in charged particle transport.

The focus of this thesis is multifold: Our first major objective is to develop a simplified spherical harmonic method for multidimensional coupled electron-photon transport; this is the first time that the SP_N method has been applied to charged

particle transport. The second major objective is the development and analysis of efficient solution techniques for the multidimensional SP_N equations.

We present an overview of the thesis:

1. In Chapter 2, we introduce the continuous transport equation, along with some physical definitions which will be used extensively throughout the thesis. We introduce the Boltzmann - Continuous Slowing Down (CSD) Equations, the fundamental model for coupled electron-photon transport. We then briefly discuss particle interactions of interest, and cross section production. We conclude with a reformulation of the Boltzmann - CSD equations into the Boltzmann equations for coupled electron-photon transport, necessary to facilitate the use of our code with the cross section generation code CEPXS.

2. In Chapter 3, we examine numerical methods for discretization of the angular variable in the Boltzmann equation. We begin by introducing the discrete ordinates or S_N method, in which the particle is allowed to travel in a discrete set of directions. We then formulate an alternate approach, the spherical harmonics or P_N method, based upon function expansion techniques. We conclude with a discussion of the equivalence between S_N and P_N methods. It is important to note that both S_N and P_N methods will be used in our development of the SP_N method.

3. In Chapter 4, we derive the simplified spherical harmonic (SP_N) equations using the original technique of Gelbard, and examine the characteristics of the SP_N method in a comparison with the P_N and S_N methods. We briefly discuss a recently developed asymptotic derivation which lends mathematical rigor to the SP_N approximation. We conclude with a derivation of the canonical form of

the SP_N equation, which permits the application of efficient numerical solution and acceleration techniques.

4. In Chapter 5, we discretize the remaining energy and spatial variables in the integrodifferential canonical equations to obtain a set of algebraic equations amenable to computational solution. We difference the energy variable using the conventional multigroup method. Spatial discretization is performed using the finite element method. In this thesis we consider one dimensional planar, two dimensional X - Y, and two dimensional R - Z geometries.

5. In Chapter 6, we address the topic of solution and acceleration of the discretized SP_N equations using iterative methods. We present and analyze the standard source iteration (SI) scheme. It is shown, through Fourier analysis, that the SI method is unconditionally stable, but can be very slow to converge in optically thick systems which are dominated by scattering. Next, we analyze and develop two new methods, P_1 diffusion synthetic acceleration and multigrid in angle acceleration, which have been devised to further accelerate the convergence. We note, these acceleration methods represent multidimensional generalizations of existing one dimensional S_N methods. We conclude with a discussion of particle production/loss rates, particle conservation and energy deposition rates.

6. In Chapter 7, we formulate one and two dimensional test problems to investigate and validate the theoretical method developed in the previous chapters. Specifically, we investigate the applicability of the SP_N method in two physical regimes: Satellite electronics shielding for geomagnetically trapped electrons, where we have uniform isotropic boundary sources; and electron beam problems. We present numerical comparisons with Monte Carlo, an examination of

accuracy and computational efficiency, and a brief discussion of our results.

7. In Chapter 8, we review and summarize the findings of this thesis. Specifically, we interpret the test problem results of the previous chapter, contrast the SP_N method to other deterministic transport methods, and conclude with some possibilities for future work.

Chapter 2

Continuous Transport Problems

2.1 Introduction

In this chapter we introduce the continuous transport equation, along with some definitions which we will use extensively throughout this thesis. We begin by defining the *Boltzmann - Continous Slowing Down Equations (Boltzmann - CSD equations)* with associated boundary conditions for an arbitrary geometry, section 2.2. This set of equations represents our fundamental physical model for coupled charged particle - photon transport. We do not derive the Boltzmann transport equation here; the derivation is presented in most transport theory textbooks [2–4], and the Boltzmann - CSD equation, an extension desirable for the treatment of charged particles, is given in [5]. We conclude, section 2.3, by reformulating the Boltzmann - CSD equations into a new more symmetric form, the *Boltzmann equations for coupled electron-photon transport*, necessary for the use of our SP_N code with the cross section generation code CEPXS.

2.2 The Boltzmann - CSD Equations

The ultimate goal of transport theory is to determine the distribution in phase space of particles in a medium, taking into account the motion of the particles and their interaction with the host medium. The fundamental model of particle transport for a coupled system of electrons and photons is given by the Boltzmann - CSD approximation. This system is coupled due to the physical fact that electrons generate

photons in their interaction with the host medium, and photons in turn generate electrons in their interaction with the host medium. Within the context of this approximation the electron distribution is described by the Boltzmann - CSD equation, and the photon distribution is described by the Boltzmann equation. For brevity, we shall refer to these two equations as the Boltzmann - CSD equations.

First, let us begin by making some fundamental physical definitions. Consider an arbitrary differential volume d^3r, about $\vec{\mathbf{r}}$, as shown in Figure 2.1. We define the particle density distribution as

> $n(\vec{\mathbf{r}}, E, \hat{\Omega}, t)d^3r dE d\hat{\Omega}$ = the expected number of particles in a volume d^3r about $\vec{\mathbf{r}}$ traveling in the solid angle $d\hat{\Omega}$ about $\hat{\Omega}$ with energies between E and $E + dE$ at time t

For most purposes it is more convenient to formulate the transport equation in terms of the *angular flux*

$$\psi(\vec{\mathbf{r}}, E, \hat{\Omega}, t) = v(E)n(\vec{\mathbf{r}}, E, \hat{\Omega}, t) \tag{2.1}$$

where $v(E)$ is the particle speed.

Let us now consider an arbitrary volume, with spatial domain D, bounded by a surface Γ, as shown in Figure 2.2, within which we wish to describe the distribution of particles. For a coupled system of electrons and photons in equilibrium the distribution is described by the steady state Boltzmann - CSD equations [5]

$$\begin{aligned}
&\hat{\Omega} \cdot \vec{\nabla}\psi_e(\vec{\mathbf{r}}, E, \hat{\Omega}) + \sigma_{te}(\vec{\mathbf{r}}, E)\psi_e(\vec{\mathbf{r}}, E, \hat{\Omega}) \\
&= \int_0^\infty dE' \int_{4\pi} d\hat{\Omega}' \sigma^*_{e\to e}(\vec{\mathbf{r}}, E' \to E, \hat{\Omega}' \cdot \hat{\Omega})\psi_e(\vec{\mathbf{r}}, E', \hat{\Omega}') \\
&+ \int_0^\infty dE' \int_{4\pi} d\hat{\Omega}' \sigma_{p\to e}(\vec{\mathbf{r}}, E' \to E, \hat{\Omega}' \cdot \hat{\Omega})\psi_p(\vec{\mathbf{r}}, E', \hat{\Omega}') \\
&+ \frac{\partial}{\partial E}[R_e(\vec{\mathbf{r}}, E)\psi_e(\vec{\mathbf{r}}, E, \hat{\Omega})] + Q_e(\vec{\mathbf{r}}, E, \hat{\Omega}) \qquad ,\vec{\mathbf{r}} \in D
\end{aligned} \tag{2.2}$$

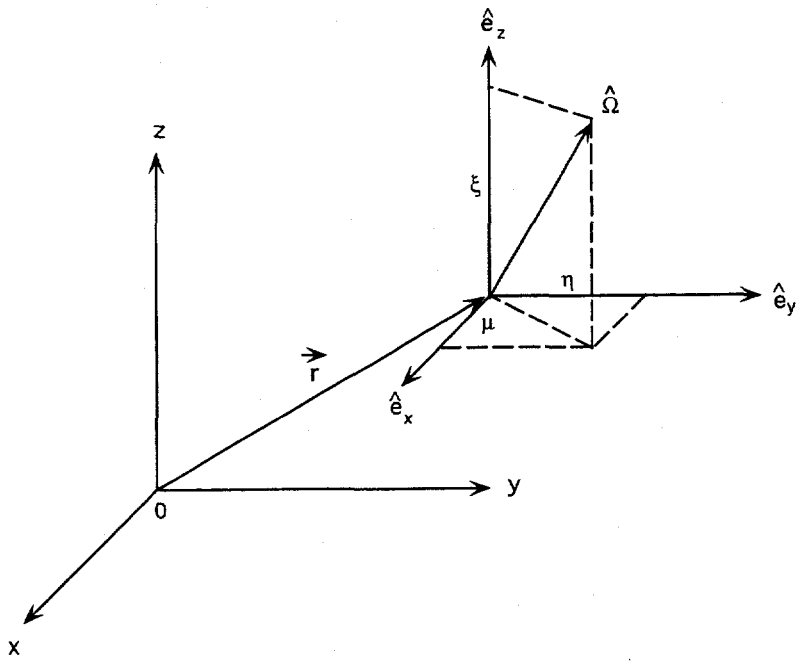

Figure 2.1: Cartesian Space-Angle Coordinate System

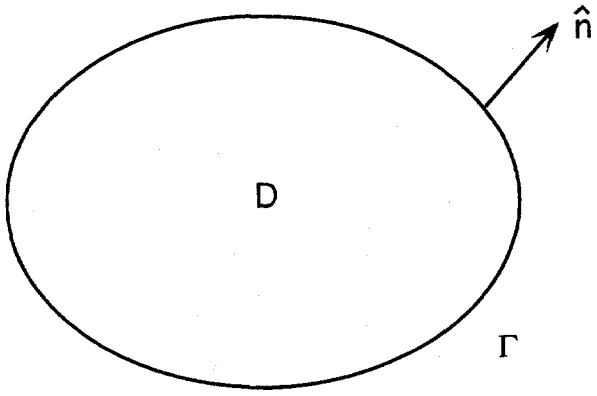

Figure 2.2: Spatial Domain D Bound by Surface Γ

$$\begin{aligned}
&\hat{\Omega}\cdot\vec{\nabla}\psi_p(\vec{\mathbf{r}},E,\hat{\Omega})+\sigma_{tp}(\vec{\mathbf{r}},E)\psi_p(\vec{\mathbf{r}},E,\hat{\Omega})\\
&\quad=\int_0^\infty dE'\int_{4\pi}d\hat{\Omega}'\sigma_{p\to p}(\vec{\mathbf{r}},E'\to E,\hat{\Omega}'\cdot\hat{\Omega})\psi_p(\vec{\mathbf{r}},E',\hat{\Omega}')\\
&\quad+\int_0^\infty dE'\int_{4\pi}d\hat{\Omega}'\sigma_{e\to p}(\vec{\mathbf{r}},E'\to E,\hat{\Omega}'\cdot\hat{\Omega})\psi_e(\vec{\mathbf{r}},E',\hat{\Omega}')\\
&\quad+Q_p(\vec{\mathbf{r}},E,\hat{\Omega})\qquad\qquad,\vec{\mathbf{r}}\in D
\end{aligned}\tag{2.3}$$

where

$\psi(\vec{\mathbf{r}},E,\hat{\Omega})$ = angular flux $(particles\ cm^{-2}s^{-1}keV^{-1})$

$\hat{\Omega}$ = particle direction

$\sigma_t(\vec{\mathbf{r}},E)$ = total cross section (cm^{-1})

$\sigma^*_{e\to e}(\vec{\mathbf{r}},E'\to E,\hat{\Omega}'\cdot\hat{\Omega})$ = electron to electron differential scattering and production cross section, where the particle scatters from initial energy E' and initial direction $\hat{\Omega}'$, to final energy E and final direction $\hat{\Omega}$. Does not include soft inelastic interactions, which are treated by the CSD operator $(cm^{-1}keV^{-1}str^{-1})$

$\sigma_{p\to e}(\vec{\mathbf{r}},E'\to E,\hat{\Omega}'\cdot\hat{\Omega})$ = photon to electron differential scattering cross section $(cm^{-1}keV^{-1}str^{-1})$

$\sigma_{p\to p}(\vec{\mathbf{r}},E'\to E,\hat{\Omega}'\cdot\hat{\Omega})$ = photon to photon differential scattering cross section $(cm^{-1}keV^{-1}str^{-1})$

$\sigma_{e\to p}(\vec{\mathbf{r}},E'\to E,\hat{\Omega}'\cdot\hat{\Omega})$ = electron to photon differential scattering cross section $(cm^{-1}keV^{-1}str^{-1})$

$R_e(\vec{\mathbf{r}},E)$ = electron restricted stopping power. Includes only contributions from soft inelastic interactions. $(cm^{-1}keV)$

$Q(\vec{\mathbf{r}},E)$ = distributed angular source $(particles\ cm^{-3}s^{-1}keV^{-1})$

and where subscripts e and p denote electron and photons, respectively. We will use this notation throughout this thesis.

Note the asymmetry which appears in a comparison of the right hand side of the electron equation, Equation (2.2), and the photon equation, Equation (2.3). The electron inelastic interactions (both collisional and radiative) are divided into two classes: "catastrophic" interactions that result in large energy losses, treated by the Boltzmann operator, and "soft" interactions that result in small energy losses, treated by the CSD operator. The cumulative effect of many soft interactions may be approximated by the continuous energy loss of an electron without angular deflection. This is the restricted slowing down or continuous slowing down approximation, and is represented in the electron equation, Equation (2.2), by the term containing the restricted stopping power.

The transport equations, Equations (2.2) and (2.3), physically express the fact that the rate at which particles, in the differential phase space volume associated with position $\vec{\mathbf{r}}$, direction $\hat{\Omega}$, and energy E, leave the volume due to leakage and collisions is equal to the rate at which they enter the volume by scattering or by a prescribed distributed source. These linear equations are valid in a physical regime in which there are no external electric or magnetic fields and the density of transporting particles is much less than the density of target atoms. It is this later restriction, the neglect of particle - particle interaction, which leads to linearity.

In addition to Equations (2.2) and (2.3), the angular flux entering the volume D, through the surface Γ, must be specified. We consider three types of boundary conditions: prescribed incoming source, vacuum, and reflective. The *prescribed incoming*

source boundary condition is given by the equation

$$\psi(\vec{\mathbf{r}}, E, \hat{\Omega}) = \psi^b(\vec{\mathbf{r}}, E, \hat{\Omega}) \qquad , \hat{\Omega} \cdot \hat{n} < 0, \vec{\mathbf{r}} \in \Gamma \tag{2.4}$$

where $\hat{n}$ is the unit outward normal vector to the surface Γ, and $\psi^b(\vec{\mathbf{r}}, E, \hat{\Omega})$ is a specified function. The case in which $\psi^b(\vec{\mathbf{r}}, E, \hat{\Omega})$ is zero is referred to as the *vacuum boundary condition*

$$\psi(\vec{\mathbf{r}}, E, \hat{\Omega}) = 0 \qquad , \hat{\Omega} \cdot \hat{n} < 0, \vec{\mathbf{r}} \in \Gamma \tag{2.5}$$

If there exists a plane of symmetry in the problem, the *reflective boundary condition* may be used to exploit this symmetry. At a reflecting boundary the incoming flux, along direction $\hat{\Omega}$, is set equal to the outgoing flux, along direction $\hat{\Omega}'$, where $\hat{\Omega}$ is the mirror reflection of $\hat{\Omega}'$. Specifically, let us consider a plane of symmetry Γ', then the reflecting boundary condition at this plane is given by the equation

$$\psi(\vec{\mathbf{r}}, E, \hat{\Omega}) = \psi(\vec{\mathbf{r}}, E, \hat{\Omega}') \qquad , \hat{\Omega} \cdot \hat{n} < 0, \vec{\mathbf{r}} \in \Gamma' \tag{2.6}$$

where

$$\hat{n} \cdot \hat{\Omega} = -\hat{n} \cdot \hat{\Omega}' \tag{2.7}$$

$$(\hat{\Omega} \times \hat{\Omega}') \cdot \hat{n} = 0 \tag{2.8}$$

We now define the *scalar flux*

$$\phi(\vec{\mathbf{r}}, E) = \frac{1}{4\pi} \int_{4\pi} d\hat{\Omega} \psi(\vec{\mathbf{r}}, E, \hat{\Omega}) \tag{2.9}$$

and the *current*

$$\vec{\mathbf{J}}(\vec{\mathbf{r}}, E) = \frac{1}{4\pi} \int_{4\pi} d\hat{\Omega} \hat{\Omega} \psi(\vec{\mathbf{r}}, E, \hat{\Omega}) \tag{2.10}$$

In this thesis we will consider two geometries to describe our space - angle coordinate system, Cartesian and cylindrical.

In Cartesian coordinates $\vec{\mathbf{r}} = (u_1, u_2, u_3) = (x, y, z)$, Figure 2.1, the streaming operator may be written as

$$\hat{\Omega} \cdot \vec{\nabla} \psi(\vec{\mathbf{r}}, E, \hat{\Omega}) = \mu \frac{\partial}{\partial x} \psi + \eta \frac{\partial}{\partial y} \psi + \xi \frac{\partial}{\partial z} \psi \tag{2.11}$$

where the direction cosines are defined as

$$\mu = \hat{\Omega} \cdot \hat{e}_1, \ \eta = \hat{\Omega} \cdot \hat{e}_2, \ \xi = \hat{\Omega} \cdot \hat{e}_3 \tag{2.12}$$

For the cylindrical coordinate system $\vec{\mathbf{r}} = (u_1, u_2, u_3) = (r, \theta, z)$, Figure 2.3, the streaming operator [6] is given by

$$\hat{\Omega} \cdot \vec{\nabla} \psi(\vec{\mathbf{r}}, E, \hat{\Omega}) = \mu \frac{\partial}{\partial r} \psi + \frac{\eta}{r} \frac{\partial}{\partial \theta} \psi + \xi \frac{\partial}{\partial z} \psi \tag{2.13}$$

with the direction cosines defined in Equation (2.12).

2.3 The Boltzmann Transport Equations

Cross sections for the SP_N method developed in this thesis will be generated by the code CEPXS [7]. Particle interactions included in CEPXS are listed in Table 2.1. Here we do not consider the actual models, but instead refer the interested reader to the literature [7].

Table 2.1: CEPXS Interactions

$e^- \rightarrow e^-$	collisional scattering, bremsstrahlung, Auger production following impact ionization
$e^- \rightarrow \gamma$	bremsstrahlung, relaxation radiation following impact ionization
$\gamma \rightarrow \gamma$	Compton scattering, relaxation radiation following photoionization
$\gamma \rightarrow e^-$	photoelectric effect, Compton scattering, pair production, Auger production following photoionization
$\gamma \rightarrow e^+$	pair production
$e^+ \rightarrow e^+$	collisional scattering, bremsstrahlung
$e^+ \rightarrow \gamma$	bremsstrahlung, pair annihilation, relaxation radiation following impact ionization
$e^+ \rightarrow e^-$	impact ionization, Auger production following impact ionization

CEPXS produces a special "pseudo" cross section for electron to electron scattering, which effectively lumps the continuous slowing down operator [8] in Equation (2.2), together with the previously defined electron to electron differential scattering cross section, $\sigma^*_{e\to e}$, which did not include the soft inelastic interactions. To facilitate the use of these cross sections, the Boltzmann - CSD equations, Equations (2.2) and (2.3), must be placed in a symmetric form, the *Boltzmann transport equations*, where the Boltzmann operator in the electron equation now effectively includes the CSD operator. The *Boltzmann transport equations* are given by

$$\begin{aligned}
&\hat{\Omega}\cdot\vec{\nabla}\psi_e(\vec{\mathbf{r}},E,\hat{\Omega})+\sigma_{te}(\vec{\mathbf{r}},E)\psi_e(\vec{\mathbf{r}},E,\hat{\Omega})\\
&\quad=\int_0^\infty dE'\int_{4\pi}d\hat{\Omega}'\sigma_{e\to e}(\vec{\mathbf{r}},E'\to E,\hat{\Omega}'\cdot\hat{\Omega})\psi_e(\vec{\mathbf{r}},E',\hat{\Omega}')\\
&\quad+\int_0^\infty dE'\int_{4\pi}d\hat{\Omega}'\sigma_{p\to e}(\vec{\mathbf{r}},E'\to E,\hat{\Omega}'\cdot\hat{\Omega})\psi_p(\vec{\mathbf{r}},E',\hat{\Omega}')\\
&\quad+Q_e(\vec{\mathbf{r}},E,\hat{\Omega})\qquad\qquad,\vec{\mathbf{r}}\in D
\end{aligned}\tag{2.14}$$

$$\begin{aligned}
&\hat{\Omega}\cdot\vec{\nabla}\psi_p(\vec{\mathbf{r}},E,\hat{\Omega})+\sigma_{tp}(\vec{\mathbf{r}},E)\psi_p(\vec{\mathbf{r}},E,\hat{\Omega})\\
&\quad=\int_0^\infty dE'\int_{4\pi}d\hat{\Omega}'\sigma_{p\to p}(\vec{\mathbf{r}},E'\to E,\hat{\Omega}'\cdot\hat{\Omega})\psi_p(\vec{\mathbf{r}},E',\hat{\Omega}')\\
&\quad+\int_0^\infty dE'\int_{4\pi}d\hat{\Omega}'\sigma_{e\to p}(\vec{\mathbf{r}},E'\to E,\hat{\Omega}'\cdot\hat{\Omega})\psi_e(\vec{\mathbf{r}},E',\hat{\Omega}')\\
&\quad+Q_p(\vec{\mathbf{r}},E,\hat{\Omega})\qquad\qquad,\vec{\mathbf{r}}\in D
\end{aligned}\tag{2.15}$$

Physical quantities are defined as before, with the exception of the electron to electron differential scattering cross section, which now includes an approximation to the soft inelastic interaction [7].

The electron equation, Equation (2.14), is now of the same form as the photon equation, Equation (2.15). That is, an invariance exists between the equations under

the transformation ($e \rightarrow p$, $p \rightarrow e$). This symmetry will allow us to use one discrete equation to represent all particle species, provided the cross sections are structured in an appropriate manner. We will return to this point in Chapter 5 when we derive the multigroup equations.

We note CEPXS also has the capability to generate cross sections for positrons, as well as electrons and photons, for the final cross section set. The consideration of positrons would involve including a third Boltzmann - CSD equation in the set, Equations (2.2) and (2.3), to represent the positrons and an update of the scattering operators to include positron to electron and positron to photon interactions. In our applications, the energy range is such that the production of positrons, via pair production ($E_\gamma > 1.02 MeV$), is a rare event. Hence, we will not consider positrons in this thesis. To summarize, the solution of the Boltzmann equations, Equations (2.14) and (2.15), with CEPXS generated cross sections effectively represents the solution of the Boltzmann - CSD equation for electrons and the the solution of the Boltzmann equation for photons.

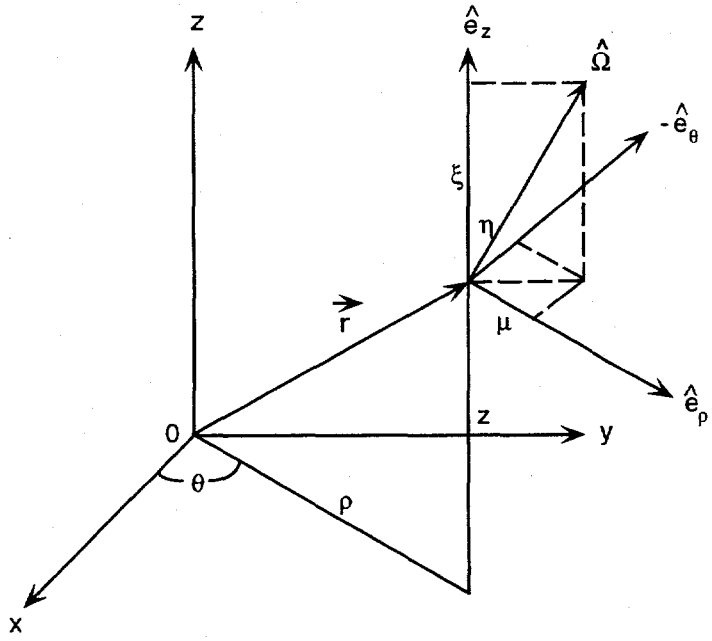

Figure 2.3: Cylindrical Space-Angle Coordinate System

Chapter 3

Numerical Methods of Solution for the Transport Equation

3.1 Introduction

In Chapter 2 we defined the continuous Boltzmann transport equation. One of our objectives is to develop accurate numerical methods for solving the *Simplified Spherical Harmonic approximation* (SP_N method) to the transport equation. However, before we formulate the SP_N method, we must first examine the discretization of the angular variable for the continous Boltzmann equation. We begin in section 3.2 by introducing the *Discrete Ordinates* or S_N method. We then formulate, section 3.3, an alternate approach, the *Spherical Harmonics* or P_N method. We conclude, section 3.4, with a discussion of the equivalence between S_N and P_N methods which exists only for the special case of one dimensional slab geometry. Both the S_N and P_N equations will be used in the derivation of the SP_N equations given in Chapter 4.

3.2 The Discrete Ordinates Method

Let us consider a general transport equation, where for simplicity in notation we have omitted the reference to particle type

$$\hat{\Omega} \cdot \vec{\nabla}\psi(\vec{\mathbf{r}}, E, \hat{\Omega}) + \sigma_t(\vec{\mathbf{r}}, E)\psi(\vec{\mathbf{r}}, E, \hat{\Omega}) =$$
$$\frac{1}{4\pi}\int_0^\infty dE' \int_{4\pi} d\hat{\Omega}'\sigma_s(\vec{\mathbf{r}}, E' \to E, \hat{\Omega}' \cdot \hat{\Omega})\psi(\vec{\mathbf{r}}, E', \hat{\Omega}') + Q(\vec{\mathbf{r}}, E, \hat{\Omega})$$
$$, \vec{\mathbf{r}} \in D \qquad (3.1)$$

In the *Discrete Ordinates* or S_N method [2], we represent the angular variable, $\hat{\Omega}$, by a discrete set of directions or *ordinates* $\hat{\Omega}_n$, where $n = 1, 2, \ldots, N$. We represent functions of $\hat{\Omega}$ by their values at each of the ordinates

$$f(\hat{\Omega}_n) \equiv f_n \qquad , n = 1, 2, \ldots, N \tag{3.2}$$

and we approximate integrals over $\hat{\Omega}$ as a summation over n

$$\frac{1}{4\pi} \int_{4\pi} f(\hat{\Omega}) d\hat{\Omega} \cong \sum_{n=1}^{N} f(\hat{\Omega}_n) w_n \tag{3.3}$$

where the w_n are the *quadrature weights*, and the set of variables $\{\hat{\Omega}_n | w_n\}$ is termed the *quadrature set.*

Frequently one encounters a one dimensional problem, in which case the angular variable reduces to the single directional cosine μ_n, n = 1, 2,..., N. We impose the following requirements on the quadrature set

1. N is an even integer
2. $w_n > 0$ and $\sum_{n=1}^{N} w_n = 1$.
3. The ordinates are symmetric about $\mu = 0$

$$\left.\begin{aligned} &\mu_n > 0 \\ &\mu_{N+1-n} = -\mu_n \\ &w_{N+1-n} = w_n \end{aligned}\right\} \quad n = 1, 2, \ldots, N/2 \tag{3.4}$$

Property one assigns equal importance to right and left particle flows and avoids ambiguities in the boundary condition that arises at $\mu = 0$ when N is odd. Even with

the restrictions imposed by Equations (3.4), substantial freedom remains in choosing a quadrature set. For our purposes we choose the *Gauss - Legendre* quadrature set defined and discussed in section 3.3. The scalar flux is then given as

$$\phi(\vec{\mathbf{r}}, E) = \sum_{n=1}^{N} \psi_n(\vec{\mathbf{r}}, E) w_n \tag{3.5}$$

and the current as

$$\vec{\mathbf{J}}(\vec{\mathbf{r}}, E) = \sum_{n=1}^{N} \hat{\Omega}_n \psi_n(\vec{\mathbf{r}}, E) w_n \tag{3.6}$$

Introducing Equations (3.2) and (3.3) into Equation (3.1), we obtain the discrete ordinates or S_N approximation to the continuous transport equation. The discrete ordinates approximation is given by the following coupled set of N equations

$$\hat{\Omega}_n \cdot \vec{\nabla} \psi_n(\vec{\mathbf{r}}, E) + \sigma_t(\vec{\mathbf{r}}, E) \psi_n(\vec{\mathbf{r}}, E) =$$
$$\sum_{n'=1}^{N} w_{n'} \int_0^{\infty} dE' \sigma_s(\vec{\mathbf{r}}, E' \rightarrow E, \hat{\Omega}_{n'} \cdot \hat{\Omega}_n) \psi_{n'}(\vec{\mathbf{r}}, E') + Q_n(\vec{\mathbf{r}}, E)$$
$$, \vec{\mathbf{r}} \in D, n = 1, 2, \ldots, N \tag{3.7}$$

with vacuum boundary conditions represented as

$$\psi_n(\vec{\mathbf{r}}, E) = 0 \qquad , \hat{\Omega}_n \cdot \hat{n} < 0, \vec{\mathbf{r}} \in \Gamma \tag{3.8}$$

and reflective boundary conditions as

$$\psi_n(\vec{\mathbf{r}}, E) = \psi_{n'}(\vec{\mathbf{r}}, E) \qquad , \hat{\Omega}_n \cdot \hat{n} < 0, \vec{\mathbf{r}} \in \Gamma' \tag{3.9}$$

where

$$\hat{n} \cdot \hat{\Omega}_n = -\hat{n} \cdot \hat{\Omega}_{n'} \tag{3.10}$$

$$(\hat{\Omega}_n \times \hat{\Omega}_{n'}) \cdot \hat{n} = 0 \tag{3.11}$$

where Γ' is the surface at which the reflective boundary condition exists, $\hat{n}$ is a normal to the surface, and $\hat{\Omega}_n$ is the direction corresponding to spectral reflection of $\hat{\Omega}_{n'}$ at Γ'.

The discrete ordinates method is a widely used method of analysis. It however, suffers from non-physical anomalies, called ray effects [2, 9], which arise in the scalar flux when there is little scattering and localized sources. These ray effects arise from the fact that particles effectively travel in a finite set of discrete directions rather than in a continuum of directions. In most cases ray effects may be reduced by increasing the order N of the S_N calculation. This, however, may be costly in terms of computational effort required. While a higher order S_N calculation will reduce ray effects, this will not eliminate them altogether. This can only be accomplished [9] if one applies a method that has rotational invariance, such as the *Spherical Harmonics* or P_N method.

3.3 The Spherical Harmonics Method

The *Spherical Harmonics* or P_N method [2, 3] is based upon the expansion of the angular dependence of the angular flux in a finite series of spherical harmonic functions. These spherical harmonics [10], $Y_{lm}(\hat{\Omega})$, form a complete set of orthogonal

functions on the unit sphere and are defined as

$$Y_{lm}(\hat{\Omega}) = Y_{lm}(\theta,\phi) = \sqrt{\frac{(2-\delta_{m,0})(l-m)!}{(l+m)!}} P_{lm}(\mu)\exp(im\phi) \tag{3.12}$$

where $\mu \equiv \cos\theta$, l is a non-negative integer $l = 0, 1, \ldots, -l \leq m \leq l$, and $P_{lm}(\mu)$ are the *associated Legendre functions* defined for non-negative integer values $m = 0, 1, \ldots, l$ by

$$P_{lm}(\mu) = (-1)^m (1-\mu^2)^{m/2} \frac{d^m}{d\mu^m} P_l(\mu) \tag{3.13}$$

and the negative integer values $m = -1, -2, \ldots, -l$ by

$$P_{l-m}(\mu) = (-1)^m \frac{(l-m)!}{(l+m)!} P_{lm}(\mu) \tag{3.14}$$

and the functions $P_l(\mu)$ are the *Legendre polynomials.* To avoid the use of complex functions, we introduce the *modified spherical harmonic functions* defined as the linear combinations

$$\tilde{Y}_{lm} = \begin{cases} \frac{1}{2}[Y_{lm} + Y_{lm}^*] & , m \geq 0 \\ (-1)^{|m|}\frac{i}{2}[Y_{lm} - Y_{lm}^*] & , m < 0 \end{cases} \tag{3.15}$$

or

$$\tilde{Y}_{lm} = \begin{cases} c_{lm} P_{lm}(\mu)\cos(m\phi) & , m \geq 0 \\ c_{lm} P_{l|m|}(\mu)\sin(|m|\phi) & , m < 0 \end{cases} \tag{3.16}$$

where

$$c_{lm} \equiv \sqrt{\frac{(2-\delta_{m,0})(l-|m|)!}{(l+|m|)!}} \tag{3.17}$$

Since the spherical harmonics form a complete set, we may express the angular flux as

$$\psi(\vec{\mathbf{r}}, E, \hat{\Omega}) = \sum_{l=0}^{\infty} \sum_{m=-l}^{l} (2l+1)\phi_{lm}(\vec{\mathbf{r}}, E)\tilde{Y}_{lm}(\hat{\Omega}) \tag{3.18}$$

In the P_N approximation, this infinite series is replaced with a finite series with $l = 0, 1, \ldots, N$. Now using the orthogonality relation

$$\frac{1}{4\pi} \int d\hat{\Omega} \tilde{Y}_{l'm'}(\hat{\Omega}) \tilde{Y}_{lm}(\hat{\Omega}) = \frac{\delta_{l'l} \delta_{m'm}}{(2l+1)} \tag{3.19}$$

where

$$\delta_{mn} = \begin{cases} 1 & m = n \\ 0 & \text{otherwise} \end{cases} \tag{3.20}$$

We define the expansion coefficients or flux moments, $\phi_{lm}(\vec{\mathbf{r}}, E)$, as

$$\phi_{lm}(\vec{\mathbf{r}}, E) = \frac{1}{4\pi} \int d\hat{\Omega} \tilde{Y}_{lm}(\hat{\Omega}) \psi(\vec{\mathbf{r}}, E, \hat{\Omega}) \tag{3.21}$$

For computational purposes it is customary to expand the differential scattering cross section, in Equation (3.1), in Legendre polynomials

$$\sigma_s(\vec{\mathbf{r}}, E' \rightarrow E, \mu_0) = \sum_{l=0}^{\infty} (2l+1) \sigma_{sl}(\vec{\mathbf{r}}, E' \rightarrow E) P_l(\mu_0) \tag{3.22}$$

where $\mu_0 \equiv \hat{\Omega} \cdot \hat{\Omega}'$ is the cosine of the scattering angle in the laboratory system. Using the orthogonality of the Legendre polynomials

$$\frac{1}{2} \int_{-1}^{1} d\mu P_m(\mu) P_n(\mu) = \frac{\delta_{mn}}{2m+1} \tag{3.23}$$

we define the scattering moments

$$\sigma_{sl}(\vec{\mathbf{r}}, E' \rightarrow E) = \frac{1}{2} \int_{-1}^{1} d\mu_0 \sigma_s(\vec{\mathbf{r}}, E' \rightarrow E, \mu_0) P_l(\mu_0) \tag{3.24}$$

It is useful at this point to review some properties of the Legendre polynomials [6,

10]. The first few Legendre polynomials are given as

$$P_0(\mu) = 1 \tag{3.25}$$

$$P_1(\mu) = \mu \tag{3.26}$$

$$P_2(\mu) = \frac{1}{2}(3\mu^2 - 1) \tag{3.27}$$

Legendre polynomials satisfy the recursion relation

$$\mu P_n(\mu) = \frac{n}{2n+1} P_{n-1}(\mu) + \frac{n+1}{2n+1} P_{n+1}(\mu) \tag{3.28}$$

and the spherical harmonic addition theorem

$$P_l(\hat{\Omega} \cdot \hat{\Omega}') = P_l(\mu) P_l(\mu') + 2 \sum_{m=1}^{l} \frac{(l-m)!}{(l+m)!} P_l^m(\mu) P_l^m(\mu') \cos[m(\phi - \phi')] \tag{3.29}$$

We may now express the integral scattering operator in Equation (3.1) in terms of the Legendre flux and cross section moments using Equations (3.21), (3.22), and (3.29). For one dimensional slab geometry, the resultant form of the scattering operator is given by the equation

$$q_s(z, E, \mu) = \sum_{l=0}^{\infty} (2l+1) P_l(\mu) \int_0^{\infty} dE' \sigma_{sl}(z, E' \rightarrow E) \phi_l(z, E') \tag{3.30}$$

where

$$\phi_l(z, E) = \frac{1}{2} \int_{-1}^{1} d\mu P_l(\mu) \psi(z, E, \mu) \tag{3.31}$$

To find the general form of the P_N equations, we substitute Equations (3.18), with the series terminated at $l = N$, and the scattering operator expansion into the continuous transport equation (3.1). We then multiply by a spherical harmonic of different order,

$\tilde{Y}_{l'm'}(\hat{\Omega})$, integrate over $\hat{\Omega}$, and utilize orthogonality. Boundary conditions are derived from the continuous transport equation in a similar manner. It is this coupled set of equations for the expansion coefficients that is referred to as the P_N *equations*. Since these equations are quite complicated for general geometries, we refer the interested reader to the literature [11] for the general form. For our purposes we need only consider the one dimensional P_N equations.

In one dimensional slab geometry an expansion in spherical harmonics reduces to an expansion in Legendre polynomials. In this case the 1 - D slab geometry P_N equations are given as

$$\frac{n+1}{2n+1}\frac{\partial}{\partial z}\phi_{n+1}(z,E) + \frac{n}{2n+1}\frac{\partial}{\partial z}\phi_{n-1}(z,E) + \sigma_t(z,E)\phi_n(z,E) = \int_0^\infty dE'\sigma_{sn}(z,E'\rightarrow E)\phi_n(z,E') + Q_n(z,E) \qquad ,n = 0,\ 1,\ldots,\ N \tag{3.32}$$

where

$$\phi_{N+1} = 0 \tag{3.33}$$

Since the P_N approximation consists of $N+1$ first order differential equations, $N+1$ boundary conditions are required. Odd order N is used, to permit $(N+1)/2$ conditions at each of the left and right boundaries. Reflective boundary conditions, at the boundary $x = x_0$, are represented by

$$\psi(x_0,\mu) = \psi(x_0,-\mu) \tag{3.34}$$

which translates to

$$\phi_l(x_0) = 0 \qquad ,l = 1,3,\ldots,N \tag{3.35}$$

Vacuum boundary conditions, for example at the right boundary of the slab, are given by

$$\psi(x_0, \mu) = 0 \qquad , -1 \leq \mu < 0 \tag{3.36}$$

This condition cannot be satisfied exactly by a finite order Legendre expansion. Two sets of boundary conditions have been devised to satisfy this condition approximately. Mark boundary conditions are given by

$$\psi(x_0, \mu_n) = 0 \qquad , n = 1, 2, \ldots, (N+1)/2 \tag{3.37}$$

where the values μ_n are given as

$$P_{N+1}(\mu_n) = 0 \tag{3.38}$$

Equation (3.38) is satisfied by the *Gauss - Legendre* quadrature cosines, defined in section 3.3. Marshak boundary conditions are given by

$$\int_{-1}^{0} d\mu P_l(\mu)\psi(x_0, \mu) = 0 \qquad , l = 1, 3, \ldots, N \tag{3.39}$$

This condition has the advantage of setting the incoming current of particles at the boundary equal to zero.

We conclude this discussion with some important properties of the P_N approximation. The P_N method is convergent as N approaches infinity, that is, we obtain the exact transport solution as N approaches infinity. For an order N calculation there are order $(N+1)^2$ unknowns in two dimensional and three dimensional geometries, and order $(N+1)$ unknowns in one dimension. The fact that electron scattering is highly anisotropic requires a high order expansion ($P_7 - P_{15}$) in calculations of interest

to us. Finally, the P_N equations are rotationally invariant, and hence do not produce ray effects.

3.4 The Equivalence between Discrete Ordinates and the Legendre Equations

Let us examine the relationship between the discrete ordinates S_N approximation and the spherical harmonic P_{N-1} approximation. We will show an equivalence exists only in one dimensional slab geometry, provided we restrict our choice of quadrature sets. For brevity, we limit our discussion to a monoenergetic problem. The one dimensional slab geometry S_N equations with P_{N-1} cross section expansion are given by

$$\mu_n \frac{\partial}{\partial x}\psi_n(x) + \sigma_t(x)\psi_n(x) = \sum_{l=0}^{N-1}(2l+1)\sigma_{sl}(x)\phi_l(x)P_l(\mu_n) + Q_n(x) \qquad ,n = 1,2,\ldots,N \quad (3.40)$$

where

$$\phi_l(x) = \sum_{n=1}^{N}\psi_n(x)P_l(\mu_n)w_n \quad (3.41)$$

we write the P_{N-1} approximation to the angular flux as

$$\psi_n(x) = \sum_{l=0}^{N-1}(2l+1)\phi_l(x)P_l(\mu_n) \qquad ,n = 1,2,\ldots,N \quad (3.42)$$

It may be shown [2, 3] that by taking Legendre moments of Equation (3.40), that is, operating by $\sum_{n=1}^{N} w_n P_{l'}(\mu_n)$, we obtain the P_{N-1} equations, provided that we place the following restrictions upon the quadrature set:

1. For an order N S_N or P_{N-1} calculation, the ordinates μ_n are the zeros of the the Nth order Legendre polynomial

$$P_N(\mu_n) = 0 \qquad , n = 1,\ 2, \ldots,\ N \tag{3.43}$$

2. The quadrature integrates the polynomials P_0 through P_{2N-1} exactly

$$\sum_{n=1}^{N} w_n P_l(\mu_n) = \delta_{l0} \qquad , l = 0,\ 1, \ldots,\ 2N-1 \tag{3.44}$$

Equations (3.43) and (3.44) specify the *Gauss - Legendre* quadrature set. The equivalence between the Gauss-S_N approximation and the Legendre P_{N-1} approximation in one dimensional slab geometry will be used in the derivation of the cannonical form of the SP_N equations in Chapter 4.

Chapter 4

The Simplified Spherical Harmonics Approximation

4.1 Introduction

The *Simplified P_N (SP_N) method* is an approximation method used to treat the angular variable. As mentioned in Chapter 1, the SP_N equations were originally proposed by Gelbard [12–14] for application to neutron transport problems. This method has been shown to produce approximate transport solutions which are significantly more accurate than diffusion theory, but significantly less expensive than discrete ordinates (S_N) or full P_N methods. The SP_N method has never before been applied to charged particle transport problems.

In this chapter we first derive the SP_N equations, section 4.2.1, using the original technique of Gelbard, and examine the characteristics of these equations in contrast with the S_N and P_N methods. We then briefly discuss, section 4.2.2, a recently developed asymptotic derivation that lends mathematical rigor to the SP_N approximation. We conclude, section 4.3, with a derivation of the canonical form of the SP_N equations, an alternate formulation which permits the application of efficient numerical solution and acceleration techniques.

4.2 The Standard SP_N Equations

4.2.1 Conventional Derivation

Let us consider the one dimensional slab geometry P_N equations

$$\frac{n+1}{2n+1}\frac{\partial}{\partial z}\phi_{n+1} + \frac{n}{2n+1}\frac{\partial}{\partial z}\phi_{n-1} + \sigma_t(z,E)\phi_n(z,E) = \int_0^\infty dE'\sigma_{sn}(z,E'\rightarrow E)\phi_n(z,E') + Q_n(z,E) \quad ,n = 0,\ 1,\ldots,\ N \tag{4.1}$$

where ϕ_n is the nth Legendre moment of the angular flux, and Q_n is the nth Legendre moment of the distributed source

$$\phi_n(z,E) = \frac{1}{2}\int_{-1}^{1} d\mu P_n(\mu)\psi(z,E,\mu) \tag{4.2}$$

$$Q_n(z,E) = \frac{1}{2}\int_{-1}^{1} d\mu P_n(\mu)Q(z,E,\mu) \tag{4.3}$$

Note that ϕ_{N+1}, which appears in Equation (4.1) when $n = N$, is defined to be zero. This produces a system of $N+1$ equations with $N+1$ unknowns.

Comparing the one dimensional P_1 equations, given by Equations (4.1) with N=1, with the three dimensional P_1 equations we may define a procedure [15] that produces the three dimensional P_1 equations from the one dimensional P_1 equations:

1. Consider the zeroth order flux moment ϕ_0, and zeroth order source moment Q_0, as scalars.

2. Consider the first order flux moment ϕ_1, and first order source moment Q_1, as vectors.

3. Replace the operator $\frac{\partial}{\partial z}$ in the one dimensional $n = 0$ equation with the divergence operator $\vec{\nabla}\cdot$.

4. Replace the operator $\frac{\partial}{\partial z}$ in the one dimensional $n = 1$ equation with the gradient operator $\vec{\nabla}$.

The derivation of the SP_N equations is motivated by this observation. Specifically, we generalize the procedure to obtain the three dimensional SP_N equations from the one dimensional P_N equations:

1. Consider the even order flux moments ϕ_l, and even order source moments Q_l, as scalars.

2. Consider the odd order flux moments ϕ_l, and odd order source moments Q_l, as vectors.

3. Replace the operator $\frac{\partial}{\partial z}$ in the one dimensional even n equations with the divergence operator $\vec{\nabla}\cdot$.

4. Replace the operator $\frac{\partial}{\partial z}$ in the one dimensional odd n equations with the gradient operator $\vec{\nabla}$.

Carrying out this procedure, we obtain

$$\frac{n+1}{2n+1}\vec{\nabla}\cdot\vec{\phi}_{n+1}(\vec{\mathbf{r}},E)+\frac{n}{2n+1}\vec{\nabla}\cdot\vec{\phi}_{n-1}(\vec{\mathbf{r}},E)$$
$$+\sigma_t(\vec{\mathbf{r}},E)\phi_n(\vec{\mathbf{r}},E)=\int_0^\infty dE'\sigma_{sn}(\vec{\mathbf{r}},E'\rightarrow E)\phi_n(\vec{\mathbf{r}},E')+Q_n(\vec{\mathbf{r}},E)$$
$$,n=0,\ 2,\ldots,\ N-1 \qquad (4.4)$$

$$\frac{n+1}{2n+1}\vec{\nabla}\phi_{n+1}(\vec{\mathbf{r}},E)+\frac{n}{2n+1}\vec{\nabla}\phi_{n-1}(\vec{\mathbf{r}},E)$$
$$+\sigma_t(\vec{\mathbf{r}},E)\vec{\phi}_n(\vec{\mathbf{r}},E)=\int_0^\infty dE'\sigma_{sn}(\vec{\mathbf{r}},E'\rightarrow E)\vec{\phi}_n(\vec{\mathbf{r}},E)+\vec{\mathbf{Q}}_n(\vec{\mathbf{r}},E)$$
$$,n=1,\ 3,\ldots,\ N \qquad (4.5)$$

where ϕ_{N+1}, which appears in Equation (4.5) when $n = N$, is defined to be zero. This closes the system of equations yielding $(N + 1)/2$ scalar equations and scalar unknowns, and $(N + 1)/2$ vector equations and vector unknowns. Equations (4.4) and (4.5) are known as the *simplified P_N equations*.

Since this procedure is exact for the P_1 equations, it follows that the P_1 and SP_1 equations are identical in all geometries. However, an equivalence does not exist for $N > 1$; that is, the SP_N equations differ from the P_N equations for $N > 1$ in two dimensional and three dimensional geometries. In one dimensional slab geometry SP_N and P_N are identical.

It is noted that for two dimensional or three dimensional geometries, the SP_N equations have order $(N+1)$ unknowns, in contrast to the P_N equations, which contain order $(N + 1)^2$, thereby offering tremendous computational savings when N is large. The condition of N large will always be met in electron transport, since an accurate representation of highly anisotropic electron scattering requires high order flux and cross section expansions. The SP_N equations maintain the rotational invariance of the P_N approximation, and hence ray effects do not appear in the solution. However, due to the asymptotic nature of the SP_N method the exact transport solution is not necessarily obtained as N approaches infinity.

4.2.2 The Diffusion Limit and an Asymptotic Derivation

There is actually no intrinsic mathematical justification for the traditional derivation of the SP_N equations. However, it has recently been shown [1] that the SP_N equations can be derived via a rigorous asymptotic expansion of the transport equation. In this section we will only briefly outline the procedure; the interested reader is referred to the above references.

Let us begin by considering a system which is optically thick, and where scattering dominates; that is, one where there is little absorption. This can be represented by the scaling

$$\Sigma_t(\vec{\mathbf{r}}) = \frac{\sigma_t(\vec{\mathbf{r}})}{\epsilon} \tag{4.6}$$

$$\Sigma_{sn}(\vec{\mathbf{r}}) = \frac{\sigma_{sn}(\vec{\mathbf{r}})}{\epsilon} \tag{4.7}$$

$$Q(\vec{\mathbf{r}}) = \epsilon q(\vec{\mathbf{r}}) \tag{4.8}$$

where $\epsilon << 1$. Equations (4.6)-(4.8) characterize a class of problems known as diffusive. The scaling is introduced into the the continuous transport equation and the equation is operated upon by $\hat{P}$ and $(\hat{I} - \hat{P})$ where the operator $\hat{P}$ is defined as

$$\hat{P}\psi(\vec{\mathbf{r}}, E, \hat{\Omega}) = \frac{1}{4\pi}\int_{4\pi} d\hat{\Omega}\psi(\vec{\mathbf{r}}, E, \hat{\Omega}) \tag{4.9}$$

and $\hat{I}$ is the identity operator. After much operator algebra, the authors arrive at a sixth order partial differential equation for the scalar flux, asymptotically equivalent to the transport equation with $O(\epsilon^7)$ error. If terms of $O(\epsilon^3)$ are ignored, the SP_1 equations are obtained. If terms of $O(\epsilon^5)$ are ignored, the SP_2 equations are obtained. Similarly, if terms of $O(\epsilon^7)$ are ignored, the SP_3 equations are obtained. The

expansion may be carried out even further, and higher order SP_N equations may be obtained. Thus, one sees that that the SP_N equations are shown to be an asymptotic approximation to the transport equation in a class of physical problems known as diffusive. That is, the SP_1 equations, or diffusion equation, are the leading order approximation to the transport equation and higher SP_N equations represent higher order corrections to diffusion theory.

4.3 The Canonical Formulation of the SP_N Equations

The SP_N equations can be put in a canonical form [15] that has several advantages relative to the conventional form. Recall, the standard derivation of the SP_N equations, section 4.2.1, began with the one dimensional slab geometry P_N equations. However, it has been demonstrated, section 3.3, that the one dimensional slab geometry P_N equations are equivalent to the one dimensional S_{N+1} equations with Gauss - Legendre quadrature and P_N cross section expansions. We begin with the one dimensional slab geometry S_{N+1} equations

$$\mu_m \frac{\partial}{\partial x}\psi_m(x,E) + \sigma_t(x,E)\psi_m(x,E) = Q_m(x,E) \qquad ,m = 1,2,\ldots,N+1 \quad (4.10)$$

$$Q_m = \sum_{n=0,1}^{N} (2n+1)P_n(\mu_m)\int_0^\infty dE'\sigma_{sn}(x,E'\rightarrow E)\phi_n(x,E') + q_m(x,E) \qquad (4.11)$$

$$\phi_n(x,E) = \sum_{m'=1}^{N+1} P_n(\mu_{m'})\psi_{m'}(x)w_{m'} \qquad \text{,for all } n \qquad (4.12)$$

where m is the angular index, $N+1$ is an even integer, q_m is the angular distributed source, ϕ_n is the angular flux moment, and all other quantities are as previously defined. The quadrature weights sum to unity over the interval $[-1,1]$. Let us now express equation (4.10) in terms of the even and odd parity components of the angular

flux. The even - parity angular flux is defined as

$$\psi^+(\mu_m) = \frac{1}{2}[\psi(\mu_m) + \psi(-\mu_m)] \tag{4.13}$$

and the odd - parity angular flux as

$$\psi^-(\mu_m) = \frac{1}{2}[\psi(\mu_m) - \psi(-\mu_m)] \tag{4.14}$$

Note from Equations (4.13) and (4.14) that

$$\psi^+(-\mu_m) = \psi^+(\mu_m) \tag{4.15}$$

$$\psi^-(-\mu_m) = -\psi^-(\mu_m) \tag{4.16}$$

In the interest of simplifying the notation, we have suppressed the spatial and energy variables. Manipulating Equations (4.10) through (4.14), we obtain the following equivalent equations [16]:

$$\mu_m \frac{\partial}{\partial x}\psi_m^- + \sigma_t \psi_m^+ = Q_m^+ \qquad , m = 1, 2, \ldots, (N+1)/2 \tag{4.17}$$

$$\mu_m \frac{\partial}{\partial x}\psi_m^+ + \sigma_t \psi_m^- = Q_m^- \qquad , m = 1, 2, \ldots, (N+1)/2 \tag{4.18}$$

where

$$Q_m^+ = \sum_{n=0,2}^{N-1} (2n+1) P_n(\mu_m) \int_0^\infty dE' \sigma_n(x, E' \to E) \phi_n(x, E') + q_m^+(x, E) \tag{4.19}$$

$$Q_m^- = \sum_{n=1,3}^{N} (2n+1) P_n(\mu_m) \int_0^\infty dE' \sigma_n(x, E' \to E) \phi_n(x, E') + q_m^-(x, E) \tag{4.20}$$

$$\phi_n = 2 \sum_{m=1}^{(N+1)/2} P_n(\mu_m)\psi_m^+ w_m \qquad \text{,for } n \text{ even} \tag{4.21}$$

$$\phi_n = 2 \sum_{m=1}^{(N+1)/2} P_n(\mu_m)\psi_m^- w_m \qquad \text{,for } n \text{ odd} \tag{4.22}$$

and where q_m^+ and q_m^- are the even - parity and odd - parity angular distributed sources, respectively. These sources are defined in analogy with the even and odd parity angular fluxes, Equations (4.13) and (4.14), and are given by

$$q^+(\mu_m) = \frac{1}{2}[q(\mu_m) + q(-\mu_m)] \tag{4.23}$$

and

$$q^-(\mu_m) = \frac{1}{2}[q(\mu_m) - q(-\mu_m)] \tag{4.24}$$

Note that one need only solve for half of the even - parity and odd - parity fluxes since defining them on either half of the interval $[-1, 1]$ also defines them on the whole interval.

Following the procedure outlined in section 4.2.1, we now obtain a set of SP_N equivalent equations by replacing the operator $\frac{\partial}{\partial z}$ in Equation (4.17) with the divergence operator, and replacing $\frac{\partial}{\partial z}$ in Equation (4.18) with the gradient operator. These equations are given as

$$\mu_m \vec{\nabla} \cdot \vec{\psi}_m^- + \sigma_t \psi_m^+ = Q_m^+ \qquad , m = 1, 2, \ldots, (N+1)/2 \tag{4.25}$$

$$\mu_m \vec{\nabla} \psi_m^+ + \sigma_t \vec{\psi}_m^- = \vec{\mathbf{Q}}_m^- \qquad , m = 1, 2, \ldots, (N+1)/2 \tag{4.26}$$

where

$$Q_m^+ = \sum_{n=0,2}^{N-1} (2n+1) P_n(\mu_m) \int_0^\infty dE' \sigma_n(x, E' \to E) \phi_n(x, E') + q_m^+(x, E) \qquad (4.27)$$

$$\vec{\mathbf{Q}}_m^- = \sum_{n=1,3}^{N} (2n+1) P_n(\mu_m) \int_0^\infty dE' \sigma_n(x, E' \to E) \vec{\phi}_n(x, E') + \vec{\mathbf{q}}_m^-(x, E) \qquad (4.28)$$

$$\phi_n = 2 \sum_{m=1}^{(N+1)/2} P_n(\mu_m) \psi_m^+ w_m \qquad \text{,for } n \text{ even} \qquad (4.29)$$

$$\vec{\phi}_n = 2 \sum_{m=1}^{(N+1)/2} P_n(\mu_m) \vec{\psi}_m^- w_m \qquad \text{,for } n \text{ odd} \qquad (4.30)$$

To obtain a second order form, we then solve Equation (4.26) for the odd parity flux $\vec{\psi}_m^-$

$$\vec{\psi}_m^- = -\frac{\mu_m}{\sigma_t} \vec{\nabla} \psi_m^+ + \frac{1}{\sigma_t} \vec{\mathbf{Q}}_m^- \qquad , m = 1, (N+1)/2 \qquad (4.31)$$

and substitute Equation(4.31) into Equation (4.25) to eliminate $\vec{\psi}_m^-$ and yield

$$-\mu_m^2 \vec{\nabla} \cdot \frac{1}{\sigma_t} \vec{\nabla} \psi_m^+ + \sigma_t \psi_m^+ = Q_m^+ - \mu_m \vec{\nabla} \cdot (\frac{\vec{\mathbf{Q}}_m^-}{\sigma_t}) \qquad , m = 1, (N+1)/2 \qquad (4.32)$$

Equations (4.31) and (4.32), are referred to as the *canonical form of the SP_N equations.*

Boundary conditions for the canonical form are obtained by generalizing the standard one dimensional S_{N+1} boundary conditions. For example, considering only $\mu_m > 0$, the one dimensional incoming source boundary condition at the left face requires

$$\psi(\mu_m) = \psi^+(\mu_m) + \psi^-(\mu_m) = f(\mu_m) \qquad , \mu_m > 0 \qquad (4.33)$$

an incoming source on the right face requires

$$\psi(-\mu_m) = \psi^+(\mu_m) - \psi^-(\mu_m) = f(\mu_m) \qquad , \mu_m > 0 \tag{4.34}$$

In the three dimensional case we generalize the incoming source boundary condition for any any point on the boundary as

$$\psi^+(\mu_m) - \vec{\psi}^-(\mu_m) \cdot \hat{n} = f(\mu_m) \qquad , \mu_m > 0 \tag{4.35}$$

where $\hat{n}$ is the unit outward normal to the surface. Reflective boundary conditions at a surface $x = x_0$

$$\psi(\mu_m) = \psi(-\mu_m) \tag{4.36}$$

are satisfied in the even odd partity formulation by inverting Equations (4.13) and (4.14) and substituting into Equation (4.36) to obtain

$$\psi^-(\mu_m) = 0 \tag{4.37}$$

which translates to the three dimensional boundary condition

$$\vec{\psi}^-(\mu_m) \cdot \hat{n} = 0 \tag{4.38}$$

The main advantages of the canonical form of the SP_N equations are

1. They require a matrix solution only for the even parity flux moments, thereby reducing the number of unknowns by a factor of four (considering the vector nature of the odd parity moments).

2. They represent a self adjoint system of equations which can be spatially discretized to produce a symmetric positive definite coefficient matrix. Efficient, robust numerical techniques exist for solving such matrix equations [17].

3. The fluxes do not become coupled at the boundaries, in contrast to the full coupling that occurs between flux moments for the standard form.

4. Since the left hand side consists of independent diffusion equations, both diffusion discretization and diffusion solution techniques can be directly applied to these equations in conjunction with a source iteration technique.

5. Standard convergence acceleration techniques for the one dimensional even parity S_{N+1} equations [16] can be generalized for application to the canonical form.

For these reasons, we will consider only the canonical form of the SP_N equations throughout the remainder of this thesis.

Chapter 5

Numerical Differencing Schemes for the SP_N Equations

5.1 Introduction

In Chapter 4 we derived the canonical form of the SP_N equations. Recall, the SP_N equations represent an angular approximation to the continuous Boltzmann equation. In this chapter we turn to the discretization of the independent variables, energy and space, in the integrodifferential canonical SP_N equations. We begin, section 5.2, by using the multigroup approximation method to discretize the energy variable and produce the *canonical multigroup SP_N equations.* We then discuss the multigroup-Legendre format for cross sections, and cross section generation for our method using the program CEPXS. A general method of solution is then developed for the multigroup equations. We conclude, section 5.3, with a finite element treatment of the spatial variables in the multigroup equations, and a derivation of appropriate boundary and source conditions.

5.2 Energy Discretization

5.2.1 The Multigroup Equations

The multigroup method is common to virtually all deterministic computational methods and is described in various references [2, 18]. Let us begin with the energy dependent, one dimensional S_{N+1} equations, Equations (4.10) through (4.12)

$$\mu_m \frac{\partial}{\partial x}\psi_m(x,E) + \sigma_t(x,E)\psi_m(x,E) = Q_m(x,E) \qquad ,m = 1,2,\ldots,N+1 \quad (5.1)$$

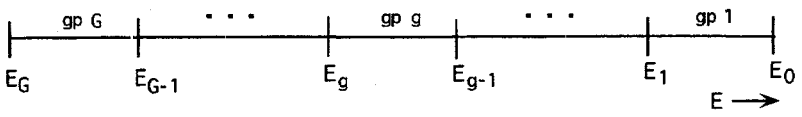

Figure 5.1: Division of the Energy Range into G Energy Groups

where

$$Q_m = \sum_{n=0,1}^{N} (2n+1) P_n(\mu_m) \int_0^\infty dE' \sigma_{sn}(x, E' \to E) \phi_n(x, E') + q_m(x, E) \qquad (5.2)$$

$$\phi_n(x, E) = \sum_{m'=1}^{N+1} P_n(\mu_{m'}) \psi_{m'}(x, E) w_{m'} \qquad \text{,for all } n \qquad (5.3)$$

and the notation is as defined in Chapter 3

To derive the multigroup equations we first divide the energy range into G intervals as shown in Figure 5.1, where $E_G = 0$ and E_0 is sufficiently large that the number of particles at energies greater than E_0 is negligible. Our objective is to discretize the S_{N+1} equations in terms of the group angular flux

$$\psi_{mg}(x) = \int_g dE \psi_m(x, E) \qquad ,m = 1, 2, \ldots, N+1 \qquad (5.4)$$

where for brevity, we introduce the notation

$$\int_g dE \equiv \int_{E_g}^{E_{g-1}} dE \qquad (5.5)$$

We proceed by dividing the energy integral in Equation (5.2) into contributions from

each energy group

$$\int_0^\infty dE' = \sum_{g'=1}^{G} \int_{g'} dE' \tag{5.6}$$

and integrating the S_{N+1} equations over the domain $E_g \leq E < E_{g-1}$, we obtain

$$\mu_m \frac{\partial}{\partial x} \int_g dE \psi_m(x,E) + \int_g dE \sigma_t(x,E)\psi_m(x,E) = \int_g dE Q_m(x,E)$$
$$, m = 1, \ldots, N+1 \tag{5.7}$$

where

$$\int_g dE\, Q_m(x,E) =$$
$$\sum_{n=0,1}^{N} (2n+1) P_n(\mu_m) \int_g dE \int_{g'} dE' \sigma_{sn}(x, E' \rightarrow E)\phi_n(x,E')$$
$$+ \int_g dE\, q_m(x,E) \tag{5.8}$$

We now assume that within each energy group, the angular flux can be separated or expressed as the product of a known function of energy $f(E)$, and the group flux $\psi_{mg}(x)$

$$\psi_m(x,E) \approx f(E)\psi_{mg}(x) \quad , E_g < E \leq E_{g-1} \tag{5.9}$$

similarly, we express the flux moments as

$$\phi_m(x,E) \approx f(E)\phi_{mg}(x) \quad , E_g < E \leq E_{g-1} \tag{5.10}$$

where the spectral weighting function $f(E)$, is normalized by the definition of the

group angular flux, Equation (5.4), to

$$\int_g dE f(E) = 1 \tag{5.11}$$

Next, we define the multigroup cross sections

$$\sigma_{tg}(x) = \int_g dE \sigma_t(x,E) f(E) \tag{5.12}$$

$$\sigma_{n g' \to g}(x) = \int_g dE \int_{g'} dE' \sigma_n(x, E' \to E) f(E') \tag{5.13}$$

and the group distributed source

$$q_{mg}(x) = \int_g dE q_m(x,E) \tag{5.14}$$

Introducing Equations (5.9) and (5.10) into Equations (5.7) and (5.8), and utilizing Equations (5.11) through (5.14) we arrive at the *one dimensional multigroup S_{N+1} equations*, given as

$$\mu_m \frac{\partial}{\partial x} \psi_{mg}(x) + \sigma_{t_g}(x) \psi_{mg}(x) = Q_{mg}(x) \qquad , m = 1, N+1, g = 1, G \tag{5.15}$$

where

$$Q_{mg}(x) = \sum_{j=1}^{G} \sum_{n=0}^{N} (2n+1) P_n(\mu_m) \sigma_{nj \to g} \phi_{nj} + q_{mg} \tag{5.16}$$

$$\phi_{ng} = \sum_{m'=1}^{N+1} P_n(\mu_{m'}) \psi_{m'g} w_{m'} \qquad \text{,for all } n \tag{5.17}$$

where g is the group index, G is the total number of groups, and $\sigma_{nj \to g}$ is the nth Legendre moment of the scattering cross section for scattering from group j to group g.

To produce the canonical multigroup SP_N equations from the multigroup S_{N+1} equations, one proceeds with exactly the same steps, section 4.3, that were used to produce the continuous energy form of the canonical SP_N equations from the continuous S_{N+1} equations. We arrive at the *canonical multigroup SP_N equations*

$$-\mu_m^2 \vec{\nabla} \cdot \frac{1}{\sigma_{tg}} \vec{\nabla} \psi_{mg}^+ + \sigma_{tg} \psi_{mg}^+ = Q_{mg}^+ - \mu_m \vec{\nabla} \cdot \left(\frac{\vec{\mathbf{Q}}_{mg}^-}{\sigma_{tg}} \right)$$
$$, m = 1, (N+1)/2, g = 1, G \tag{5.18}$$

$$\vec{\psi}_{mg}^- = -\frac{\mu_m}{\sigma_{tg}} \vec{\nabla} \psi_{mg}^+ + \frac{1}{\sigma_{tg}} \vec{\mathbf{Q}}_{mg}^-$$
$$, m = 1, (N+1)/2, g = 1, G \tag{5.19}$$

where

$$Q_{mg}^+ = \sum_{j=1}^{G} \sum_{n=0,2,}^{N-1} (2n+1) P_n(\mu_m) \sigma_{n,j \to g} \phi_{nj} + q_{mg}^+ \tag{5.20}$$

$$\vec{\mathbf{Q}}_{mg}^- = \sum_{j=1}^{G} \sum_{n=1,3,}^{N} (2n+1) P_n(\mu_m) \sigma_{n,j \to g} \vec{\phi}_{nj} + \vec{\mathbf{q}}_{mg}^- \tag{5.21}$$

$$\phi_{ng} = 2 \sum_{m=1}^{(N+1)/2} P_n(\mu_m) \psi_{mg}^+ w_m \qquad , n \text{ even} \tag{5.22}$$

$$\vec{\phi}_{ng} = 2 \sum_{m=1}^{(N+1)/2} P_n(\mu_m) \vec{\psi}_{mg}^- w_m \qquad , n \text{ odd} \tag{5.23}$$

5.2.2 Multigroup Cross Section Generation

As we have shown in sections 3.3 and 5.2.1, the energy and angular variations of the cross sections can be represented by multigroup-Legendre expansions. The coefficients of these expansions are called multigroup-Legendre cross sections. As discussed in Chapter 2, cross sections for our multigroup SP_N code will be generated

by the code CEPXS. CEPXS produces coupled electron-photon cross sections in a multigroup-Legendre format over the energy range 1 keV to 100 MeV for materials of arbitrary composition. We note, electron cross sections are not generally available below 1 keV for materials of arbitrary composition.

In CEPXS the energy domain is the same for all species of particles. For example, in coupled electron-photon transport, the lower energy bound E_G, and the upper energy bound E_0, will be the same for both the electrons and photons. If we consider a electron source problem with G total groups, and n electron groups, CEPXS assigns group indices $g = 1, 2, \ldots, n$ to the electrons, and group indices $g = n+1, n+2, \ldots, G$ to the photons. Electron to photon scattering then looks like downscattering, and photon to electron scattering looks like upscattering. This format [19] allows one to use only one set of multigroup equations; where, the subscript g now refers to both particle type and energy.

5.2.3 Numerical Solution of the Multigroup Equations

Let us develop a general solution algorithm for solving the multigroup equations. We begin with these equations

$$\left(\hat{\Omega}\cdot\vec{\nabla} + \sigma_{tg}(\vec{\mathbf{r}})\right)\psi_g(\vec{\mathbf{r}},\hat{\Omega}) = \sum_{g'=1}^{G}\int_{4\pi} d\hat{\Omega}'\sigma_{g'\to g}(\vec{\mathbf{r}},\hat{\Omega}'\cdot\hat{\Omega})\psi_{g'}(\vec{\mathbf{r}},\hat{\Omega}') + q_g(\vec{\mathbf{r}},\hat{\Omega}) \quad , g = 1, 2, \ldots, G \tag{5.24}$$

We introduce a general operator notation to condense these equations. Define the group g streaming-collision operator, $\hat{H}^0_{gg}$,as

$$\hat{H}^0_{gg}\psi_g = \left(\hat{\Omega}\cdot\vec{\nabla} + \sigma_{tg}(\vec{\mathbf{r}})\right)\psi_g(\vec{\mathbf{r}},\hat{\Omega}) \tag{5.25}$$

and the group g' to g scattering operator, $\hat{H}^1_{gg'}$, as

$$\hat{H}^1_{gg'}\psi_{g'} = \int_{4\pi} d\hat{\Omega}'\sigma_{g'\to g}(\vec{\mathbf{r}},\hat{\Omega}'\cdot\hat{\Omega})\psi_{g'}(\vec{\mathbf{r}},\hat{\Omega}') \tag{5.26}$$

we may then express Equation (5.24) as

$$\sum_{g'=1}^{G}\left(\delta_{g'g}\hat{H}^0_{gg} - \hat{H}^1_{gg'}\right)\psi_{g'} = q_g \qquad ,g = 1,2,\ldots,G \tag{5.27}$$

and defining the multigroup transport operator

$$\hat{H}_{gg'} \equiv \delta_{g'g}\hat{H}^0_{gg} - \hat{H}^1_{gg'} \tag{5.28}$$

we may write Equations (5.27) as the coupled set of operator equations

$$\sum_{g'=1}^{G}\hat{H}_{gg'}\psi_{g'} = q_g \qquad\qquad ,g = 1,2,\ldots,G \tag{5.29}$$

or

$$\begin{bmatrix} \hat{H}_{11} & \hat{H}_{12} & \ldots & \hat{H}_{1G} \\ \hat{H}_{21} & \hat{H}_{22} & \ldots & \hat{H}_{2G} \\ \vdots & & & \\ \hat{H}_{G1} & \hat{H}_{G2} & \ldots & \hat{H}_{GG} \end{bmatrix}\begin{bmatrix} \psi_1 \\ \psi_2 \\ \vdots \\ \psi_G \end{bmatrix} = \begin{bmatrix} q_1 \\ q_2 \\ \vdots \\ q_G \end{bmatrix} \tag{5.30}$$

For many problems there is no scattering of particles from lower energy to higher energy, or *no upscatter*, this implies

$$\hat{H}_{gg'} = 0 \qquad , g' > g \tag{5.31}$$

matrix **H** is now lower triangular, and the group fluxes may be obtained systematically starting with the highest energy group, group 1

$$\begin{aligned}
\psi_1 &= \hat{H}_{11}^{-1} q_1 \\
\psi_2 &= \hat{H}_{22}^{-1} \left(q_2 - \hat{H}_{21} \psi_1 \right) \\
&\vdots \\
\psi_g &= \hat{H}_{gg}^{-1} \left(q_g - \sum_{g'<g} \hat{H}_{gg'} \psi_{g'} \right) \\
&\vdots \\
\psi_G &= \hat{H}_{GG}^{-1} \left(q_G - \sum_{g'<G} \hat{H}_{Gg'} \psi_{g'} \right)
\end{aligned} \tag{5.32}$$

Each one of these G equations represents an equation for the flux in group g, and a sweep through all groups, $g = 1, 2, \ldots, G$, is referred to as an *outer iteration*. We defer the development of a solution method for the group equations until section 5.3, and Chapter 6. For the general case where upscatter is included an iterative method must be employed. We write equation (5.29) as

$$\hat{H}_{gg} \psi_g + \sum_{g'<g} \hat{H}_{gg'} \psi_{g'} + \sum_{g'>g} \hat{H}_{gg'} \psi_{g'} = q_g \qquad , g = 1, 2, \ldots, G \tag{5.33}$$

The first term on the left physically represents all interactions within the gth group which result in a loss of particles from the gth group. The second term, known as the downscatter source, represents the transfer of particles from higher energy groups to the gth group. The third term, the upscatter source, represents transfer of particles from lower energy groups to the gth group. We now specify the iteration scheme

$$\psi_g^{(l)} = \hat{H}_{gg}^{-1}\left(q_g - \sum_{g'<g}\hat{H}_{gg'}\psi_{g'}^{(l)} - \sum_{g'>g}\hat{H}_{gg'}\psi_{g'}^{(l-1)}\right) \quad ,g = 1,2,\ldots,G \tag{5.34}$$

where l is the outer iteration index.

The iteration process begins (l=1) with some initial guess of the group fluxes $\psi_g^{(0)}$, where $g = 1,2,\ldots,G$. We first solve the group 1 equation for the group 1 flux. We then use this value to construct the downscatter source for group 2, and solve the group 2 equation for the group 2 flux. Next, we use the group 1 and 2 fluxes for the construction of the downscatter source for group 3, and solve the group 3 equation. This process is continued until the first outer iteration is complete. We may now update the initial flux guess with the new group fluxes, which we have just calculated, and then proceed with the next outer iteration (l=2). After 2 outer iterations a convergence test is performed. The error is calculated for each group using the L^2 norm of the scalar flux, and the L^2 norm of the residual of the scalar flux, and is given by

$$e_g^{(l)} = \sqrt{\frac{\sum_k |\phi_{kg}^{(l)} - \phi_{kg}^{(l-1)}|^2}{\sum_k |\phi_{kg}^{(l)}|^2}} \quad ,g = 1,2,\ldots,G \tag{5.35}$$

where k is the spatial index. If the error criterion

$$\max |e_g^{(l)}| < \epsilon \qquad \text{,for all } g = 1, 2, \ldots, G \tag{5.36}$$

is not satisfied, where ϵ is typically 10^{-5}, a global flux update is made, and another outer iteration is performed. When the error criterion is satisfied, the calculation is terminated.

As we have seen in the case of no upscatter, we have the complete solution after one outer iteration, at which point we may terminate the calculation. We turn now to the topic of spatial discretization of the group equations.

5.3 Spatial Differencing - Bilinear Continuous Finite Element Methods

5.3.1 Two Dimensional R - Z Geometry

The canonical multigroup equations represent a self adjoint system of equations. Upon discretization, self adjoint systems yield matrix equations with symmetric positive definite coefficient matrices. Efficient, robust numerical methods exist for the solution of such matrix equations. In this section the group g equation will be spatially discretized using bilinear continuous finite element methods (BLCFEM) to produce a discrete set of equations. Let us begin with the group g canonical SP_N equations, Equations (5.18) and (5.19), given by

$$-\mu_m^2 \vec{\nabla} \cdot \frac{1}{\sigma_t} \vec{\nabla} \psi_m^+ - \sigma_t \psi_m^+ = Q_m^+ - \mu_m \vec{\nabla} \cdot \left(\frac{\vec{\mathbf{Q}}_m^-}{\sigma_t} \right) \qquad \text{,} m = 1, (N+1)/2 \tag{5.37}$$

$$\vec{\psi}_m^- = -\frac{\mu_m}{\sigma_t} \vec{\nabla} \psi_m^+ + \frac{1}{\sigma_t} \vec{\mathbf{Q}}_m^- \qquad \text{,} m = 1, (N+1)/2 \tag{5.38}$$

where for brevity, we have omitted the group index g, and the source terms, Q_m^+, $\vec{\mathbf{Q}}_m^-$, which appear on the right hand side of each equation are known functions. In the interest of simplifying the calculation, we choose to proceed with a first order form of the SP_N equations obtained by solving Equation (5.38) for $\vec{\nabla}\psi_m^+$ and substituting into Equation (5.37)

$$\mu_m \vec{\nabla} \cdot \vec{\psi}_m^- + \sigma_t \psi_m^+ = Q_m^+ \quad , m = 1, (N+1)/2 \tag{5.39}$$

Here we consider two dimensional R - Z geometry, which is characteristic of cylindrical geometry with azimuthal symmetry. We proceed by dividing the problem domain into an R - Z mesh of (I X J) rectangular cells as shown in Figure 5.2; where the mesh deltas are defined as

$$\Delta r_i \equiv r_{i+1} - r_i \tag{5.40}$$

$$\Delta z_j \equiv z_{j+1} - z_j \tag{5.41}$$

Within each cell we require the material properties to be constant, allowing for discontinuities, if any, to exist only at cell edges. Thus the total cross section within the (i,j)th cell is defined as

$$\sigma_t(\vec{r}) = \sigma_t(r, z) \equiv \sigma_{tij} \quad , r_i < r \leq r_{i+1},\ z_j < z \leq z_{j+1} \tag{5.42}$$

Next, we assume that the even parity angular flux is represented as a bilinear function of r and z within each cell. That is, for the (i,j)th cell the even parity flux is given by

$$\begin{aligned}\psi_m^+(r,z) &= \psi_{i,j}^{--}\left(\frac{r_{i+1}-r}{\Delta r_i}\right)\left(\frac{z_{j+1}-z}{\Delta z_j}\right)+\psi_{i,j+1}^{+}\left(\frac{r_{i+1}-r}{\Delta r_i}\right)\left(\frac{z-z_j}{\Delta z_j}\right)\\ &+ \psi_{i+1,j+1}^{--}\left(\frac{r-r_i}{\Delta r_i}\right)\left(\frac{z-z_j}{\Delta z_j}\right)+\psi_{i+1,j}^{+}\left(\frac{r-r_i}{\Delta r_i}\right)\left(\frac{z_{j+1}-z}{\Delta z_j}\right)\\ &\qquad ,r_i \le r \le r_{i+1}, z_j \le z \le z_{j+1} \quad (5.43)\end{aligned}$$

where the even parity flux is continuous across cell edges. We define the node based unknowns, where we have supressed the subscript m, as

$$\begin{aligned}\psi^+(r_i,z_j) &\equiv \psi_{i,j}^+\\ \psi^+(r_i,z_{j+1}) &\equiv \psi_{i,j+1}^+\\ \psi^+(r_{i+1},z_{j+1}) &\equiv \psi_{i+1,j+1}^+\\ \psi^+(r_{i+1},z_j) &\equiv \psi_{i+1,j}^+ \quad (5.44)\end{aligned}$$

and approximate the even parity source in an analogous manner

$$\begin{aligned}Q_m^+(r,z) &= Q_{i,j}^+\left(\frac{r_{i+1}-r}{\Delta r_i}\right)\left(\frac{z_{j+1}-z}{\Delta z_j}\right)+Q_{i,j+1}^+\left(\frac{r_{i+1}-r}{\Delta r_i}\right)\left(\frac{z-z_j}{\Delta z_j}\right)\\ &+ Q_{i+1,j+1}^+\left(\frac{r-r_i}{\Delta r_i}\right)\left(\frac{z-z_j}{\Delta z_j}\right)+Q_{i+1,j}^+\left(\frac{r-r_i}{\Delta r_i}\right)\left(\frac{z_{j+1}-z}{\Delta z_j}\right)\\ &\qquad ,r_i \le r \le r_{i+1}, z_j \le z \le z_{j+1} \quad (5.45)\end{aligned}$$

Continuing, we must next consider the odd parity angular flux. The odd parity angular flux is also represented bilinearly within each (i,j) cell. It however, is defined not in terms of node based unknowns, but in terms of corner based unknowns, as shown in Figure 5.3. For the (i,j)th cell, the odd parity angular flux is given as

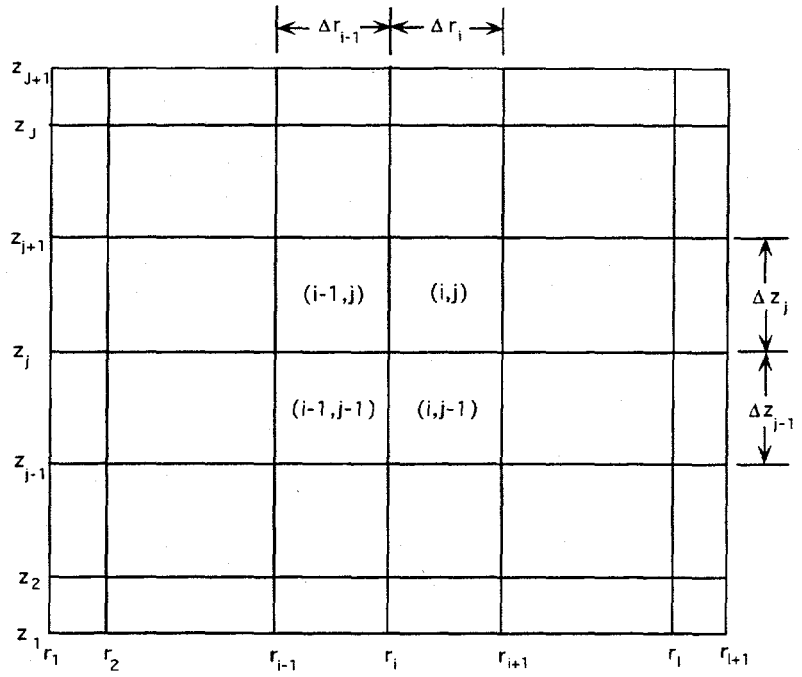

Figure 5.2: Two Dimensional R-Z Geometry Spatial Mesh

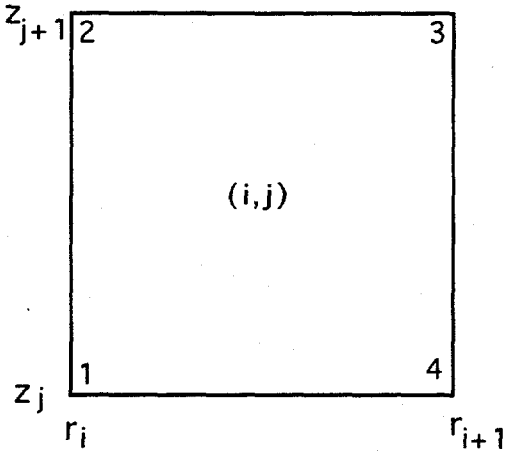

Figure 5.3: Corner Numbering System for Cell (i,j)

$$\vec{\psi}^{-}_{m}(r,z) = \vec{\psi}^{-(1)}_{i,j}\left(\frac{r_{i+1}-r}{\Delta r_i}\right)\left(\frac{z_{j+1}-z}{\Delta z_j}\right) + \vec{\psi}^{-(2)}_{i,j}\left(\frac{r_{i+1}-r}{\Delta r_i}\right)\left(\frac{z-z_j}{\Delta z_j}\right) + \vec{\psi}^{-(3)}_{i,j}\left(\frac{r-r_i}{\Delta r_i}\right)\left(\frac{z-z_j}{\Delta z_j}\right) + \vec{\psi}^{-(4)}_{i,j}\left(\frac{r-r_i}{\Delta r_i}\right)\left(\frac{z_{j+1}-z}{\Delta z_j}\right) \quad , r_i < r \leq r_{i+1}, z_j < z \leq z_{j+1} \tag{5.46}$$

and the odd parity source as

$$\vec{\mathbf{Q}}^{-}_{m}(r,z) = \vec{\mathbf{Q}}^{-(1)}_{i,j}\left(\frac{r_{i+1}-r}{\Delta r_i}\right)\left(\frac{z_{j+1}-z}{\Delta z_j}\right) + \vec{\mathbf{Q}}^{-(2)}_{i,j}\left(\frac{r_{i+1}-r}{\Delta r_i}\right)\left(\frac{z-z_j}{\Delta z_j}\right) + \vec{\mathbf{Q}}^{-(3)}_{i,j}\left(\frac{r-r_i}{\Delta r_i}\right)\left(\frac{z-z_j}{\Delta z_j}\right) + \vec{\mathbf{Q}}^{-(4)}_{i,j}\left(\frac{r-r_i}{\Delta r_i}\right)\left(\frac{z_{j+1}-z}{\Delta z_j}\right) \quad , r_i < r \leq r_{i+1}, z_j < z \leq z_{j+1} \tag{5.47}$$

We define a set of basis functions $\gamma^{(k)}_{i,j}(r,z)$, which represent the behavior of the flux within each (i,j) cell

$$\gamma^{(1)}_{i,j}(r,z) = \begin{cases} \left(\frac{r_{i+1}-r}{\Delta r_i}\right)\left(\frac{z_{j+1}-z}{\Delta z_j}\right) & , r_i < r \leq r_{i+1}, z_j < z \leq z_{j+1} \\ 0 & \text{otherwise} \end{cases} \tag{5.48}$$

$$\gamma^{(2)}_{i,j}(r,z) = \begin{cases} \left(\frac{r_{i+1}-r}{\Delta r_i}\right)\left(\frac{z-z_j}{\Delta z_j}\right) & , r_i < r \leq r_{i+1}, z_j < z \leq z_{j+1} \\ 0 & \text{otherwise} \end{cases} \tag{5.49}$$

$$\gamma^{(3)}_{i,j}(r,z) = \begin{cases} \left(\frac{r-r_i}{\Delta r_i}\right)\left(\frac{z-z_j}{\Delta z_j}\right) & , r_i < r \leq r_{i+1}, z_j < z \leq z_{j+1} \\ 0 & \text{otherwise} \end{cases} \tag{5.50}$$

$$\gamma^{(4)}_{i,j}(r,z) = \begin{cases} \left(\frac{r-r_i}{\Delta r_i}\right)\left(\frac{z_{j+1}-z}{\Delta z_j}\right) & , r_i < r \leq r_{i+1}, z_j < z \leq z_{j+1} \\ 0 & \text{otherwise} \end{cases} \tag{5.51}$$

Here the superscript k, where $k = 1, 2, \ldots, 4$, corresponds to the kth corner of the (i,j)th cell, as shown in Figure 5.3. An important property of these basis functions derives from the fact that the functions vanish except in a small region within the

(i,j)th cell. This property, called compact support, guarantees that the coefficient matrices resulting from the finite element approximation are sparse. Numerical solution of matrix equations with sparse coefficient matrices requires fewer arithmetic operations and less memory than would otherwise be the case. For two dimensional R - Z geometry the differential volume element is

$$dV = 2\pi r dr dz \tag{5.52}$$

Let us operate on Equation (5.39) by $2\pi \int_{r_1}^{r_{I+1}} r dr \int_{z_1}^{z_{J+1}} dz\ w(r,z)$, where $w(r,z)$ is an arbitrary function defined throughout the domain of the problem. For brevity, we introduce the notation

$$\int_V dV \equiv 2\pi \int_{r_1}^{r_{I+1}} r dr \int_{z_1}^{z_{J+1}} dz \tag{5.53}$$

to signify the integration over the total problem volume. We obtain

$$\mu_m \int_V dV w \vec{\nabla} \cdot \vec{\psi}_m^- + \int_V dV w \sigma_t \psi_m^+ = \int_V dV w Q_m^+ \tag{5.54}$$

The first term of Equation (5.54) may be simplified through the use of the vector identity

$$\vec{\nabla} \cdot (\phi \vec{\mathbf{A}}) = \vec{\nabla}\phi \cdot \vec{\mathbf{A}} + \phi \vec{\nabla} \cdot \vec{\mathbf{A}} \tag{5.55}$$

and Gauss' divergence theorem to

$$\int_V dV w \vec{\nabla} \cdot \vec{\psi}_m^- = \int_V dV \vec{\nabla} \cdot w \vec{\psi}_m^- - \int_V dV \vec{\nabla} w \cdot \vec{\psi}_m^- \tag{5.56}$$

$$= \oint_S w \vec{\psi}_m^- \cdot \hat{n} dA - \int_V dV \vec{\nabla} w \cdot \vec{\psi}_m^- \tag{5.57}$$

If we now substitute the basis function $\gamma_{i,j}^{(1)}(r,z)$ for $w(r,z)$, where (i,j) is an interior node, the surface integral term vanishes. This can be seen from the fact that $\gamma_{i,j}^{(1)}(r,z)$ is zero on the surface. The integration over the total volume then collapses to an integration over the volume of the (i,j)th cell.

$$\begin{aligned} - \quad & \mu_m \int_{r_i}^{r_{i+1}} r dr \int_{z_j}^{z_{j+1}} dz \vec{\nabla} \gamma_{i,j}^{(1)} \cdot \vec{\psi}_m^- + \int_{r_i}^{r_{i+1}} r dr \int_{z_j}^{z_{j+1}} dz \gamma_{i,j}^{(1)} \sigma_t \psi_m^+ \\ & = \int_{r_i}^{r_{i+1}} r dr \int_{z_j}^{z_{j+1}} dz \gamma_{i,j}^{(1)} Q_m^+ \end{aligned} \tag{5.58}$$

Substituting Equations (5.48), and (5.43) through (5.46) into Equation (5.58), and proceding with the integration, we then obtain the contribution from the (i,j)th cell

$$\frac{\mu_m \Delta z_j}{6} \left[(2r_i + r_{i+1})(\frac{1}{3}\psi_{rij}^{-(1)} + \frac{1}{6}\psi_{rij}^{-(2)}) + (r_i + 2r_{i+1})(\frac{1}{6}\psi_{rij}^{-(3)} + \frac{1}{3}\psi_{rij}^{-(4)}) \right]$$

$$+ \quad \frac{\mu_m \Delta r_i}{24} \left[(3r_i + r_{i+1})(\psi_{zij}^{-(1)} + \psi_{zij}^{-(2)}) + (r_i + r_{i+1})(\psi_{zij}^{-(3)} + \psi_{zij}^{-(4)}) \right]$$

$$+ \quad \frac{\Delta r_i \Delta z_j}{36} \sigma_{tij} \left[(3r_i + r_{i+1})(\psi_{i,j}^{+} + \frac{1}{2}\psi_{i,j+1}^{+}) + (r_i + r_{i+1})(\frac{1}{2}\psi_{i+1,j+1}^{+} + \psi_{i+1,j}^{+}) \right]$$

$$= \quad \frac{\Delta r_i \Delta z_j}{36} \left[(3r_i + r_{i+1})(Q_{i,j}^{+} + \frac{1}{2}Q_{i,j+1}^{+}) + (r_i + r_{i+1})(\frac{1}{2}Q_{i+1,j+1}^{+} + Q_{i+1,j}^{+}) \right] \tag{5.59}$$

where ψ_{rij}^- and ψ_{zij}^- are defined to be the radial and axial components, respectively, of the odd parity angular flux $\vec{\psi}_{ij}^-$.

To complete our derivation of an equation for node (i,j), we must next consider the contributions from the 3 other cells surrounding node (i,j), that is cells (i,j-1), (i-1,j-1), and (i-1,j). We define an analogous procedure to derive equations for these

cells using the BLCFEM:

1. cell (i,j-1) - multiply Equation (5.39) by $\gamma^{(2)}_{i,j-1}(r,z)$ and integrate over the volume of the cell

2. cell (i-1,j-1) - multiply Equation (5.39) by $\gamma^{(3)}_{i-1,j-1}(r,z)$ and integrate over the volume of the cell

3. cell (i-1,j) - multiply Equation (5.39) by $\gamma^{(4)}_{i-1,j}(r,z)$ and integrate over the volume of the cell

The resulting 4 equations, from the 4 cells surrounding node (i,j), are then summed, and the odd parity angular flux, $\vec{\psi}^{-}_{m}$, is eliminated using equation (5.38)

$$\vec{\psi}^{-}_{m} = -\frac{\mu_m}{\sigma_t}\vec{\nabla}\psi^{+}_{m} + \frac{1}{\sigma_t}\vec{\mathbf{Q}}^{-}_{m} \tag{5.60}$$

where the radial components of (5.60) are given by

$$\psi^{-(1)}_{rij} = -\frac{\mu_m}{\sigma_{tij}}\left(\frac{\psi^{+}_{i+1,j} - \psi^{+}_{i,j}}{\Delta r_i}\right) + \frac{Q^{-(1)}_{rij}}{\sigma_{tij}} \tag{5.61}$$

$$\psi^{-(2)}_{rij} = -\frac{\mu_m}{\sigma_{tij}}\left(\frac{\psi^{+}_{i+1,j+1} - \psi^{+}_{i,j+1}}{\Delta r_i}\right) + \frac{Q^{-(2)}_{rij}}{\sigma_{tij}} \tag{5.62}$$

$$\psi^{-(3)}_{rij} = -\frac{\mu_m}{\sigma_{tij}}\left(\frac{\psi^{+}_{i+1,j+1} - \psi^{+}_{i,j+1}}{\Delta r_i}\right) + \frac{Q^{-(3)}_{rij}}{\sigma_{tij}} \tag{5.63}$$

$$\psi^{-(4)}_{rij} = -\frac{\mu_m}{\sigma_{tij}}\left(\frac{\psi^{+}_{i+1,j} - \psi^{+}_{i,j}}{\Delta r_i}\right) + \frac{Q^{-(4)}_{rij}}{\sigma_{tij}} \tag{5.64}$$

and the axial components of (5.60) are given by

$$\psi^{-(1)}_{zij} = -\frac{\mu_m}{\sigma_{tij}}\left(\frac{\psi^{+}_{i,j+1} - \psi^{+}_{i,j}}{\Delta z_j}\right) + \frac{Q^{-(1)}_{zij}}{\sigma_{tij}} \tag{5.65}$$

$$\psi^{-(2)}_{zij} = -\frac{\mu_m}{\sigma_{tij}}\left(\frac{\psi^{+}_{i,j+1} - \psi^{+}_{i,j}}{\Delta z_j}\right) + \frac{Q^{-(2)}_{zij}}{\sigma_{tij}} \tag{5.66}$$

$$\psi_{zij}^{-(3)} = -\frac{\mu_m}{\sigma_{tij}}\left(\frac{\psi_{i+1,j+1}^{+} - \psi_{i+1,j}^{+}}{\Delta z_j}\right) + \frac{Q_{zij}^{-(3)}}{\sigma_{tij}} \tag{5.67}$$

$$\psi_{zij}^{-(4)} = -\frac{\mu_m}{\sigma_{tij}}\left(\frac{\psi_{i+1,j+1}^{+} - \psi_{i+1,j}^{+}}{\Delta z_j}\right) + \frac{Q_{zij}^{-(4)}}{\sigma_{tij}} \tag{5.68}$$

Finally, we obtain the equation for the (i,j)th interior node

$$\begin{aligned} & c_1\,\psi_{i-1,j-1}^{+} + c_2\,\psi_{i,j-1}^{+} + c_3\,\psi_{i+1,j-1}^{+} \\ + \;& c_4\,\psi_{i-1,j}^{+} + c_5\,\psi_{i,j}^{+} + c_6\,\psi_{i+1,j}^{+} \\ + \;& c_7\,\psi_{i-1,j+1}^{+} + c_8\,\psi_{i,j+1}^{+} + c_9\,\psi_{i+1,j+1}^{+} = S_{i,j} \\ & \qquad\qquad i = 2,3,\ldots,I \\ & \qquad\qquad j = 2,3,\ldots,J \end{aligned} \tag{5.69}$$

where the coefficients $c_k \equiv c_k(i,j)$, $k = 1,\ldots,9$, are defined as

$$\begin{aligned} c_1 &= \left[-\frac{\mu_m^2\Delta z_{j-1}}{\Delta r_{i-1}\sigma_{i-1,j-1}} - \frac{\mu_m^2\Delta r_{i-1}}{\Delta z_{j-1}\sigma_{i-1,j-1}} + \frac{1}{6}\sigma_{i-1,j-1}\Delta r_{i-1}\Delta z_{j-1}\right] \\ &\times \frac{1}{12}(r_{i-1} + r_i) \end{aligned}$$

$$\begin{aligned} c_2 &= \left[\frac{1}{\Delta r_{i-1}\sigma_{i-1,j-1}}(r_{i-1} + r_i) + \frac{1}{\Delta r_i\sigma_{i,j-1}}(r_i + r_{i+1})\right]\frac{1}{12}\mu_m^2\Delta z_{j-1} \\ &+ \left[-\frac{\mu_m^2}{\Delta z_{j-1}\sigma_{i,j-1}} + \frac{1}{6}\sigma_{i,j-1}\Delta z_{j-1}\right]\frac{1}{12}\Delta r_i(3r_i + r_{i+1}) \\ &+ \left[-\frac{\mu_m^2}{\Delta z_{j-1}\sigma_{i-1,j-1}} + \frac{1}{6}\sigma_{i-1,j-1}\Delta z_{j-1}\right]\frac{1}{12}\Delta r_{i-1}(r_{i-1} + 3r_i) \end{aligned}$$

$$\begin{aligned} c_3 &= \left[-\frac{\mu_m^2\Delta z_{j-1}}{\Delta r_i\sigma_{i,j-1}} - \frac{\mu_m^2\Delta r_i}{\Delta z_{j-1}\sigma_{i,j-1}} + \frac{1}{6}\sigma_{i,j-1}\Delta r_i\Delta z_{j-1}\right] \\ &\times \frac{1}{12}(r_i + r_{i+1}) \end{aligned}$$

$$
\begin{aligned}
c_4 &= \left[-\frac{\mu_m^2 \Delta z_{j-1}}{\Delta r_{i-1}\sigma_{i-1,j-1}} - \frac{\mu_m^2 \Delta z_j}{\Delta r_{i-1}\sigma_{i-1,j}} + \frac{\mu_m^2 \Delta r_{i-1}}{2\Delta z_{j-1}\sigma_{i-1,j-1}} \right. \\
&+ \left. \frac{\mu_m^2 \Delta r_{i-1}}{2\Delta z_j \sigma_{i-1,j}} + \frac{1}{6}\sigma_{i-1,j-1}\Delta r_{i-1}\Delta z_{j-1} + \frac{1}{6}\sigma_{i-1,j}\Delta r_{i-1}\Delta z_j \right] \\
&\times \frac{1}{6}(r_{i-1} + r_i)
\end{aligned}
$$

$$
\begin{aligned}
c_5 &= \left[\frac{\mu_m^2 \Delta z_j}{\Delta r_i \sigma_{i,j}} + \frac{\mu_m^2 \Delta z_{j-1}}{\Delta r_i \sigma_{i,j-1}} \right] \frac{1}{6}(r_i + r_{i+1}) \\
&+ \left[\frac{\mu_m^2 \Delta z_{j-1}}{\Delta r_{i-1}\sigma_{i-1,j-1}} + \frac{\mu_m^2 \Delta z_j}{\Delta r_{i-1}\sigma_{i-1,j}} \right] \frac{1}{6}(r_{i-1} + r_i) \\
&+ \left[\frac{\mu_m^2 \Delta r_i}{\Delta z_j \sigma_{i,j}} + \frac{\mu_m^2 \Delta r_i}{\Delta z_{j-1}\sigma_{i,j-1}} \right] \frac{1}{12}(3r_i + r_{i+1}) \\
&+ \left[\frac{\mu_m^2 \Delta r_{i-1}}{\Delta z_{j-1}\sigma_{i-1,j-1}} + \frac{\mu_m^2 \Delta r_{i-1}}{\Delta z_j \sigma_{i-1,j}} \right] \frac{1}{12}(r_{i-1} + 3r_i) \\
&+ \left[\sigma_{i,j}\Delta r_i \Delta z_j + \sigma_{i,j-1}\Delta r_i \Delta z_{j-1} \right] \frac{1}{36}(3r_i + r_{i+1}) \\
&+ \left[\sigma_{i-1,j-1}\Delta r_{i-1}\Delta z_{j-1} + \sigma_{i-1,j}\Delta r_{i-1}\Delta z_j \right] \frac{1}{36}(r_{i-1} + 3r_i)
\end{aligned}
$$

$$
\begin{aligned}
c_6 &= \left[-\frac{\mu_m^2 \Delta z_j}{\Delta r_i \sigma_{i,j}} - \frac{\mu_m^2 \Delta z_{j-1}}{\Delta r_i \sigma_{i,j-1}} + \frac{\mu_m^2 \Delta r_i}{2\Delta z_j \sigma_{i,j}} \right. \\
&+ \left. \frac{\mu_m^2 \Delta r_i}{2\Delta z_{j-1}\sigma_{i,j-1}} + \frac{1}{6}\sigma_{i,j}\Delta r_i \Delta z_j + \frac{1}{6}\sigma_{i,j-1}\Delta r_i \Delta z_{j-1} \right] \\
&\times \frac{1}{6}(r_i + r_{i+1})
\end{aligned}
$$

$$
\begin{aligned}
c_7 &= \left[-\frac{\mu_m^2 \Delta z_j}{\Delta r_{i-1}\sigma_{i-1,j}} - \frac{\mu_m^2 \Delta r_{i-1}}{\Delta z_j \sigma_{i-1,j}} + \frac{1}{6}\sigma_{i-1,j}\Delta r_{i-1}\Delta z_j \right] \\
&\times \frac{1}{12}(r_{i-1} + r_i)
\end{aligned}
$$

$$
c_8 = \left[\frac{1}{\Delta r_{i-1}\sigma_{i-1,j}}(r_{i-1} + r_i) + \frac{1}{\Delta r_i \sigma_{i,j}}(r_i + r_{i+1}) \right] \frac{1}{12}\mu_m^2 \Delta z_j
$$

$$
\begin{aligned}
&+ \left[-\frac{\mu_m^2}{\Delta z_j \sigma_{i,j}} + \frac{1}{6}\sigma_{i,j}\Delta z_j\right] \frac{1}{12}\Delta r_i(3r_i + r_{i+1}) \\
&+ \left[-\frac{\mu_m^2}{\Delta z_j \sigma_{i-1,j}} + \frac{1}{6}\sigma_{i-1,j}\Delta z_j\right] \frac{1}{12}\Delta r_{i-1}(r_{i-1} + 3r_i)
\end{aligned}
$$

$$
\begin{aligned}
c_9 &= \left[-\frac{\mu_m^2 \Delta z_j}{\Delta r_i \sigma_{i,j}} - \frac{\mu_m^2 \Delta r_i}{\Delta z_j \sigma_{i,j}} + \frac{1}{6}\sigma_{i,j}\Delta r_i \Delta z_j\right] \\
&\times \frac{1}{12}(r_i + r_{i+1}) \qquad (5.70)
\end{aligned}
$$

and the source term $S_{i,j}$ is given by

$$
\begin{aligned}
S_{i,j} &= \frac{1}{72}\Delta r_{i-1}\Delta z_{j-1}(r_{i-1} + r_i)Q^+_{i-1,j-1} \\
&+ \left[\Delta r_{i-1}(r_{i-1} + 3r_i) + \Delta r_i(3r_i + r_{i+1})\right] \frac{1}{72}\Delta z_{j-1} Q^+_{i,j-1} \\
&+ \frac{1}{72}\Delta r_i \Delta z_{j-1}(r_i + r_{i+1})Q^+_{i+1,j-1} \\
&+ \left[\Delta z_{j-1} + \Delta z_j\right] \frac{1}{36}\Delta r_{i-1}(r_{i-1} + r_i)Q^+_{i-1,j} \\
&+ \left[\Delta r_{i-1}(r_{i-1} + 3r_i) + \Delta r_i(3r_i + r_{i+1})\right] \frac{1}{36}(\Delta z_{j-1} + \Delta z_j)Q^+_{i,j} \\
&+ \left[\Delta z_{j-1} + \Delta z_j\right] \frac{1}{36}\Delta r_i(r_i + r_{i+1})Q^+_{i+1,j} \\
&+ \frac{1}{72}\Delta r_{i-1}\Delta z_j(r_{i-1} + r_i)Q^+_{i-1,j+1} \\
&+ \left[\Delta r_{i-1}(r_{i-1} + 3r_i) + \Delta r_i(3r_i + r_{i+1})\right] \frac{1}{72}\Delta z_j Q^+_{i,j+1} \\
&+ \frac{1}{72}\Delta r_i \Delta z_j(r_i + r_{i+1})Q^+_{i+1,j+1} \\
&- \frac{\mu_m \Delta z_j}{(\Delta r_i)^2 \sigma_{i,j}} \left[\frac{a_i}{3}Q^{-(1)}_{r,i,j} + \frac{a_i}{6}Q^{-(2)}_{r,i,j} + \frac{b_i}{6}Q^{-(3)}_{r,i,j} + \frac{b_i}{3}Q^{-(4)}_{r,i,j}\right] \\
&- \frac{\mu_m \Delta z_{j-1}}{(\Delta r_i)^2 \sigma_{i,j-1}} \left[\frac{a_i}{6}Q^{-(1)}_{r,i,j-1} + \frac{a_i}{3}Q^{-(2)}_{r,i,j-1} + \frac{b_i}{3}Q^{-(3)}_{r,i,j-1} + \frac{b_i}{6}Q^{-(4)}_{r,i,j-1}\right] \\
&+ \frac{\mu_m \Delta z_{j-1}}{(\Delta r_{i-1})^2 \sigma_{i-1,j-1}} \left[\frac{c_i}{6}Q^{-(1)}_{r,i-1,j-1} + \frac{c_i}{3}Q^{-(2)}_{r,i-1,j-1} + \frac{d_i}{3}Q^{-(3)}_{r,i-1,j-1} + \frac{d_i}{6}Q^{-(4)}_{r,i-1,j-1}\right] \\
&+ \frac{\mu_m \Delta z_j}{(\Delta r_{i-1})^2 \sigma_{i-1,j}} \left[\frac{c_i}{3}Q^{-(1)}_{r,i-1,j} + \frac{c_i}{6}Q^{-(2)}_{r,i-1,j} + \frac{d_i}{6}Q^{-(3)}_{r,i-1,j} + \frac{d_i}{3}Q^{-(4)}_{r,i-1,j}\right]
\end{aligned}
$$

$$
\begin{aligned}
- \quad & \frac{\mu_m \Delta r_i}{24\sigma_{i,j}} \left[(3r_i + r_{i+1})(Q^{-(1)}_{z,i,j} + Q^{-(2)}_{z,i,j}) \right. \\
+ \quad & \left. (r_i + r_{i+1})(Q^{-(3)}_{z,i,j} + Q^{-(4)}_{z,i,j}) \right] \\
+ \quad & \frac{\mu_m \Delta r_i}{24\sigma_{i,j-1}} \left[(3r_i + r_{i+1})(Q^{-(1)}_{z,i,j-1} + Q^{-(2)}_{z,i,j-1}) \right. \\
+ \quad & \left. (r_i + r_{i+1})(Q^{-(3)}_{z,i,j-1} + Q^{-(4)}_{z,i,j-1}) \right] \\
+ \quad & \frac{\mu_m \Delta r_{i-1}}{24\sigma_{i-1,j-1}} \left[(r_{i-1} + r_i)(Q^{-(1)}_{z,i-1,j-1} + Q^{-(2)}_{z,i-1,j-1}) \right. \\
+ \quad & \left. (r_{i-1} + 3r_i)(Q^{-(3)}_{z,i-1,j-1} + Q^{-(4)}_{z,i-1,j-1}) \right] \\
- \quad & \frac{\mu_m \Delta r_{i-1}}{24\sigma_{i-1,j}} \left[(r_{i-1} + r_i)(Q^{-(1)}_{z,i-1,j} + Q^{-(2)}_{z,i-1,j}) \right. \\
+ \quad & \left. (r_{i-1} + 3r_i)(Q^{-(3)}_{z,i-1,j} + Q^{-(4)}_{z,i-1,j}) \right]
\end{aligned}
\tag{5.71}
$$

where

$$a_i = \frac{1}{6}\Delta r_i^2 (2r_i + r_{i+1}) \tag{5.72}$$

$$b_i = \frac{1}{6}\Delta r_i^2 (r_i + 2r_{i+1}) \tag{5.73}$$

$$c_i = a_{i-1} = \frac{1}{6}\Delta r_{i-1}^2 (2r_{i-1} + r_i) \tag{5.74}$$

$$d_i = b_{i-1} = \frac{1}{6}\Delta r_{i-1}^2 (r_{i-1} + 2r_i) \tag{5.75}$$

This equation is valid for all interior nodes, that is $i = 2, 3, \ldots, I$, $j = 2, 3, \ldots, J$; special consideration must be given to nodes which occur at corners and edges. We address the topic of corner and edge nodes, including boundary and source conditions in section 5.3.3.

5.3.2 Two Dimensional X - Y Geometry

To extend the range of application of the SP_N method, we have also derived the finite element equations for two dimensional X - Y geometry. These equations represent a simple modification of the R - Z equations. Specifically, we proceed by dividing the problem domain into an X - Y mesh of (I x J) rectangular cells, Figure 5.4, where material properties are again constant within a cell.

Let us examine the differential volume element dV in orthogonal curvilinear coordinates

$$dV = h_1 h_2 h_3 du_1 du_2 du_3 \tag{5.76}$$

where $h_i, i = 1, 2, 3$ are the scale factors. Then

R-Z geometry - $(u_1, u_2, u_3) = (r, \theta, z),\ dV = 2\pi r dr dz$

X-Y geometry - $(u_1, u_2, u_3) = (x, y, z),\ dA = dx dy$

We may then define a procedure that transforms the R-Z geometry finite element equations to the X-Y geometry finite element equations:

1. calculate mesh deltas $\Delta r_i, \Delta z_j$
2. set all $r_i = 1$
3. transform constant $C = 2\pi \rightarrow 1$
4. relabel variables $r_i \rightarrow x_i, z_j \rightarrow y_j$

When the X-Y geometry option is choosen by the user, this procedure is performed internally.

5.3.3 Boundary Conditions and Sources

In the derivation of the finite element equations, section 5.3.1, we have thus far considered only the interior nodes: $i = 2, 3, \ldots, I,\ j = 2, 3, \ldots, J$, in which case the surface integral contribution to Equation (5.57)

$$I_s = \oint_S \gamma_{i,j}^{(k)} \vec{\psi}_m^- \cdot \hat{n} dA \tag{5.77}$$

was found to be zero. If we consider the node (i,j) to lie on the boundary, that is any of the 4 corner nodes: $(1,1), (I+1,1), (1,J+1), (I+1,J+1)$, or any of the 4 edge nodes:

left edge - $(1,j)$, where $j = 2, \ldots, J$

right edge - $(I+1,j)$, where $j = 2, \ldots, J$

bottom edge - $(i,1)$, where $i = 2, \ldots, I$

top edge - $(i,J+1)$, where $i = 2, \ldots, I$

then the basis function $\gamma_{i,j}^{(k)}$ will be nonzero for at least one k value; and the surface integral, Equation (5.77), will not necessarily be zero. Furthermore, the finite element procedure applied to a corner node will involve integration over only one cell, and the procedure applied to a edge node will involve integration over two cells, this is in contrast to an interior node which required integration over the four cells surrounding the node (i,j). The reflective boundary condition, Equation (4.38), is given as

$$\vec{\psi}_m^- \cdot \hat{n} = 0 \qquad ,m = 1, (N+1)/2 \tag{5.78}$$

Substitution of Equation (5.78) into the surface integral gives zero, thus the refective boundary condition requires no modification of the interior equation. We refer to such a boundary condition (one which is satisfied automatically) as a *natural boundary condition.* The prescribed source boundary conditon, Equation (4.35), is given by

$$\vec{\psi}_m^- \cdot \hat{n} = \psi_m^+ - f_m \qquad ,m = 1,(N+1)/2 \tag{5.79}$$

and will produce a nonzero surface integral

$$\begin{aligned} \oint_S \gamma_{i,j}^{(k)} \vec{\psi}_m^- \cdot \hat{n} dA &= \oint_S \gamma_{i,j}^{(k)} [\psi_m^+ - f_m] dA \\ &\neq 0 \end{aligned} \tag{5.80}$$

Recall, the vacuum boundary condition is a special case of the incoming source boundary condition where $f_m = 0$, and a homogeneous isotropic boundary source is given as $f_m = \text{constant} \equiv \psi^{BDRY}$.

To illustrate the analysis of a corner/edge cell, let us consider the node (I+1,1) in the corner cell $(I,1)$, Figure 5.5, with reflective boundary conditions on the bottom surface, and incoming source boundary conditions on the right surface of the problem. The equation for (I+1,1) node will involve only coefficients c_4, c_5, c_7, c_8, in Equation (5.69). We calculate the surface integral contribution for the incoming source boundary condition, where the differential area element over the right surface is given by

$$dA = 2\pi r_{I+1} dz \tag{5.81}$$

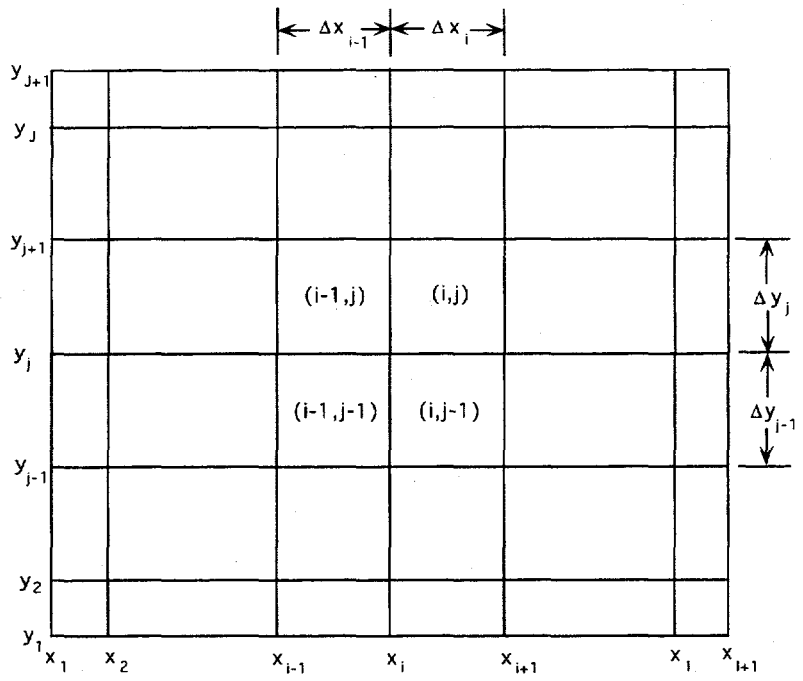

Figure 5.4: Two Dimensional X-Y Geometry Spatial Mesh

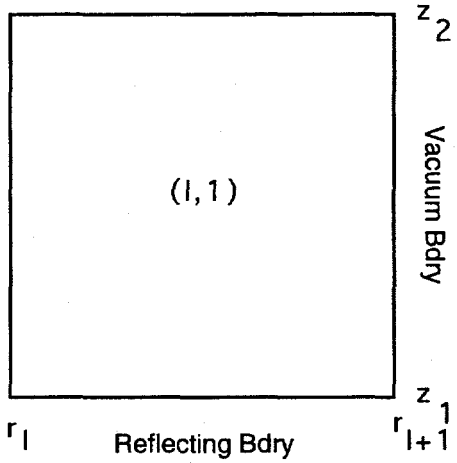

Figure 5.5: Corner Cell (I,1)

The surface integral then becomes

$$\begin{aligned}\frac{1}{2\pi}I_s &= \mu_m r_{I+1}\left[\int_{z_1}^{z_2} dz\gamma^{(4)}_{I+1,1}(r_{I+1},z)\psi^+_m(r_{I+1},z)\right. \\ &\quad \left. - \psi^{BDRY}\int_{z_1}^{z_2} dz\gamma^{(4)}_{I+1,1}(r_{I+1},z)\right] \\ &= \frac{1}{3}\mu_m r_{I+1}\Delta z_1\left(\psi^+_{I+1,1}+\frac{1}{2}\psi^+_{I+1,2}\right) \\ &\quad -\frac{1}{2}\mu_m r_{I+1}\Delta z_1\psi^{BDRY} \end{aligned} \tag{5.82}$$

The coefficients c_5, and c_8 are then modified

$$\begin{aligned} c'_5 &= c_5+\frac{1}{3}\mu_m r_{I+1}\Delta z_1 \\ c'_8 &= c_8+\frac{1}{6}\mu_m r_{I+1}\Delta z_1 \end{aligned} \tag{5.83}$$

and the boundary source term moved to the right hand side of the equation. The other corner/edge nodes may be analyzed in an analogous manner.

The boundary source may be specified as monoenergetic, or distributed in energy. We define the spectral distribution function χ_g, as

χ_g - the fraction of source particles emitted with energy E, in the range $E_g < E \leq E_{g-1}$

where

$$\sum_{g=1}^{G}\chi_g = 1 \tag{5.84}$$

and

$$\psi^{BDRY}_g = \chi_g\psi^{BDRY} \tag{5.85}$$

This completes the discretization of the multigroup canonical SP_N equations, and we now turn to the topic of their solution.

Chapter 6

Solution and Acceleration of the SP_N Equations

6.1 Introduction

In Chapters 2 through 5, we have derived and discretized the canonical SP_N equations. In this chapter, we address the topic of solution of the SP_N equations via iterative methods. We begin, section 6.2, by presenting the standard iterative procedure, the *Source Iteration* (SI) method; we then provide a abbreviated discussion of Fourier analysis, a mathematical technique used to examine the the stability and convergence rate of iterative schemes, and we perform a Fourier analysis of the continuous SP_N equations solved with the SI scheme. It is shown that in certain physical problems, that is optically thick systems with a scattering ratio $c \equiv \frac{\sigma_0}{\sigma_t}$ near unity, the SI method can converge very slowly. We then examine two methods which have been devised to accelerate the SI method. The first of these, the *Diffusion Synthetic Acceleration* (DSA) method, is developed in section 6.3, and a Fourier analysis is performed. The *Angular Multigrid* method, an extension of the DSA technique shown to be much more effective than DSA when scattering is highly forward peaked, is formulated in section 6.4, and applied to the electron groups. A comparison of the three iterative schemes is provided, and numerical results presented in Chapter 7, section 7.4. In the development of these acceleration schemes for the SP_N equations, we also discuss their effectiveness for the 1-D and 2-D S_N method. We conclude, section 6.5, with a discussion of particle conservation, particle production/loss rates, and energy deposition rates.

6.2 The Source Iteration Method

6.2.1 Description

Let us consider the group g canonical SP_N equations

$$-\mu_m^2 \vec{\nabla} \cdot \frac{1}{\sigma_t} \vec{\nabla} \psi_m^+ + \sigma_t \psi_m^+ = Q_m^+ - \mu_m \vec{\nabla} \cdot \left(\frac{\vec{\mathbf{Q}}_m^-}{\sigma_t} \right) \quad , m = 1, N/2 \tag{6.1}$$

$$\vec{\psi}_m^- = -\frac{\mu_m}{\sigma_t} \vec{\nabla} \psi_m^+ + \frac{1}{\sigma_t} \vec{\mathbf{Q}}_m^- \quad , m = 1, N/2 \tag{6.2}$$

where

$$Q_m^+ = \sum_{n=0,2}^{N-1} (2n+1) P_n(\mu_m) \sigma_n \phi_n + q_m^+ \tag{6.3}$$

$$\vec{\mathbf{Q}}_m^- = \sum_{n=1,3}^{N} (2n+1) P_n(\mu_m) \sigma_n \vec{\phi}_n + \vec{\mathbf{q}}_m^- \tag{6.4}$$

$$\phi_n = 2 \sum_{m=1}^{N/2} P_n(\mu_m) \psi_m^+ w_m \qquad \text{,for } n \text{ even} \tag{6.5}$$

$$\vec{\phi}_n = 2 \sum_{m=1}^{N/2} P_n(\mu_m) \vec{\psi}_m^- w_m \qquad \text{,for } n \text{ odd} \tag{6.6}$$

here, we have supressed the group index g, and the fixed source terms q_m^+, $\vec{\mathbf{q}}_m^-$, include the distributed sources, and the g' to g scattering sources, where $g' \neq g$. The sum terms in Q_m^+, $\vec{\mathbf{Q}}_m^-$ are referred to as the within-group scattering sources. The problem

can be solved iteratively by the *Source Iteration* (SI) *method*, which is described by

$$-\mu_m^2 \vec{\nabla} \cdot \frac{1}{\sigma_t} \vec{\nabla} \psi_m^{+(l+1)} + \sigma_t \psi_m^{+(l+1)} = Q_m^{+(l)} - \mu_m \vec{\nabla} \cdot \left(\frac{\vec{\mathbf{Q}}_m^{-(l)}}{\sigma_t} \right) \quad , m = 1, N/2 \tag{6.7}$$

$$\vec{\psi}_m^{-(l+1)} = -\frac{\mu_m}{\sigma_t} \vec{\nabla} \psi_m^{+(l+1)} + \frac{1}{\sigma_t} \vec{\mathbf{Q}}_m^{-(l)} \quad , m = 1, N/2 \tag{6.8}$$

$$\phi_n^{(l+1)} = 2 \sum_{m=1}^{N/2} P_n(\mu_m) \psi_m^{+(l+1)} w_m \qquad \text{,for } n \text{ even} \tag{6.9}$$

$$\vec{\phi}_n^{(l+1)} = 2 \sum_{m=1}^{N/2} P_n(\mu_m) \vec{\psi}_m^{-(l+1)} w_m \qquad \text{,for } n \text{ odd} \tag{6.10}$$

$$Q_m^{+(l+1)} = \sum_{n=0,2}^{N-1} (2n+1) P_n(\mu_m) \sigma_n \phi_n^{(l+1)} + q_m^+ \tag{6.11}$$

$$\vec{\mathbf{Q}}_m^{-(l+1)} = \sum_{n=1,3}^{N} (2n+1) P_n(\mu_m) \sigma_n \vec{\phi}_n^{(l+1)} + \vec{\mathbf{q}}_m^- \tag{6.12}$$

where l is the inner iteration index. The iteration process begins with some initial guess for the even and odd parity sources $Q_m^{+(0)}, \vec{\mathbf{Q}}_m^{-(0)}$. One then calculates the even-parity fluxes for all m, by solving Equation (6.7), and then the odd-parity fluxes for all m, using Equation (6.8). Next, the flux moments are calculated, Equations (6.9) and (6.10), and new source terms are calculated using Equations (6.11) and (6.12). After two inner iterations a convergence test is performed. The relative error is calculated using the L^2 norm of the scalar flux, and the L^2 norm of the scalar flux residual

$$e^{(l+1)} = \sqrt{\frac{\sum_k |\phi_k^{(l+1)} - \phi_k^{(l)}|^2}{\sum_k |\phi_k^{(l+1)}|^2}} \tag{6.13}$$

where k is the spatial index. If the error criterion

$$e^{(l+1)} < \epsilon \left(1 - \rho^{(l+1)}\right) \tag{6.14}$$

is not satisfied, where $\rho^{(l)}$ is the spectral radius defined in Equation (6.15), and ϵ is typically 10^{-6}, new within-group scattering sources are calculated, and another iteration is performed. When the error criterion is satisfied, the group g calculation is terminated. Furthermore, we require $\epsilon_{inner} < \epsilon_{outer}$, where ϵ_{inner} is the error tolerance on the inner iterations, and ϵ_{outer} is the error tolerance on the outer iterations.

6.2.2 Continuous Fourier Analysis

The convergence rate of an iterative scheme is determined by the spectral radius ρ [2] (see Appendix A), which is defined as

$$\rho \equiv \lim_{l \to \infty} \left| \frac{\phi - \phi^{(l+1)}}{\phi - \phi^{(l)}} \right| \tag{6.15}$$

The spectral radius can be interpreted as the smallest possible reduction in the relative error between successive iterates, that is $e \approx \rho^l$. We may estimate the number of iterations required to reach a specified convergence criterion ($e < \epsilon$) using

$$N \approx \frac{\log \epsilon}{\log \rho} \tag{6.16}$$

An iteration scheme is stable if $\rho \leq 1$, and convergent if $\rho < 1$. Note from Equation (6.16) that the smaller the value of ρ, the fewer number of iterations required to converge. Fourier analysis is a mathematical technique that allows one to examine the stability and convergence rate of an iterative scheme by providing an estimate of

the spectral radius. Let us proceed with a Fourier analysis of the SI scheme for the continuous SP_N equations. To begin, we make the following definitions

$$\epsilon_m^{+(l+1)} = \psi_m^+ - \psi_m^{+(l+1)} \tag{6.17}$$

$$\vec{\epsilon}_m^{-(l+1)} = \vec{\psi}_m^- - \vec{\psi}_m^{-(l+1)} \tag{6.18}$$

where $\epsilon_m^{+(l)}$ and $\vec{\epsilon}_m^{-(l)}$ represent the error at the lth iterate. Subtracting Equation (6.7) from (6.1), and Equation (6.8) from (6.2), we obtain the error equations

$$-\mu_m^2 \vec{\nabla} \cdot \frac{1}{\sigma_t} \vec{\nabla} \epsilon_m^{+(l+1)} + \sigma_t \epsilon_m^{+(l+1)} = \hat{S}^+ \epsilon_m^{+(l)} - \mu_m \vec{\nabla} \cdot \left(\frac{\hat{S}^- \vec{\epsilon}_m^{-(l)}}{\sigma_t} \right) \tag{6.19}$$

$$\vec{\epsilon}_m^{-(l+1)} = -\frac{\mu_m}{\sigma_t} \vec{\nabla} \epsilon_m^{+(l+1)} + \frac{1}{\sigma_t} \hat{S}^- \vec{\epsilon}_m^{-(l)} \tag{6.20}$$

where, for simplicity, we have represented the sources

$$Q_m^{+(l)} = \hat{S}^+ \psi_m^{+(l)} + q_m^+ \tag{6.21}$$

$$\vec{\mathbf{Q}}_m^{-(l)} = \hat{S}^- \vec{\psi}_m^{-(l)} + \vec{\mathbf{q}}_m^- \tag{6.22}$$

in terms of the scattering operators $\hat{S}^+, \hat{S}^-$. We now assume a homogeneous, infinite medium in X - Y geometry, and substitute the Fourier ansatz

$$\epsilon_m^{+(l)}(\vec{\mathbf{r}}, \lambda_x, \lambda_y) = \epsilon_m^{+(l)} \exp\left[i(\lambda_x x + \lambda_y y)\right] \tag{6.23}$$

$$\vec{\epsilon}_m^{-(l)}(\vec{\mathbf{r}}, \lambda_x, \lambda_y) = \vec{\epsilon}_m^{-(l)} \exp\left[i(\lambda_x x + \lambda_y y)\right] \tag{6.24}$$

where $i = \sqrt{-1}$, $-\infty < \lambda_x < \infty$, and $-\infty < \lambda_y < \infty$. We obtain the following coupled set of equations

$$\frac{\mu_m^2}{\sigma_t}(\lambda_x^2 + \lambda_y^2)\epsilon_m^{+(l+1)} + \sigma_t \epsilon_m^{+(l+1)} = \hat{S}^+ \epsilon_m^{+(l)} - \frac{i\mu_m}{\sigma_t}(\lambda_x \hat{S}^- \epsilon_{x,m}^{-(l)} + \lambda_y \hat{S}^- \epsilon_{y,m}^{-(l)}) \quad (6.25)$$

$$\epsilon_{x,m}^{-(l+1)} + \frac{i\lambda_x \mu_m}{\sigma_t}\epsilon_m^{+(l+1)} = \frac{\hat{S}^-}{\sigma_t}\epsilon_{x,m}^{-(l)} \quad (6.26)$$

$$\epsilon_{y,m}^{-(l+1)} + \frac{i\lambda_y \mu_m}{\sigma_t}\epsilon_m^{+(l+1)} = \frac{\hat{S}^-}{\sigma_t}\epsilon_{y,m}^{-(l)} \quad (6.27)$$

An analysis of the SI scheme has been performed for an S_4 calculation, after calculating the scattering operators, we arrive at the matrix form of Equations (6.25) - (6.27)

$$\mathbf{A}\begin{bmatrix} \epsilon_1^+ \\ \epsilon_2^+ \\ \epsilon_{x,1}^- \\ \epsilon_{y,1}^- \\ \epsilon_{x,2}^- \\ \epsilon_{y,2}^- \end{bmatrix}^{(l+1)} = \mathbf{B}\begin{bmatrix} \epsilon_1^+ \\ \epsilon_2^+ \\ \epsilon_{x,1}^- \\ \epsilon_{y,1}^- \\ \epsilon_{x,2}^- \\ \epsilon_{y,2}^- \end{bmatrix}^{(l)} \quad (6.28)$$

where

$$\mathbf{A} = \begin{bmatrix} \alpha_1 & 0 & 0 & 0 & 0 & 0 \\ 0 & \alpha_2 & 0 & 0 & 0 & 0 \\ \beta_1 & 0 & 1 & 0 & 0 & 0 \\ \gamma_1 & 0 & 0 & 1 & 0 & 0 \\ 0 & \beta_2 & 0 & 0 & 1 & 0 \\ 0 & \gamma_2 & 0 & 0 & 0 & 1 \end{bmatrix} \quad (6.29)$$

$$\mathbf{B} = \begin{bmatrix} c_1^{(1)} & c_1^{(2)} & -\beta_1 c_1^{(3)} & -\gamma_1 c_1^{(3)} & -\beta_1 c_1^{(4)} & -\gamma_1 c_1^{(4)} \\ c_2^{(1)} & c_2^{(2)} & -\beta_2 c_2^{(3)} & -\gamma_2 c_2^{(3)} & -\beta_2 c_2^{(4)} & -\gamma_2 c_2^{(4)} \\ 0 & 0 & \frac{c_1^{(3)}}{\sigma_t} & 0 & \frac{c_1^{(4)}}{\sigma_t} & 0 \\ 0 & 0 & 0 & \frac{c_1^{(3)}}{\sigma_t} & 0 & \frac{c_1^{(4)}}{\sigma_t} \\ 0 & 0 & \frac{c_2^{(3)}}{\sigma_t} & 0 & \frac{c_2^{(4)}}{\sigma_t} & 0 \\ 0 & 0 & 0 & \frac{c_2^{(3)}}{\sigma_t} & 0 & \frac{c_2^{(4)}}{\sigma_t} \end{bmatrix} \tag{6.30}$$

and the matrix elements are given by

$$\alpha_m \equiv \frac{\mu_m^2}{\sigma_t}(\lambda_x^2 + \lambda_y^2) + \sigma_t \tag{6.31}$$

$$\beta_m \equiv \frac{i\lambda_x \mu_m}{\sigma_t} \tag{6.32}$$

$$\gamma_m \equiv \frac{i\lambda_y \mu_m}{\sigma_t} \tag{6.33}$$

$$\hat{S}^+ \epsilon_m^{+(l)} \equiv c_m^{(1)} \epsilon_1^{+(l)} + c_m^{(2)} \epsilon_2^{+(l)} \tag{6.34}$$

$$\hat{S}^- \epsilon_{x,m}^{-(l)} \equiv c_m^{(3)} \epsilon_{x,1}^{-(l)} + c_m^{(4)} \epsilon_{x,2}^{-(l)} \tag{6.35}$$

$$\hat{S}^- \epsilon_{y,m}^{-(l)} \equiv c_m^{(3)} \epsilon_{y,1}^{-(l)} + c_m^{(4)} \epsilon_{y,2}^{-(l)} \tag{6.36}$$

The spectral radius is given as the largest eigenvalue moduli of the iteration matrix [2] (see Appendix A) $\mathbf{M} = \mathbf{A}^{-1}\mathbf{B}$.

$$\rho = \max_{\lambda} \|\omega(\lambda)\| \tag{6.37}$$

Let us now list the results of our analysis: For an infinite medium problem the SI method is shown to be unconditionally stable, but has arbitrarily poor convergence as $c \to 1$. For a finite medium problem $\rho < c$ because of leakage; however, as the

medium becomes optically thick $\rho \to c$. This is the same behavior exhibited by the S_N method in all dimensions.

6.3 The Diffusion Synthetic Acceleration Method

6.3.1 Description

The *Diffusion Synthetic Acceleration Scheme* (DSA) has been shown to be an effective method of accelerating the convergence rate of the SI method [20] in 1-D S_N calculations. This two stage iterative procedure is based upon solving a "low order" S_2 (or P_1) calculation to produce additive correction terms which are then used to accelerate the "high order" transport calculation.

Neglecting spatial discretization, the Diffusion Synthetic Acceleration Scheme (DSA) is given as

$$-\mu_m^2 \vec{\nabla} \cdot \frac{1}{\sigma_t} \vec{\nabla} \psi_m^{+(l+\frac{1}{2})} + \sigma_t \psi_m^{+(l+\frac{1}{2})} = Q_m^{+(l)} - \mu_m \vec{\nabla} \cdot \left(\frac{\vec{\mathbf{Q}}_m^{-(l)}}{\sigma_t} \right) \quad ,m = 1, N/2 \tag{6.38}$$

$$\vec{\psi}_m^{-(l+\frac{1}{2})} = -\frac{\mu_m}{\sigma_t} \vec{\nabla} \psi_m^{+(l+\frac{1}{2})} + \frac{1}{\sigma_t} \vec{\mathbf{Q}}_m^{-(l)} \quad ,m = 1, N/2 \tag{6.39}$$

$$\phi_n^{(l+\frac{1}{2})} = 2 \sum_{m=1}^{N/2} P_n(\mu_m) \psi_m^{+(l+\frac{1}{2})} w_m \qquad \text{,for } n \text{ even} \tag{6.40}$$

$$\vec{\phi}_n^{(l+\frac{1}{2})} = 2 \sum_{m=1}^{N/2} P_n(\mu_m) \vec{\psi}_m^{-(l+\frac{1}{2})} w_m \qquad \text{,for } n \text{ odd} \tag{6.41}$$

$$R_0^{(l+\frac{1}{2})} = \sigma_0 (\phi_0^{(l+\frac{1}{2})} - \phi_0^{(l)}) \tag{6.42}$$

$$\vec{\mathbf{R}}_1^{(l+\frac{1}{2})} = \sigma_1(\vec{\phi}_1^{(l+\frac{1}{2})} - \vec{\phi}_1^{(l)}) \tag{6.43}$$

$$-\frac{1}{3}\vec{\nabla}\cdot\frac{1}{\sigma_{tr}}\vec{\nabla}c_0^{(l+\frac{1}{2})} + \sigma_a c_0^{(l+\frac{1}{2})} = R_0^{(l+\frac{1}{2})} - \vec{\nabla}\cdot\left(\frac{\vec{\mathbf{R}}_1^{(l+\frac{1}{2})}}{\sigma_{tr}}\right) \tag{6.44}$$

$$\vec{\mathbf{c}}_1^{-(l+\frac{1}{2})} = -\frac{1}{3\sigma_{tr}}\vec{\nabla}c_0^{(l+\frac{1}{2})} + \frac{1}{\sigma_{tr}}\vec{\mathbf{R}}_1^{(l+\frac{1}{2})} \tag{6.45}$$

$$\psi_m^{+(l+1)} = \psi_m^{+(l+\frac{1}{2})} + c_0^{(l+\frac{1}{2})} \tag{6.46}$$

$$\vec{\psi}_m^{-(l+1)} = \vec{\psi}_m^{-(l+\frac{1}{2})} + 3\mu_m\vec{\mathbf{c}}_1^{(l+\frac{1}{2})} \tag{6.47}$$

where the transport and absorption cross sections are defined as

$$\sigma_{tr} \equiv \sigma_t - \sigma_1 \tag{6.48}$$

$$\sigma_a \equiv \sigma_t - \sigma_0 \tag{6.49}$$

Equations (6.38) through (6.41) correspond to the standard unaccelerated source iteration scheme. One first solves the SP_N equations using sources constructed from the previous iterate flux moments, and then one calculates new fluxes using the latest iterate angular fluxes. If there were no acceleration, these two steps would constitute a complete iteration. Convergence acceleration is achieved by calculating additive correction terms for the angular fluxes by solving Equations (6.44) and (6.45). The motivation for Equations (6.44) and (6.45) derives from the fact that the exact correction for the angular flux at the $(l+\frac{1}{2})$ iterate is given by

$$\epsilon_m^{+(l+\frac{1}{2})} = \psi_m^{+} - \psi_m^{+(l+\frac{1}{2})} \tag{6.50}$$

$$\vec{\epsilon}_m^{-(l+\frac{1}{2})} = \vec{\psi}_m^{-} - \vec{\psi}_m^{-(l+\frac{1}{2})} \tag{6.51}$$

where $\psi_m^+, \vec{\psi}_m^-$ represent the exact solution, and the corrections satisfy

$$-\mu_m^2 \vec{\nabla} \cdot \frac{1}{\sigma_t} \vec{\nabla} \epsilon_m^{+(l+\frac{1}{2})} + \sigma_t \epsilon_m^{+(l+\frac{1}{2})} = (Q_m^+ - Q_m^{+(l)}) - \mu_m \vec{\nabla} \cdot \left(\frac{\vec{\mathbf{Q}}_m^- - \vec{\mathbf{Q}}_m^{-(l)}}{\sigma_t} \right) \tag{6.52}$$

$$\vec{\epsilon}_m^{-(l+\frac{1}{2})} = -\frac{\mu_m}{\sigma_t} \vec{\nabla} \epsilon_m^{+(l+\frac{1}{2})} + \frac{1}{\sigma_t} \left(\vec{\mathbf{Q}}_m^- - \vec{\mathbf{Q}}_m^{-(l)} \right) \tag{6.53}$$

These equations are exact, but just as difficult to solve as the original problem. In the DSA procedure we replace Equations (6.52) and (6.53) with a S_2 (P_1) aproximation or *diffusion* approximation, and Equations (6.44) and (6.45) result. Boundary conditions for the correction equations are the same as the original equations, with the exception of the incoming source boundary condition which is replaced by a vacuum boundary condition, so as not to include the source twice. Once c_0, and $\vec{\mathbf{c}}_1$ have been obtained, the angular fluxes are corrected or updated according to Equations (6.46) and (6.47). This completes the iteration.

6.3.2 Continuous Fourier Analysis

The analysis of the DSA scheme is made for a S_4 calculation following the same procedure outlined in section 6.2.2 for the SI method. In this section we will only display the results. We substitute the Fourier ansatz

$$\epsilon_m^{+(l)}(\vec{\mathbf{r}}, \lambda_x, \lambda_y) = \epsilon_m^{+(l)} f(\vec{\mathbf{r}}, \lambda_x, \lambda_y) \tag{6.54}$$

$$\vec{\epsilon}_m^{-(l)}(\vec{\mathbf{r}}, \lambda_x, \lambda_y) = \vec{\epsilon}_m^{-(l)} f(\vec{\mathbf{r}}, \lambda_x, \lambda_y) \tag{6.55}$$

$$R_0^{(l)}(\vec{\mathbf{r}}, \lambda_x, \lambda_y) = R_0^{(l)} f(\vec{\mathbf{r}}, \lambda_x, \lambda_y) \tag{6.56}$$

$$\vec{\mathbf{R}}_1^{(l)}(\vec{\mathbf{r}}, \lambda_x, \lambda_y) = \vec{\mathbf{R}}_1^{(l)} f(\vec{\mathbf{r}}, \lambda_x, \lambda_y) \tag{6.57}$$

where

$$f(\vec{\mathbf{r}}, \lambda_x, \lambda_y) = \exp\left[i(\lambda_x x + \lambda_y y)\right] \tag{6.58}$$

and arrive at the final matrix equation

$$\begin{aligned} \vec{\mathbf{E}}^{(l+1)} &= \left[\mathbf{A}^{-1}\mathbf{B} + \mathbf{G}\,\mathbf{D}^{-1}\mathbf{F}\,\mathbf{C}(\mathbf{A}^{-1}\mathbf{B} - \mathbf{I})\right]\vec{\mathbf{E}}^{(l)} \\ &\equiv \mathbf{M}\vec{\mathbf{E}}^{(l)} \end{aligned} \tag{6.59}$$

where $\mathbf{M}$ is the iteration matrix, $\mathbf{I}$ is the identity matrix, matrices $\mathbf{A}$ and $\mathbf{B}$ are previously defined, Equations (6.27), (6.28), and the remaining matrices are given as

$$\mathbf{C} = 2\begin{bmatrix} \sigma_0 w_1 & \sigma_0 w_2 & 0 & 0 & 0 & 0 \\ 0 & 0 & \sigma_1 P_1(\mu_1) w_1 & 0 & \sigma_1 P_1(\mu_2) w_2 & 0 \\ 0 & 0 & 0 & \sigma_1 P_1(\mu_1) w_1 & 0 & \sigma_1 P_1(\mu_2) w_2 \end{bmatrix} \tag{6.60}$$

$$\mathbf{D} = \begin{bmatrix} \frac{1}{3\sigma_{tr}}(\lambda_x^2 + \lambda_y^2) + \sigma_a & 0 & 0 \\ \frac{i\lambda_x}{\sqrt{3}\sigma_{tr}} & 1 & 0 \\ \frac{i\lambda_y}{\sqrt{3}\sigma_{tr}} & 0 & 1 \end{bmatrix} \tag{6.61}$$

$$\mathbf{F} = \begin{bmatrix} 1 & \frac{-i\lambda_x}{\sigma_{tr}} & \frac{-i\lambda_y}{\sigma_{tr}} \\ 0 & \frac{\sqrt{3}}{\sigma_{tr}} & 0 \\ 0 & 0 & \frac{\sqrt{3}}{\sigma_{tr}} \end{bmatrix} \tag{6.62}$$

$$\mathbf{G} = \begin{bmatrix} 1 & 0 & 0 \\ 1 & 0 & 0 \\ 0 & \sqrt{3}\mu_1 & 0 \\ 0 & 0 & \sqrt{3}\mu_1 \\ 0 & \sqrt{3}\mu_2 & 0 \\ 0 & 0 & \sqrt{3}\mu_2 \end{bmatrix} \tag{6.63}$$

In the analysis of the DSA procedure we obtain a spectral radius ρ =.184 for $c = 1$; this is in contrast to the SI procedure which produced a spectral radius ρ =1 for $c = 1$. Fourier analysis of the 1-D and 2-D SP_N equations produced identical results. We wish to emphasize that previous analyses indicate the DSA method is stable for 1-D S_N, but unstable for the multidimensional case.

6.4 The Angular Multigrid Acceleration Method

The DSA method becomes ineffective as scattering becomes increasingly forward peaked. An *Angular Multigrid* method [21] is developed in this section, which is effective in acceleration of the electron groups. Let us begin by considering the general matrix problem

$$\mathbf{H}f = q \tag{6.64}$$

which may be solved iteratively by splitting the coefficient matrix

$$\mathbf{H} = \mathbf{A} - \mathbf{B} \tag{6.65}$$

and specifying an iteration scheme

$$f^{(l+1)} = \mathbf{A}^{-1}\mathbf{B}f^{(l)} + \mathbf{A}^{-1}q \tag{6.66}$$

By manipulating Equations (6.64), (6.65), and (6.66), it may be shown that the exact error in f at the $(l+1)$th iterate satisfies

$$\mathbf{H}\epsilon^{(l+1)} = r^{(l+1)} \tag{6.67}$$

where the error is defined by

$$\epsilon^{(l+1)} = f - f^{(l+1)} \tag{6.68}$$

and the residual is defined as

$$r^{(l+1)} = q - \mathbf{H}f^{(l+1)} \tag{6.69}$$

We may then obtain the exact error in $f^{(l+1)}$ by solving Equation (6.67); however, Equation (6.67) is just as difficult to solve as the original problem ,Equation (6.64). The main idea of synthetic acceleration is to obtain an estimate of the error in $f^{(l+1)}$ by solving Equation (6.67) with a low-rank approximation to $\mathbf{H}$. The accelerated scheme then takes the form

$$f^{(l+\frac{1}{2})} = \mathbf{A}^{-1}\mathbf{B}f^{(l)} + \mathbf{A}^{-1}q \tag{6.70}$$

$$r^{(l+\frac{1}{2})} = q - \mathbf{H}f^{(l+\frac{1}{2})} \tag{6.71}$$

$$c^{(l+\frac{1}{2})} = \mathbf{H}_L^{-1}\mathbf{P}r^{(l+\frac{1}{2})} \tag{6.72}$$

$$f^{(l+1)} = f^{(l+\frac{1}{2})} + \mathbf{T}c^{(l+\frac{1}{2})} \tag{6.73}$$

where

$\mathbf{H}_L$=low-rank operator

P=projection operator that maps the high-rank residual to the low-rank space of $\mathbf{H}_L$

T=interpolation operator that maps the low-rank correction to the high-rank space of **H**

Synthetic acceleration is effective if the low-rank operator is easy to invert, and the low-rank operator attenuates the error modes which are not well attenuated by the basic iteration scheme. The DSA scheme, presented in section 6.3, may be viewed as a SP_N transport sweep followed by a diffusion solve, where the P_1 diffusion operator is the low rank approximation to the transport operator (i.e. a 2 grid method). The projection and interpolation operators are defined in terms of the Legendre moments. To illustrate the angular multigrid method, we now specify the angular multigrid acceleration scheme for the canonical SP_N equations for a S_{16} calculation.

1. Transport sweep on S_{16} grid

$$-\mu_m^{(1)2}\vec{\nabla}\cdot\frac{1}{\sigma_t^{(1)}}\vec{\nabla}\psi_m^{+(l+\frac{1}{2})}+\sigma_t^{(1)}\psi_m^{+(l+\frac{1}{2})} = Q_m^{+(l)}-\mu_m^{(1)}\vec{\nabla}\cdot\left(\frac{\vec{\mathbf{Q}}_m^{-(l)}}{\sigma_t^{(1)}}\right) \quad ,m=1,2,\ldots,8 \tag{6.74}$$

$$\vec{\psi}_m^{-(l+\frac{1}{2})} = -\frac{\mu_m^{(1)}}{\sigma_t^{(1)}}\vec{\nabla}\psi_m^{+(l+\frac{1}{2})}+\frac{1}{\sigma_t^{(1)}}\vec{\mathbf{Q}}_m^{-(l)} \quad ,m=1,2,\ldots,8 \tag{6.75}$$

$$\phi_n^{(l+\frac{1}{2})} = 2\sum_{m=1}^{8}P_n[\mu_m^{(1)}]\psi_m^{+(l+\frac{1}{2})}w_m^{(1)} \qquad ,n=0,2,\ldots,6 \tag{6.76}$$

$$\vec{\phi}_n^{(l+\frac{1}{2})} = 2\sum_{m=1}^{8}P_n[\mu_m^{(1)}]\vec{\psi}_m^{-(l+\frac{1}{2})}w_m^{(1)} \qquad ,n=1,3,\ldots,7 \tag{6.77}$$

2. Transport sweep on S_8 grid (first coarse grid) with P_7 expansion for the S_{16} residual

$$-\mu_m^{(2)2}\vec{\nabla}\cdot\frac{1}{\sigma_t^{(2)}}\vec{\nabla}c_m^{(2)}+\sigma_t^{(2)}c_m^{(2)} = \sum_{n=0,2}^{6}(2n+1)\sigma_n^{(1)}(\phi_n^{l+\frac{1}{2}}-\phi_n^l)P_n[\mu_m^{(2)}] - \mu_m^{(2)}\vec{\nabla}\cdot\frac{1}{\sigma_t^{(2)}}\sum_{n=1,3}^{7}(2n+1)\sigma_n^{(1)}(\vec{\phi}_n^{l+\frac{1}{2}}-\vec{\phi}_n^l)P_n[\mu_m^{(2)}] \quad ,m=1,2,\ldots,4 \qquad (6.78)$$

$$\vec{c}_m^{(2)} = -\frac{\mu_m^{(2)}}{\sigma_t^{(2)}}\vec{\nabla}c_m^{(2)}+\frac{1}{\sigma_t^{(2)}}\sum_{n=1,3}^{7}(2n+1)\sigma_n^{(1)}(\vec{\phi}_n^{l+\frac{1}{2}}-\vec{\phi}_n^l)P_n[\mu_m^{(2)}] \quad ,m=1,2,\ldots,4 \qquad (6.79)$$

$$\xi_n^{(2)}=2\sum_{m=1}^{4}P_n[\mu_m^{(2)}]c_m^{(2)}w_m^{(2)} \qquad ,n=0,2,\ldots,6 \qquad (6.80)$$

$$\vec{\xi}_n^{(2)}=2\sum_{m=1}^{4}P_n[\mu_m^{(2)}]\vec{c}_m^{(2)}w_m^{(2)} \qquad ,n=1,3,\ldots,7 \qquad (6.81)$$

3. Transport sweep on S_4 grid (second coarse grid) with P_3 expansion for the S_8 residual

$$-\mu_m^{(3)2}\vec{\nabla}\cdot\frac{1}{\sigma_t^{(3)}}\vec{\nabla}c_m^{(3)}+\sigma_t^{(3)}c_m^{(3)} = \sum_{n=0}^{2}(2n+1)\sigma_n^{(2)}\xi_n^{(2)}P_n[\mu_m^{(3)}] - \mu_m^{(3)}\vec{\nabla}\cdot\frac{1}{\sigma_t^{(3)}}\sum_{n=1}^{3}(2n+1)\sigma_n^{(2)}\vec{\xi}_n^{(2)}P_n[\mu_m^{(3)}] \quad ,m=1,2 \qquad (6.82)$$

$$\vec{c}_m^{(3)} = -\frac{\mu_m^{(3)}}{\sigma_t^{(3)}}\vec{\nabla}c_m^{(3)}+\frac{1}{\sigma_t^{(3)}}\sum_{n=1}^{3}(2n+1)\sigma_n^{(2)}\vec{\xi}_n^{(2)}P_n[\mu_m^{(3)}] \quad ,m=1,2 \qquad (6.83)$$

$$\xi_n^{(3)} = 2\sum_{m=1}^{2} P_n[\mu_m^{(3)}]c_m^{(3)}w_m^{(3)} \qquad ,n = 0,2 \tag{6.84}$$

$$\vec{\xi}_n^{(3)} = 2\sum_{m=1}^{2} P_n[\mu_m^{(3)}]\vec{c}_m^{(3)}w_m^{(3)} \qquad ,n = 1,3 \tag{6.85}$$

4. Solve the diffusion equation with P_1 expansion for the S_4 residual as an inhomogeneous source

$$-\vec{\nabla}\cdot D\vec{\nabla}\xi_0^{(4)} + \sigma_a^{(3)}\xi_0^{(4)} = \sigma_0^{(3)}\xi_0^{(3)} - \vec{\nabla}\cdot\frac{\sigma_1^{(3)}}{\sigma_{tr}^{(3)}}\vec{\xi}_1^{(3)} \tag{6.86}$$

$$\vec{\xi}_1^{(4)} = -D\vec{\nabla}\xi_0^{(4)} + \frac{\sigma_1^{(3)}}{\sigma_{tr}^{(3)}}\vec{\xi}_1^{(3)} \tag{6.87}$$

5. Update angular fluxes

$$\psi_m^{+(l+1)} = \psi_m^{+(l+\frac{1}{2})} + \sum_{n=0,2}^{6}(2n+1)\xi_n P_n[\mu_m^{(1)}] \tag{6.88}$$

$$\vec{\psi}_m^{-(l+1)} = \vec{\psi}_m^{-(l+\frac{1}{2})} + \sum_{n=1,3}^{7}(2n+1)\vec{\xi}_n P_n[\mu_m^{(1)}] \qquad ,m = 1,2,\ldots,8 \tag{6.89}$$

where

$$\begin{aligned}
\xi_0 &= \xi_0^{(2)} + \xi_0^{(3)} + \xi_0^{(4)} \\
\vec{\xi}_1 &= \vec{\xi}_1^{(2)} + \vec{\xi}_1^{(3)} + \vec{\xi}_1^{(4)} \\
\xi_2 &= \xi_2^{(2)} + \xi_2^{(3)} \\
\vec{\xi}_3 &= \vec{\xi}_3^{(2)} + \vec{\xi}_3^{(3)} \\
\xi_4 &= \xi_4^{(2)} \\
\vec{\xi}_5 &= \vec{\xi}_5^{(2)}
\end{aligned}$$

$$\begin{aligned} \xi_6 &= \xi_6^{(2)} \\ \vec{\xi}_7 &= \vec{\xi}_7^{(2)} \end{aligned} \tag{6.90}$$

and

$\mu_m^{(i)}$=cosine for direction m on grid i

$w_m^{(i)}$=weight for direction m on grid i

$D = \frac{1}{3\sigma_{tr}}$

$\sigma_l^{(i)}$=Legendre moment of degree l of the cross section for grid i, where

$$\begin{aligned} \delta\sigma^{(i)} &\equiv \frac{1}{2}(\sigma_{N/2}^{(i-1)} + \sigma_{N-1}^{(i-1)}) \\ \sigma_l^{(i)} &= \sigma_l^{(i-1)} - \delta\sigma^{(i)} \qquad , l = 0, \ldots, N-1 \end{aligned} \tag{6.91}$$

The transport sweep attenuates the errors in the *upper half* of the Legendre flux moments, provided the cross sections are "corrected" on each grid, as given by Equation (6.91). This cross section correction modifies the convergence rate of the transport sweep, while the equation solution remains invariant. Again, boundary conditions for the correction equations are the same as the original equations with the exception of incoming source boundary condition, which is replaced by a vacuum boundary condition. The net effect of a single transport sweep in conjunction with a projection to lower order space is the attenuation of the errors in the *upper three quarters* of the Legendre flux moments. One may then continue this process through multiple levels, attenuating a larger fraction of the error modes with an increasing number of grids. The diffusion solve on the final grid attenuates errors not attenuated by the transport sweeps on the upper levels.

It may at first appear as if a large number of coarse grids would require an inordinate amount of computational work. However, it is easily shown that this is not the case. To illustrate, let us measure computational work in a system where 1 unit equals the work required to solve the fine grid problem. Let us also assume that the work required to solve each equation is constant, and that the fine grid problem involves X equations. Then a 2 grid problem (fine grid plus a single coarse grid) would involve X plus $X/2$ equations, and the total work required is 3/2. We may then continue this summing process through an indefinite number of grids, and we see that the total work required is bounded by a limiting value of 2. That is, a problem with an infinite number of grids would require twice the amount of work as is required to solve the unaccelerated or fine grid problem. Multigrid acceleration becomes increasingly effective, relative to DSA, as N increases. For 1-D S_N multigrid acceleration is stable. Since DSA is unstable for multigeometry S_N, and is contained in the multigrid method, then multigrid is also unstable for multigeometry S_N.

6.5 Particle Conservation and the Calculation of Energy Deposition Rates

Particle production (distributed sources, boundary sources) and loss (absorption, leakage) rates are calculated for each group using:

$$\text{abs. rate} = \int_V \sigma_a \phi dV \tag{6.92}$$

$$\text{dist. source} = 2 \sum_{m=1}^{N/2} \int_V q_m^+ w_m dV \tag{6.93}$$

$$\text{bdry. source} = \sum_{m=1}^{N/2} \oint_S \psi^{BDRY} \mu_m w_m dA \tag{6.94}$$

$$\text{leak. rate} = 2 \sum_{m=1}^{N/2} \oint_S (\psi_m^+ - \frac{1}{2} \psi^{BDRY}) \mu_m w_m dA \tag{6.95}$$

where V is the total problem volume, S is the problem surface, and

$$\sigma_{ag} \equiv \sigma_{tg} - \sum_{g'=1}^{G} \sigma_{s0,g\to g'} \tag{6.96}$$

Rates are then summed over appropriate groups, and tabulated for electrons and photons. Particle balance is calculated using the equation

$$\text{bal} = \frac{(\text{dist. source} + \text{bdry. source} - \text{abs. rate} - \text{leak. rate})}{(\text{dist. source} + \text{bdry. source})} \tag{6.97}$$

and checked to be zero to verify particle conservation.

Energy deposition rates are calculated for each group, using the CEPXS energy deposition cross sections. Three different average rates are calculated volumetric, axial, and radial, given as

$$EDR = \frac{1}{V}\int_V \sigma^{(ED)}\phi dV \tag{6.98}$$

$$f(z) = \frac{1}{\pi R^2}\left[2\pi\int_0^R \sigma^{(ED)}\phi r dr\right] \tag{6.99}$$

$$h(r) = \frac{1}{Z}\int_0^Z \sigma^{(ED)}\phi dz \tag{6.100}$$

and summed over all groups.

Chapter 7

Numerical Results

7.1 Introduction

In this chapter we consider various computational problems to investigate and validate the theoretical method developed in the previous chapters. One and two dimensional test problems have been formulated, and comparison tests have been performed using a SP_N code, written by the author, and the Monte Carlo code CYLTRAN [22]. CYLTRAN will serve as our benchmark. For each problem we will investigate the accuracy of the numerical solutions, the computational efficiency of the methods, and provide a brief discussion of results. An extended discussion and interpretation of results will be presented in the next chapter. CYLTRAN is a member of the integrated TIGER series (ITS) of coupled electron-photon transport codes developed by Sandia National Laboratory; cross sections for CYLTRAN are generated using the ITS code XGEN [22]. All calculations were performed on a CRAY YMP at Los Alamos National Laboratory.

7.2 Test Problem One

Let us begin by analyzing a simple problem: a one dimensional homogeneous slab of aluminum with an isotropic boundary source of electrons (1 electron/cm^2 s). The problem is of thickness 25 mil (.0635 cm), with the source located at the plane $z = 0$ cm. The source electrons are distributed in a flat energy spectrum as shown in Figure 7.1. We have calculated the energy deposition rate (EDR) as a function of

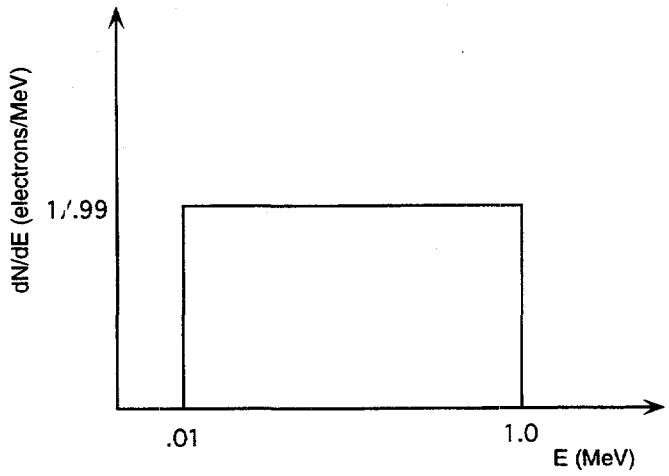

Figure 7.1: Problem One: Electron Differential Spectrum

Table 7.1: Problem One: Results

	EDR (MeV/cm^3s)	CPU time
SP_{15}	1.55	41 s
MC	$1.52 \pm 1\%$	2 hr 22 min

penetration, and the energy deposition rate in a test region defined as 24 mil $\leq z \leq$ 25 mil. For the SP_N calculation, we have performed an order P_{15} calculation with 80 energy groups (50 e^-, 30 γ) and 50 spatial cells of uniform mesh spacing (Δz = 1.27 x 10^{-3} cm). For the Monte Carlo calculation we ran 10^6 histories. In a comparison of SP_N and Monte Carlo results, Figure 7.2 and Table 7.1, we note that the EDR curves are almost identical, the test region energy deposition rates differ less than 2%, and the SP_N method is over 200 times faster than Monte Carlo.

7.3 Test Problem Two

The second problem is a one dimensional, deep penetration, multi-media problem, shown in Figure 7.3. Deep penetration problems are problems in which we wish to calculate the dose in a region surrounded by many mean free paths of material. An isotropic geosynchronous trapped electron source [23], Table 7.2, is incident at the plane z = 0 cm. The source is normalized to 1 particle/cm^2 s. This source-geometry configuration is characteristic of space shielding benchmark problems [23], with the silicon region representing a semiconductor device, and the aluminum and tungsten regions representing the shield. We have written a FORTRAN code to produce the SP_N and Monte Carlo input spectrum from the tabular electron spectra data. For the SP_N calculation have performed an order P_{15} calculation, with 70 spatial cells of nonuniform mesh spacing ($\Delta_{Al,Si}$ = 1.27 x 10^{-3} cm, Δ_W = 7.5197 x 10^{-4} cm). To obtain a low standard deviation on the Monte Carlo solution, it was necessary to run a large number of histories (1 x 10^7). We display the results of the calculation, the EDR in the silicon region, in Table 7.3.

We have performed a convergence study of the SP_N method, where we investigated the effects of the order N upon the solution. The results of the convergence study are

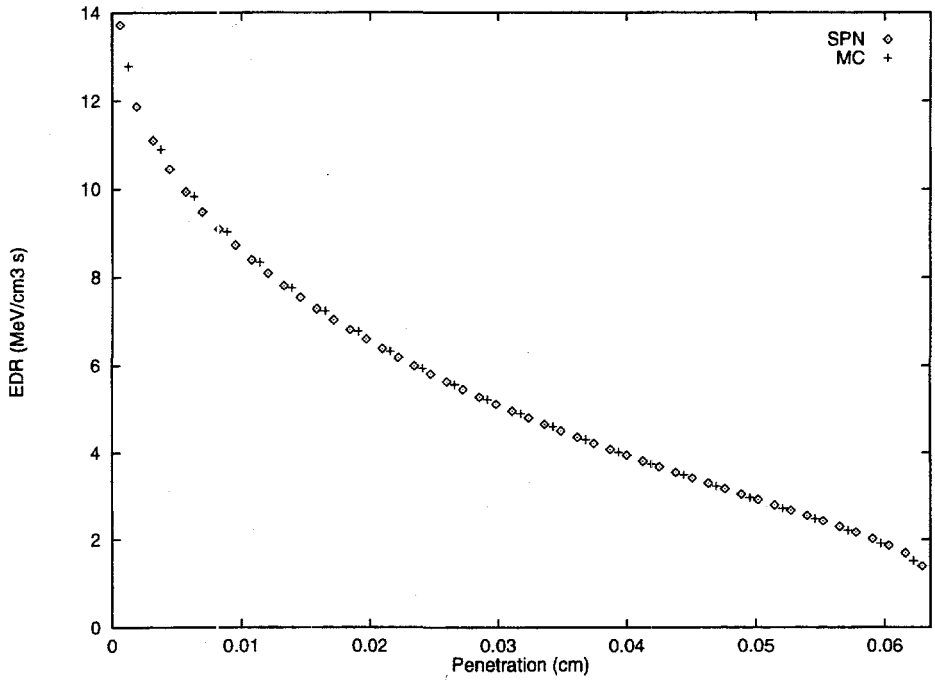

Figure 7.2: Problem One: Energy Deposition Rate vs Penetration

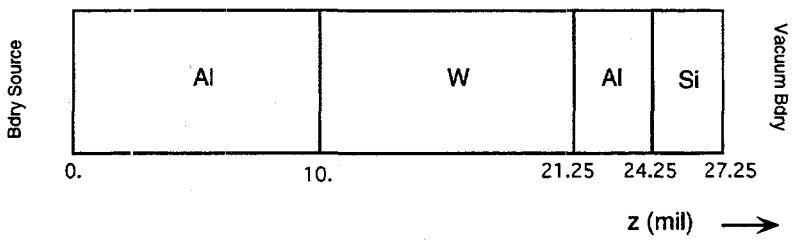

Figure 7.3: Problem Two: Geometry

Table 7.2: Geosynchronous Electron Spectrum

Energy (MeV)	Integral Spectrum[a] (e/cm^2)	Differential Spectrum (e/cm^2MeV)
0.1	1.878 (12)[b]	1.227 (13)
0.5	2.789 (11)	1.047 (12)
1.0	5.861 (10)	1.661 (11)
1.5	1.375 (10)	4.082 (10)
2.0	3.224 (09)	8.685 (09)
2.5	8.832 (08)	2.409 (09)
3.0	2.419 (08)	4.678 (08)
3.5	1.313 (08)	1.278 (08)
4.0	7.122 (07)	1.074 (08)
4.5	3.153 (07)	4.899 (07)
5.0	1.396 (07)	2.868 (07)
5.5	3.862 (06)	1.092 (07)
6.0	1.069 (06)	2.194 (06)

[a]The integral spectrum is given for a period of one day. The integral spectrum value at energy E_i is defined as the integral spectrum between E_i and ∞.
[b]value read as 1.878 x 10^{12}

Table 7.3: Problem Two: Results

	EDR (MeV/cm^3s)	CPU time	HWM memory[a]
SP_1	1.67 x 10^{-3}	09 s	499 K
SP_3	2.02 x 10^{-3}	20 s	837 K
SP_7	2.11 x 10^{-3}	45 s	1513 K
SP_{15}	2.14 x 10^{-3}	91 s	2884 K
MC	2.26 x 10^{-3} $\pm$ 3%	6 hr 4 min	715 K

[a]1 high water mark (HWM) memory unit = 512 words (64 bits/word)

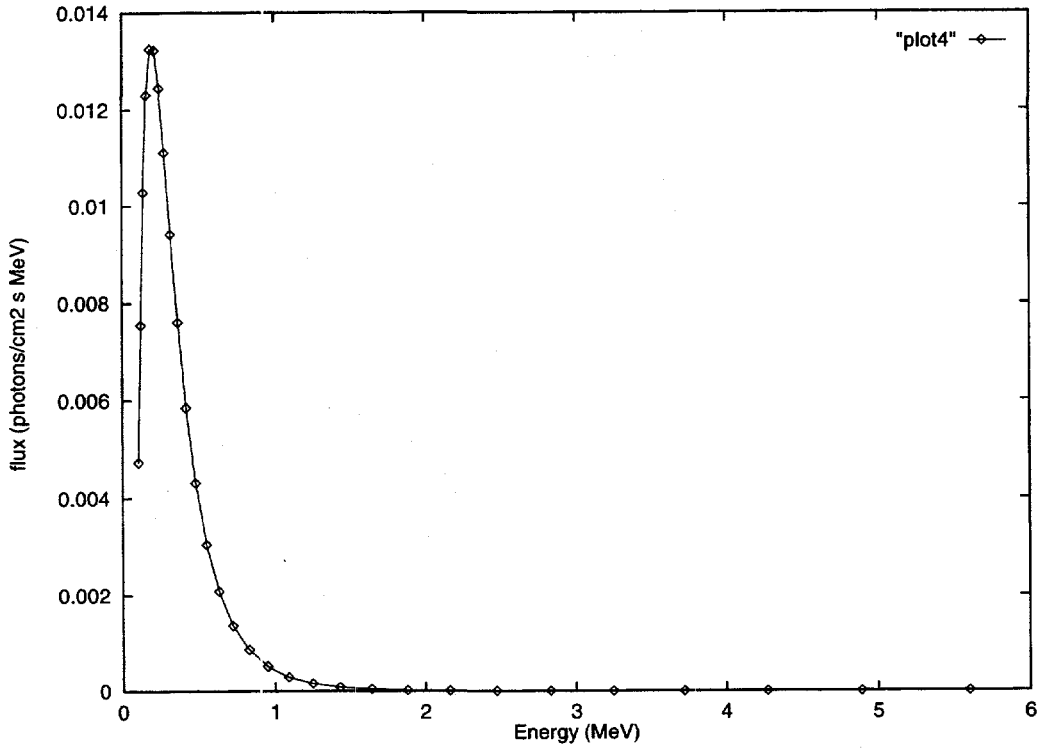

Figure 7.4: Problem Two: Photon Flux vs Energy

displayed in Table 7.3. We observed that the largest change in the solution occurs between SP_1 and SP_3. After SP_7 the solution changes relatively little, while the required CPU time increases proportional to N. We will consider the SP_{15} calculation as the final answer for our comparison with Monte Carlo, although it appears as if an order SP_7 calculation would be sufficient. We observed that the SP_{15} and Monte Carlo results differ by 5%, with the Monte Carlo CPU time exceeding the SP_{15} CPU time by over two orders of magnitude.

We have calculated the unshielded or free space dose to the silicon region. This value was found to be 12.0 MeV/cm^3s, indicating 4 orders of magnitude attenuation by the shield. This calculation verifies that we are in a well shielded regime.

All space shielding calculations, up until now, have been performed without including the effects of positrons. Our justification for neglecting positrons, thus far, lies in the geosynchronous electron spectrum, where 97% of the electrons in the spectrum have energy E $<$ 1.0 MeV. Recall, for positron production we require photons with energies E $>$ 1.02 MeV. To investigate the significance of positrons we have performed the following two calculations: We have repeated the test problem two calculation with positrons, and we note that the energy deposition rate increases from the previous value of 2.14 x 10^{-3} MeV/cm^3s (no positrons) to 2.16 x 10^{-3} MeV/cm^3s. To understand this result, we calculated the photon spectrum at the midpoint of the silicon region, Figure 7.4. From this differential spectrum we found that relatively few photons have energies E $>$ 1.02 MeV, the threshold energy for positron production. Thus, we conclude that positrons do not significantly contribute to the dose in space shielding problems, and hence we are justified in neglecting their effect in our calculations.

7.4 Test Problem Three

The third problem, Figure 7.5, is a difficult two dimensional, R - Z geometry, four region, deep penetration problem. Each region represents a coaxial cylinder of uniform composition. A geosynchronous trapped electron source is uniformly incident along the outer periphery. Again, this geometry-source configuration is characteristic of satellite shielding benchmark problems. We note that for the calculation of the dose in a region deep within a multidimensional problem, Monte Carlo requires a large number of histories and often a corresponding large CPU time. For the SP_N calculation we have again performed an order P_7 calculation, with 35 x 35 spatial cells of nonuniform mesh spacing ($\Delta_{Al,Si}$ = 2.54 x 10^{-3} cm, Δ_W = 1.504 x 10^{-3} cm). For the Monte Carlo calculation we ran 2 x 10^7 histories. We display the results of the calculation, the EDR in the silicon region, in Table 7.4.

The unshielded or free space dose to the silicon region was calculated to be 25.8 MeV/cm^3s, indicating 3 orders of magnitude attenuation by the shield, and again verifying that the silicon region is highly shielded.

We have performed a convergence study for the two dimensional SP_N method, where we have investigated the effects of the order N upon the solution, Table 7.4. We again observed that the largest change in the solution occurs between SP_1 and SP_3, with a relatively small change between SP_3 and SP_7. For our comparison with Monte Carlo, we shall consider the SP_7 result as the final answer. We observed that the SP_7 result significantly overshoots the Monte Carlo answer; however, there is a relatively large uncertainty in the Monte Carlo answer. Unfortunately, the current Monte Carlo calculation required over nine hours. To reduce the uncertainty to 4% would require an excessive run time of 37 hrs. Furthermore, we wish to indicate that

solution overshoots have been observed in previous SP_N studies [15]. Finally, we note that the SP_7 and Monte Carlo results differ by 8%, with the Monte Carlo CPU time exceeding the SP_7 CPU time by over two orders of magnitude.

We have investigated the effects of including positrons in this two dimensional test problem. With positrons the EDR increased from the previous value of 1.97 x 10^{-2} MeV/cm^3s (no positrons) to 2.00 x 10^{-2} MeV/cm^3s, a change of only 1.5%, while, the CPU time required increased a factor of four. Again, this calculation validates the assumption that positrons may be neglected in our space shielding calculations.

The computational efficiency of the SP_N code with various acceleration schemes is displayed in Table 7.5. In this particular calculation, the MGA scheme with a conjugate gradient (CG) solver is shown to be the most efficient. However, we note that in problems involving a void region, the multigrid (MG) matrix solver [17] can surpass the conjugate gradient solver in efficiency. In general, if we have a system of well-conditioned equations, CG is the recommended method of solution. However, if the equations are ill-conditioned, as those that result in a void calculation, MG can be more efficient.

We have performed a separate study to further investigate the effectiveness of the angular multigrid (MGA) method when applied to two dimensional SP_N calculations. In this study we compared the computational spectral radius of the one and two dimensional SP_N methods with the computational spectral radius of the one dimensional S_N method for one group, highly forward peaked Fokker-Planck scattering [21]. Recall, SP_N is equivalent to S_N in one dimension; therefore, we would expect to see the same spectral radius in one dimensional SP_N as one dimensional S_N. Furthermore, our previous Fourier analysis indicated that the P_1 diffusion synthetic acceleration scheme exhibits exactly the same effectiveness on two dimensional SP_N

calculations that it does on one dimensional SP_N calculations. This would suggest that MGA should have the same effectiveness on two dimensional SP_N calculations as one dimensional SP_N calculations. Finally, we wish to remind the readed that both the DSA and MGA methods are unstable (with sufficiently forward-peaked scattering and sufficiently small absorption) for two dimensional S_N calculations, yet are both very effective for one dimensional S_N calculations. We display the results of our investigation in Table 7.6, and we observe the following: The one dimensional results are identical for S_N and SP_N. Furthermore, the one dimensional and two dimensional SP_N results are identical. Therefore, we conclude that the angular multigrid method exhibits exactly the same effectiveness on two dimensional SP_N calculations that it does one dimensional SP_N calculations.

Table 7.4: Problem Three: Results

	EDR (MeV/cm^3s)	CPU time	HWM memory
SP_1	1.60 x 10^{-2}	63 s	2782 K
SP_3	1.93 x 10^{-2}	138 s	6755 K
SP_7	1.97 x 10^{-2}	286 s	14753 K
MC	1.82 x 10^{-2} $\pm$ 8%	9 hr 22 min	715 K

7.5 Test Problem Four

To decrease the uncertainty in the Monte Carlo results of problem three without increasing the CPU time, we have formulated a two dimensional space shielding problem with reduced shield thickness. This problem is identical to test problem three

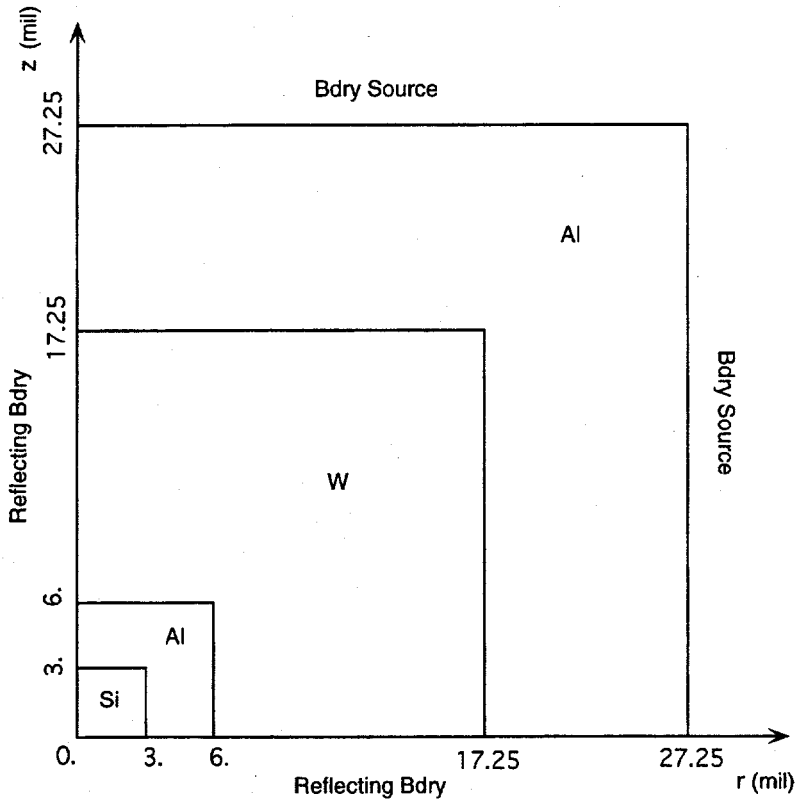

Figure 7.5: Problem Three: Geometry

Table 7.5: Problem Three: SP_N Acceleration Scheme Performance

acceleration scheme	matrix solver	CPU time (s)
none	CG	891
DSA all gps	CG	414
MGA e^- gps, DSA γ gps	CG	286
MGA e^- gps, DSA γ gps	MG	310

Table 7.6: Performance of Angular Multigrid and Diffusion Synthetic Methods

acceleration	order	1-D S_N Spectral Radius	1-D SP_N Spectral Radius	2-D SP_N Spectral Radius
MGA	4	0.36	0.35	0.35
DSA	4	0.36	0.35	0.35
MGA	8	0.47	0.47	0.47
DSA	8	0.81	0.81	0.82
MGA	16	0.54	0.54	0.54
DSA	16	0.95	0.95	0.95

with the outer aluminum and tungsten regions each reduced to 5 mil thickness. For the SP_N calculation we have performed order P_1, P_3, and P_7 calculations, with 35 x 35 spatial cells of nonuniform mesh spacing ($\Delta_{inner\,Al,Si}$ = 2.54 x 10^{-3} cm, Δ_W = 6.684 x 10^{-4} cm, $\Delta_{outer\,Al}$ = 1.27 x 10^{-3} cm). For the Monte Carlo calculation we ran 5 x 10^6 histories. We display the results in Table 7.7, and note that the uncertainty in the Monte Carlo solution is reduced from $\pm$ 8% (test problem three) to $\pm$ 2% in this problem. Recall, the unshielded or free space dose to the silicon region was calculated to be 25.8 $MeV/cm^3 s$, indicating two orders of magnitude attenuation by the shield, and again verifying that the silicon region is well shielded.

7.6 Test Problem Five

The fifth problem, Figure 7.6, is a difficult two dimensional, R - Z geometry, three region void problem. Again, this geometry-source configuration is characteristic of satellite shielding benchmark problems. Deterministic transport problems with a void region are often times very slow to converge when using a code with a conjugate

Table 7.7: Problem Four: Results

	EDR (MeV/cm^3s)	CPU time	HWM memory
SP_1	2.49 x 10^{-1}	066 s	2782 K
SP_3	2.62 x 10^{-1}	145 s	6755 K
SP_7	2.67 x 10^{-1}	305 s	14753 K
MC	2.48 x 10^{-1} $\pm$ 2%	2 hr 23 min	715 K

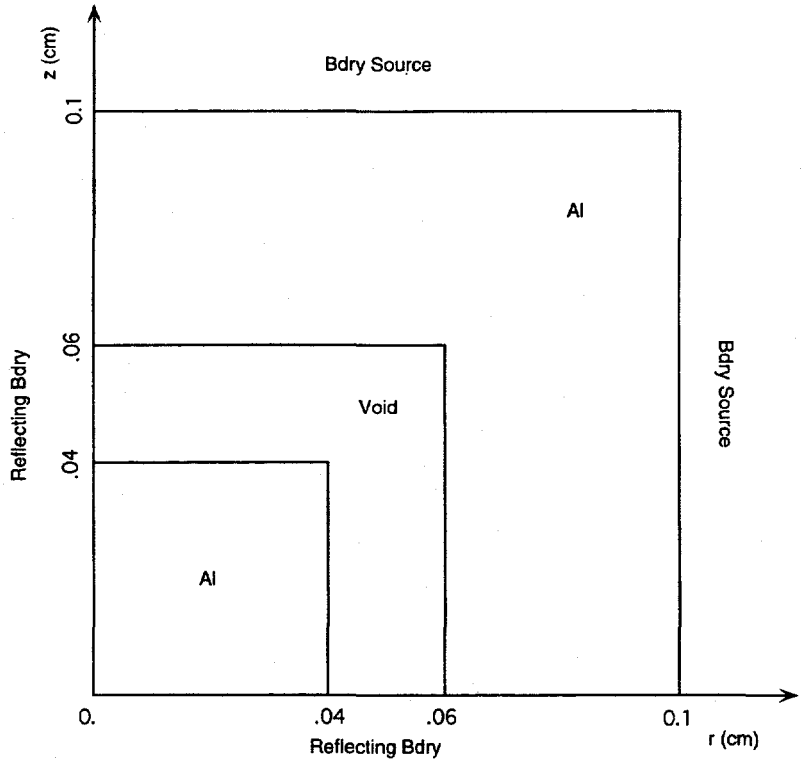

Figure 7.6: Problem Five: Geometry

gradient solver. We have employed a multigrid matrix solver [17] within our SP_N code to handle the ill-conditioned equations that result from the modeling of the void. Each region represents a coaxial cylinder of uniform composition. A geosynchronous trapped electron source is again incident along the outer periphery. For the SP_N calculation we have performed an order P_7 calculation with 35 x 35 spatial cells of nonuniform mesh spacing ($\Delta_{Al,Si}$ = 2.67 x $10^{-3}cm$, Δ_W = 4.0 x 10^{-3} cm). Low density nitrogen gas ($10^{-7}g/cm^3$) is used to simulate the void region in the SP_N calculation, while Monte Carlo allows the explicit modeling of a void. For the Monte Carlo calculation we ran 2 x 10^6 histories. We display the results of the calculation, the EDR in the inner aluminum region, in Table 7.8.

Table 7.8: Problem Five: Results

	EDR (MeV/cm^3s)	CPU time	HWM memory
SP_7	2.24	478 s	14739 K
MC	2.25 ± 1%	53 min 13 s	715 K

7.7 Test Problem Six

We conclude with a monodirectional electron beam problem. A cylindrical beam is incident along the z axis of an aluminum cylinder, where the beam radius is 1/20 th of the radius of the cylinder. The cylinder is of dimension radius = height = 10 mil (2.54 x 10^{-2} cm). Electrons are distributed in a flat energy spectrum as shown in Figure 7.1. For the SP_N calculation we have performed an order P_{15} calculation.

For the Monte Carlo calculation we ran 10^5 histories. Axial energy deposition rate as a function of penetration is displayed in Figure 7.7. We have observed that the SP_N method appears to be a poor approximation in this case, with an average error of approximately 30%. Specifically, the SP_N method appears to be too diffusive an approximation for beam problems. This result, however, is in agreement with theoretical expectations.

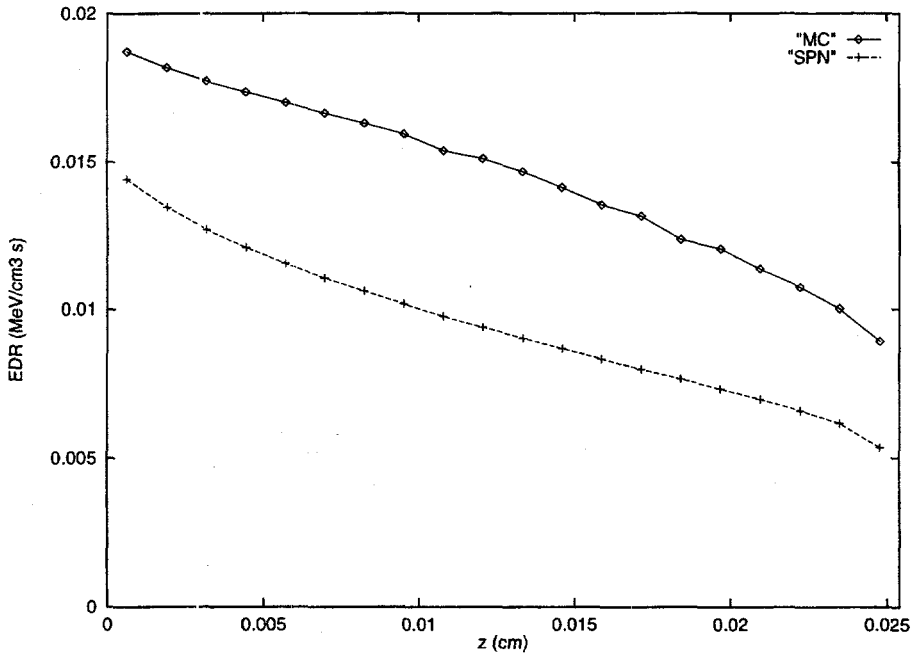

Figure 7.7: Problem Six: Axial Energy Deposition Rate vs Penetration

Chapter 8

Summary and Discussion

8.1 Conclusions

There is a strong need for accurate and efficient numerical methods for solving the Boltzmann - CSD transport equations. The purpose of this thesis was multifold: Our first major objective was to develop a simplified spherical harmonic method (SP_N method) for multidimensional coupled electron-photon transport; this is the first time that the SP_N method has been applied to charged particle transport. The second major objective was the development and analysis of efficient solution techniques for the multidimensional SP_N equations. We have met these objectives. In this chapter we review and summarize some important properties of the SP_N method in contrast to other transport methods, examine and interpret the test problem results of Chapter 7, and conclude with some possibilities for future work.

The SP_N equations were proposed in the early 1960's by Gelbard for application to neutron transport problems. As has been stated earlier, the SP_N method is an approximation used to treat the angular variable. This method has been shown to produce approximate transport solutions which are significantly more accurate than diffusion theory, but significantly less expensive than discrete-ordinates (S_N), or full P_N methods. The initial derivation of the SP_N equations was not rigorous. This lack of theoretical foundation has undoubtedly acted as an obstruction to the widespread use of these equations. However, a recent paper [1] in the literature shows that the SP_N equations represent a formal asymptotic solution to the Boltzmann transport

equation in the diffusion limit.

The SP_N equations are an approximation in the sense that one does not obtain the exact transport solution as N approaches infinity. Such a method is said to be nonconvergent. This is in contrast to the S_N and P_N methods which are convergent. The number of unknowns in multidimensional SP_N is of order $(N+1)$, while in multidimensional P_N the number of unknowns is of order $(N+1)^2$. Electron scattering is highy anisotropic; hence, an accurate representation of the electron flux requires high order $(P_7 - P_{15})$ flux and cross section expansions. Thus, SP_N offers tremendous computational savings over P_N when N is large, as is always the case in electron-photon transport problems. SP_N retains the rotational invariance of the P_N method; hence, ray effects do not appear in the solution. The SP_N equations can be put in a canonical form which allows the application of standard diffusion discretization techniques and a source iteration solution strategy. In addition, convergence acceleration techniques can be applied to the canonical form.

We have developed codes for the multigroup SP_N equations in one dimensional slab, two dimensional X-Y, and two dimensional R-Z geometries. We have performed a Fourier analysis of the standard source iteration (SI) solution scheme, and have shown the method to be unconditionally stable. The SI method, however, can be very slow to converge in optically thick systems where the scattering ratio, $c = \frac{\sigma_0}{\sigma_t}$, is near one. This behavior is also exhibited by the S_N method in all dimensions. We have analyzed and generalized two acceleration schemes, P_1 diffusion synthetic acceleration and multigrid in angle acceleration, which significantly reduce the spectral radius and accelerate the convergence. We have performed a Fourier analysis of the P_1 diffusion synthetic acceleration scheme (P_1 DSA) for multidimensional SP_N, and have shown the method to be stable and effective. Fourier analysis of the one dimensional and two

dimensional SP_N equations produced identical results. The stability of P_1 DSA for two dimensional case is indeed a suprising result. Previous analyses [24] have shown that P_1 DSA is stable for one dimensional S_N, but unstable for two dimensional S_N. We have generalized the one dimensional P_1 DSA method to two dimensions and have implemented this method in our code. We have developed a multigrid in angle (MGA) convergence acceleration routine, and have demonstrated that MGA is more effective than P_1 DSA when scattering is highly forward peaked. That is, MGA becomes increasingly effective, relative to DSA, as N increases. We note for the one dimensional S_N equations multigrid acceleration is stable. However, since P_1 DSA is unstable for multigeometry S_N and P_1 DSA is contained in the multigrid method, then multigrid is also unstable for multigeometry S_N.

To investigate the accuracy and computational efficiency of the SP_N method, we have performed numerical comparisons with Monte Carlo, in the form of six test problems. We have investigated the applicability of the SP_N approximation to two different physical classes of problems: satellite electronics shielding from geomagnetically trapped electrons, and electron beam problems. In the space shielding study, the SP_N method produced solutions that are accurate within 10% of the benchmark Monte Carlo code solutions. We observed that we obtain better agreement with Monte Carlo for one dimensional than two dimensional problems. This is intuitively satisfying, since SP_N and P_N are identical in one dimensional geometry, and P_N is convergent. In two and three dimensions, this equivalence between SP_N and P_N does not exist for $N > 1$. In an examination of computational efficiency, we have demonstrated in space shielding applications that the SP_N method is often orders of magnitude faster than Monte Carlo, with the difference in CPU time particularly pronounced in deep penetration problems. For reasonable statistics on the dose in

deeply shielded regions, Monte Carlo often requires a large number of histories and a corresponding long run time. We observed that SP_N often requires more memory than Monte Carlo. However, SP_N is capable of producing detailed scalar flux and current profiles whereas CYLTRAN is not.

In deterministic transport calculations, void problems often lead to excessive solution times when a simple conjugate gradient (CG) matrix solver is used. We have successfully modeled quasi-void problems, by implementing a spatial multigrid (MG) matrix solver within our code, and have obtained excellent agreement with Monte Carlo. In general, if we have a system of well-conditioned equations, CG is the recommended method of solution. However, if the equations are ill-conditioned, as in the case of strong material discontinuities across an interface, MG can be more efficient.

We have investigated the effects of positrons in one dimensional and two dimensional space shielding applications. Specifically, we have performed calculations of the energy deposition rates with and without positrons and compared solutions. In the comparison study we observed less than 1.5% change in calculated energy deposition rates when we included positrons, while the required CPU time increased up to a factor of four. To understand this result, we calculated the photon spectrum at the midpoint of the silicon region. We found that relatively few photons are present at energies greater than the threshold for positron production, which is consistent with our results.

We have calculated the unshielded or free space dose to the silicon region in the one and two dimensional space shielding problems. We have observed from two to four orders of magnitude attenuation in the scalar flux. Thus we conclude that we are in a highly shielded regime.

We have performed a convergence study of the SP_N method for space shielding

applications. We observed that the largest change in the solution occurs between SP_1 and SP_3. The SP_N solution changes relatively little for N > 3, while the required CPU time increases proportional to N. We conclude that the optimal approximation varies from SP_3 to SP_7 for space shielding applications. Increasing the order does not necessarily increase the accuracy of the solution in multidimensional calculations.

We have further investigated the effectiveness of the angular multigrid (AMG) method when applied to two dimensional SP_N calculations. By performing certain benchmark calculations appearing in the literature [21], we have computationally demonstrated that the AMG method exhibits exactly the same effectiveness on two dimensional SP_N calculations that it does on one dimensional SP_N calculations. This was suggested by the Fourier analysis we originally performed indicating that the diffusion-synthetic acceleration (DSA) scheme exhibits exactly the same effectiveness on two dimensional SP_N calculations that it does on one dimensional SP_N calculations. Remember that both the DSA and AMG methods are unstable (with sufficiently forward-peaked scattering and sufficiently small absorption) for two dimensional S_N calculations, yet are both very effective for one dimensional S_N calculations.

We have investigated the applicability of the SP_N method to beam problems. We have observed that the SP_N method appears to be too diffusive an approximation for beam problems. This result, however, is in agreement with theoretical expectations.

8.2 Future Goals

Some possible future goals include:

1. Investigate the biasing of coupled electron-photon Monte Carlo using SP_N adjoint solutions.

2. Replacement of diamond-difference in energy scheme [25], which can lead to numerical oscillations in transport solutions when the boundary source is monoenergetic and spatial cells are optically thin. This will require a considerably more complex solution strategy.

3. Extend the method to three dimensional geometry for orthogonal mesh.

4. Extend the method to three dimensional geometry for unstructured mesh.

5. Develop optimal v cycle strategy for the use of spatial multigrid in angular multigrid scheme.

Bibliography

[1] E. W. Larsen, J. E. Morel, and J. M. McGhee, "Asymptotic Derivation of the Simplified P_N Equations," *Proc. ANS Topical Meeting, Mathematical Methods and Supercomputing in Nuclear Applications, M&C + SNA '93*, vol. 1, April 1993. Karlsruhe, Germany.

[2] E. E. Lewis and W. F. Miller, Jr., *Computational Methods of Neutron Transport.* New York: Wiley, 1984.

[3] G. I. Bell and S. Glasstone, *Nuclear Reactor Theory.* New York: Van Nostrand Reinhold, 1970.

[4] K. M. Case and P. F. Zweifel, *Linear Transport Theory.* Reading, MA: Addison-Wesley, 1967.

[5] K. Przybylski and J. Ligou, "Numerical Analysis of the Boltzmann Equation Including Fokker-Planck Terms," *Nuclear Science and Engineering*, vol. 81, pp. 92–109, 1982.

[6] M. R. Spiegel, *Mathematical Handbook.* New York: McGraw-Hill, 1968.

[7] L. J. Lorence, Jr., J. E. Morel, and G. D. Valdez, "Physics Guide to CEPXS: A Multigroup Coupled Electron-Photon Cross Section Generating Code," Tech. Rep. SAND89-1685, Sandia National Laboratory, Albuquerque, NM 87185, 1989.

[8] J. E. Morel, "Multigroup Legendre Coefficients for the Diamond Difference Continuous Slowing Down Operator," *Nuclear Science and Engineering*, vol. 91, pp. 324–331, 1985.

[9] K. D. Lathrop, "Remedies for Ray Effects," *Nuclear Science and Engineering*, vol. 45, p. 255, 1971.

[10] J. D. Jackson, *Classical Electrodynamics*. New York: Wiley, 1975.

[11] J. K. Fletcher, "The Solution of the Multigroup Neutron Transport Equation Using Spherical Harmonics," *Nuclear Science and Engineering*, vol. 84, pp. 33–46, 1983.

[12] E. M. Gelbard, "Application of Spherical Harmonics Method to Reactor Problems," *WAPD-BT-20*, September 1960.

[13] E. M. Gelbard, "Simplified Spherical Harmonics Equations and Thier Use in Shielding Problems," *WAPD-T-1182*, February 1961.

[14] E. M. Gelbard, "Applications of the Simplified Spherical Harmonics Equations in Spherical Geometry," *WAPD-TM-294*, April 1962.

[15] J. E. Morel, J. M. McGhee, and E. W. Larsen, "A 3-D Time Dependent Unstructured Tetrahedral Mesh SP_N Method," *International Conference on Mathematics and Computations, Reactor Physics, and Environmental Analyses*, April-May 1995.

[16] J. E. Morel, L. A. Olvey, J. M. McGhee, G. W. Claborn, and J. A. Josef, "Diffusion-Accelerated Solution of the Even-Parity S_N Equations with Anisotropic Scattering," *Proceedings of the International Topical Meeting on Advances in Mathematics, Computations, and Reactor Physics*, April-May 1991. Pittsburgh, PA.

[17] J. E. Dendy, Jr., "Black Box Multigrid," *Journal of Computational Physics*, vol. 48, pp. 366–386, 1982.

[18] J. J. Duderstadt and L. J. Hamilton, *Nuclear Reactor Analysis.* New York: Wiley, 1979.

[19] T. R. Hill, "ONETRAN: A Discrete Ordinates Finite Element Code for the Solution of the One-Dimensional Multigroup Transport Equation," Tech. Rep. LA-5990-MS, Los Alamos National Laboratory, Los Alamos, NM 87545, 1975.

[20] L. J. Lorence, Jr., J. E. Morel, and E. W. Larsen, "An S_2 Synthetic Acceleration Scheme for the One-Dimensional S_N Equations with Linear Discontinuous Spatial Differencing," *Nuclear Science and Engineering*, vol. 101, pp. 341–351, 1989.

[21] J. E. Morel and T. A. Manteuffel, "An Angular Multigrid Acceleration Technique for S_N Equations with Highly Forward-Peaked Scattering," *Nuclear Science and Engineering*, vol. 107, pp. 330–342, 1991.

[22] J. A. Halbleib *et al.*, "ITS Version 3.0: The Integrated Tiger Series of Coupled Electron/Photon Monte Carlo Transport Codes," Tech. Rep. SAND91-1634, Sandia National Laboratory, Albuquerque, NM 87185, 1992.

[23] R. Saqui *et al.*, "Computataional Benchmarks for Electron Total Dose Shielding Methodology," Tech. Rep. WL-TR-90-59, Weapons Laboratory, Air Force Systems Command, Kirtland Air Force Base, NM 87117-6008, 1991.

[24] M. L. Adams and T. A. Wareing, "Diffusion-Synthetic Acceleration Given Anisotropic Scattering, General Quadratures, and Multidimensions," *Transactions of the American Nuclear Society*, vol. 68, June 1993. San Diego, CA.

[25] M. S. Lazo, "A Linear Discontinuous Galerkin Approximation for the Continuous Slowing Down Operator," *Nuclear Science and Engineering*, vol. 92, pp. 98–109, 1986.

Appendix A

Iterative Solution of Matrix Equations

In this appendix we demonstrate that the stability and convergence of a specified iteration scheme is determined by the properties of the iteration matrix. Consider the inhomogeneous matrix equation

$$\mathbf{A}\vec{x} = \vec{y} \tag{A.1}$$

we may split the coefficient matrix

$$\mathbf{A} = \mathbf{M} - \mathbf{N} \tag{A.2}$$

and write Equation (A.1) as

$$\mathbf{M}\vec{x} = \mathbf{N}\vec{x} + \vec{y} \tag{A.3}$$

To solve the equation iteratively we guess the value of $\vec{x}$ on the right hand side of Equation (A.3), defined to be $\vec{x}^{(0)}$, and calculate successive iterates $\vec{x}^{(1)}, \vec{x}^{(2)}, \ldots$ according to

$$\mathbf{M}\vec{x}^{(l)} = \mathbf{N}\vec{x}^{(l-1)} + \vec{y} \tag{A.4}$$

or

$$\vec{x}^{(l)} = \mathbf{B}\vec{x}^{(l-1)} + \tilde{y} \tag{A.5}$$

where $\mathbf{B} \equiv \mathbf{M}^{-1}\mathbf{N}$ is called the iteration matrix. We may obtain a recursion relation for the error, $\vec{\epsilon}^{(l)} = \vec{x}^{(l)} - \vec{x}$, by subtracting Equation (A.3) from (A.4)

$$\vec{\epsilon}^{(l)} = \mathbf{B}\vec{\epsilon}^{(l-1)} \tag{A.6}$$

hence

$$\vec{\epsilon}^{(l)} = \mathbf{B}^l \vec{\epsilon}^{(0)} \tag{A.7}$$

For the sequence of vectors $\vec{x}^{(l)}$ to converge to $\vec{x}$, we then require

$$\lim_{l\to\infty} \vec{\epsilon}^{(l)} = \vec{0} \tag{A.8}$$

Next, assume the iteration matrix has a complete, linearly independent set of eigenvectors $\vec{\eta}_i$ and associated eigenvalues λ_i; this is always true for the symmetric positive definite matrices that result in our work. Then, expand the error $\vec{\epsilon}^{(0)}$ in terms of these eigenvectors

$$\mathbf{B}\vec{\eta}_i = \lambda_i \vec{\eta}_i \tag{A.9}$$

$$\vec{\epsilon}^{(0)} = \sum_{i=1}^{J} \alpha_i \vec{\eta}_i \tag{A.10}$$

Then, substituting Equation (A.10) into (A.7) and using (A.9), we obtain

$$\vec{\epsilon}^{(l)} = \sum_i \alpha_i \lambda_i^l \vec{\eta}_i \tag{A.11}$$

For the error to approach zero as $l \to \infty$ we then require

$$\|\lambda_i\| < 1 \qquad\qquad i = 1, 2, \ldots, J \tag{A.12}$$

This is the stability condition for iteration methods. If we order the eigenvalue moduli as

$$\|\lambda_1\| > \|\lambda_2\| > \|\lambda_3\| > \dots \tag{A.13}$$

then $\|\lambda_1\|$ is referred to as the spectral radius, and the stability of the iterative scheme is determined by the spectral radius

$$\|\lambda_1\| \begin{cases} < 1 & \text{stable, convergent} \\ = 1 & \text{stable, nonconvergent} \\ > 1 & \text{unstable} \end{cases} \tag{A.14}$$

In Fourier analysis, we first derive a matrix equation for the error, expand the error in a Fourier series, and then determine the spectral radius of the iteration matrix of the resultant equation.

Appendix B

CEPXS Cross Section Format

The SP_N code utilizes multigroup-Legendre cross sections generated by the program CEPXS. CEPXS produces cross sections data in a format where each material and each Legendre order (l = 0, 1,..., NLEG) is described by a block of data of IHM rows by IGM columns. The parameter IHM is determined internally, and the parameter IGM is equal to the number of energy groups specified by the user. Non scattering cross sections are stored in the l = 0 data block. The row position of cross sections is specified relative to the total cross section, σ_t (row IHT), and the within group scattering cross section, $\sigma_{s,g\to g}$ (row IHS). The row order for group g is as follows

cross section	row
⋮	⋮
σ_t	IHT
$\sigma_{s,g+N\to g}$	IHT + 1
⋮	⋮
$\sigma_{s,g+2\to g}$	IHS − 2
$\sigma_{s,g+1\to g}$	IHS − 1
$\sigma_{s,g\to g}$	IHS
$\sigma_{s,g-1\to g}$	IHS + 1
⋮	⋮
$\sigma_{s,g-M\to g}$	IHS+M

(B.1)

M is the number of downscatter groups, and N is the number of upscatter groups. The scattering matrix need not be square. Cross sections are stored in a final three dimensional array of size IHM x IGM x NSETS, where

$$\text{NSETS} = \text{NMAT}(\text{NLEG}+1) \tag{B.2}$$

NMAT is the number of materials, and NLEG is the maximum Legendre order.